U.S. Department
of Transportation
**National Highway
Traffic Safety
Administration**

NHTSA
www.nhtsa.gov

DOT HS 811 102 **March 2009**

Evaluation of the Ribeye Deflection Measurement System in the 50th Percentile Hybrid III Dummy

Final Report

This document is available to the public from the National Technical Information Service, Springfield, Virginia 22161

1. Report No.	2. Government Accession No.	3. Recipient's Catalog No.
DOT HS 811 102		

4. Title and Subtitle	5. Report Date
Evaluation of the RibEye deflection measurement system in the 50th percentile Hybrid III dummy	March 2009
	6. Performing Organizational Code
7. Author(s) Narayan Yoganandan, Frank A. Pintar, James Rinaldi	8. Performing Organization Report No.
9. Performing Organization Name and Address Department of Neurosurgery Medical College of Wisconsin Milwaukee, WI 53226	10. Work Unit No. (TRAIS)
	11. Contract or Grant No. DTNH-22-07-H00173
12. Sponsoring Agency Name and Address National Highway Traffic Safety Administration U.S. Department of Transportation 1300 New Jersey Avenue SE. Washington, DC 20590	13. Type of Report and Period Covered Interim July 2007 - December 2008
	14. Sponsoring Agency Code

15. Supplementary Notes

16. Abstract

This report describes experiments aimed to evaluate the performance of the RibEye system, using quasi-static and dynamic tests. Signal drop-out evaluations included mid-sternum compression tests replicating symmetrical, and offset and diagonal compression tests replicating asymmetric loading to the chest. Accuracy assessment evaluations included tests using sternum-mounted LEDs, rib-mounted LEDs with and without initial chest rotation, and indenter-mounted LEDs. The Hybrid III dummy internal chest potentiometer was included in some tests. For dynamic evaluations, pendulum tests were conducted in the neutral and oblique positions. A full-scale vehicle frontal offset test was conducted with the system in the dummy positioned in the right front passenger seat. In both static and dynamic tests, the system captured both x- and y-components of rib deflection. LEDs on the sternum responded similar to the chest potentiometer. System accuracy depends on the LED location on the rib, magnitude of rib deformation, and potential interference from devices such as the presence of the internal chest potentiometer. Optimum locations appear to be at a distance of 9 cm measured along the outer curvilinear path of the rib from mid-sternum on either side. At suboptimal positions, drop-out may occur. Eccentric positioning LEDs away from the rib center may result in accuracy loss. Signal drop-out depended on the type of loading, asymmetric loading produced more signal loss. The deflection response along the x-and y-directions were deemed reasonable in oblique loading tests. Results from the full-scale vehicle frontal offset test indicated that deflections from the system were in-line with the frontal offset principal direction of force with x-direction component magnitudes more on the left chest than the right chest, and the y-direction components of all ribs were from left-to-right. These evaluations provide a fundamental understating of the performance of the system and its ability to measure x- and y-component rib deflections at multiple locations including the sternum for frontal impact simulations.

17. Key Words	18. Distribution Statement
Biomechanics, deflection profiles, Ribeye system	

19. Security Classif. (of this report)	20. Security Classif. (of this page)	21. No. of Pages	22. Price
Unclassified	Unclassified	77	

Form DOT F 1700.7 (8-72) Per FORM PRO/Delrina 04/04/94 Reproduction of completed page authorized

EXECUTIVE SUMMARY

This report presents an evaluation of a new deflection measuring system. Briefly, the optically-based RibEye system developed by Robert A. Denton, Inc., for the 50th percentile male Hybrid III dummy is capable of providing deflections at 12 locations within the ribcage. Illumination from each light emitting diode (LED) positioned on the inside rib surface or sternum is captured by two sensors placed on either side of the spine box in the dummy. Deflections can be derived from processed optical signals, gathered along the x and y, i.e., frontal and side (antero-posterior and lateral) directions. Quasi-static and dynamic tests were done during the evaluation process.

Quasi-static tests consisted of signal drop-out and accuracy assessment tests. This included mid-sternum compression tests using cylindrical and square indenters replicating symmetrical chest loading, and offset and diagonal compression tests using a "belt type" indenter replicating asymmetric loading. Accuracy assessment of deflections from the system was also quasi-static. This included compression tests using sternum-mounted LEDs, rib-mounted LEDs with and without initial chest rotation about the z-axis, and indenter-mounted LEDs. All tests were conducted using an electro-hydraulic testing device. Signal drop-out tests to evaluate conditions where the RibEye system cannot record rib/sternum deflections were performed with the indenter positioned to deliver loading to the mid-sternum, left side offset, and diagonal belt-type loads inducing chest displacements of magnitudes ranging from one to three inches. In some tests, the available internal chest potentiometer of the dummy was included to assess the potential light interference to capture optical data from the LED-sensor combination, and to compare LED-measured deflections with the "standard" sternum displacements, albeit the latter is along one direction.

Results indicated that the RibEye system captures ribcage deformations effectively. LEDs on the sternum respond similar to the available internal chest potentiometer. The accuracy of the system depends on where the LEDs are positioned on the rib, the magnitude of rib deformation, and the potential interference from devices such as the presence of the internal chest potentiometer. Optimum locations appear to be at a distance of 9 cm measured along the outer curvilinear path of the rib from mid-sternum on either side. At this positioning, the system

showed no signal drop-out at deflections representative of current frontal impact Injury Assessment Reference Values (IARV). However, at suboptimal positions, drop-out may occur. Positioning LEDs away from the center of the rib, i.e., eccentric z-axis placement resulted in loss of accuracy. In addition, the signal drop-out depended on the type of indenter, with the belt-type indenter producing more signal loss. The deflections response along the x-and y-directions were deemed reasonable in oblique loading tests.

While quasi-static loading tests provided fundamental information on the performance of the RibEye system, pendulum and full-scale vehicle crash tests were conducted to evaluate the system under dynamic conditions. Pendulum tests were conducted at velocities ranging from 3.0 to 6.6 m/s with the LEDs positioned at the optimal location of 9 cm, determined from quasi-static tests. These experiments were conducted with and without the internal chest potentiometer with the dummy in the neutral position. Tests were also conducted with the dummy oriented at an angle of 25-degrees, i.e., oblique tests. In addition, a full-scale vehicle frontal offset test was conducted with the RibEye-equipped dummy (the standard chest potentiometer was not used) positioned in the right front passenger seat and the SID-H3 dummy in the driver seat.

Results from dynamic tests indicated that light interference from internal components restricts the ability of the system to obtain deflections including signal drop-out. In oblique tests, the system captured the asymmetric motions of the chest by demonstrating greater deflections on all left side ribs than right side ribs, demonstrating its potential under this loading condition. Results from the full-scale vehicle frontal offset test indicated that the RibEye performed well with minor signal drop-outs. The deflections from the RibEye system were in-line with the frontal offset principal direction of force with x-direction component magnitudes more on the left chest than the right chest, and the y-direction components of all ribs were from left-to-right. These quasi-static and dynamic evaluations have provided a fundamental understanding of the performance of the RibEye system as installed in the 50^{th} percentile Hybrid III dummy and its ability to measure both x- and y-components of rib deflections at multiple locations including the sternum for frontal impact applications.

TABLE OF CONTENTS

1.0 BACKGROUND 1

2.0 RIBEYE SYSTEM 3

2.1 RibEye specifications 8

3.0 EVALUATIONS BASED ON QUASI-STATIC LOADING 10

3.1 LED positioning and drop-out 10

3.1.1 LED positioning: 11

3.1.2 LED signal drop-out assessment tests: 13

3.1.3 Mid-Sternum compression tests: 17

3.1.3.1 Round indenter loading: 17

3.1.3.2 Plate indenter loading: 19

3.1.4 Left side offset tests: 27

3.1.5 Diagonal belt loading tests: 30

3.2 Accuracy assessment 33

3.2.1 Sternum-mounted LED tests: 34

3.2.2 Rib-mounted LED tests: 36

3.2.3 Rib-mounted LED tests with rotated chest: 43

3.2.4 Indenter-mounted LED tests: 45

4.0 EVALUATIONS BASED ON DYNAMIC LOADING 49

4.1 Pendulum Tests 50

4.2 Full-scale vehicle frontal offset pole test 58

5.0 OTHER CONSIDERATIONS 64

6.0 SUMMARY 64

7.0 NOMENCLATURE 66

8.0 Bibliography 67

TABLE OF FIGURES

Figure 1: RibEye system showing the LEDs (A), two sensor heads located on either side of the dummy thoracic spine (B), interface box (C and E), dummy thoracic spine box (D), and LED connector block (F). 4

Figure 2: RibEye system components showing the controller (A), sensor heads (B), interface box (C), and LED connector block (D). 4

Figure 3: RibEye system shown installed in the 50th percentile male Hybrid III dummy. The photo shows an LED fixed to right sixth rib (A), sensors (B). The standard Hybrid III sternum displacement slider arm (C), dummy thoracic spine box (D), and internal chest potentiometer assembly (E) are also shown....5

Figure 4: The top illustration shows the LED case design: flat back LED (A), 20-deg angled back LED (B), and 35-deg angled back LED (C). The bottom illustration shows the 35-deg angled back LED (A) and the sternum mounting plate (B)....5

Figure 5: Hybrid III dummy chest showing the sternum assembly (A), sternum mounting plate (B), upper right and left sternum LEDs (C and D). 6

Figure 6: Inferior view of the sternum-mounted LED: sternum mounting plate (A), lower right and left sternum LEDs (B and C), and upper sternum LED (D). 6

Figure 7: RibEye use interface 7

Figure 8: The specified range LED x-y positions for the Hybrid III dummy. 9

Figure 9: The specified range LED x-z positions for the Hybrid III dummy. 9

Figure 10: RibEye system showing LED positions on the sternum and at 6, 8, 9, 10, 11, and 13 cm along the rib path measured from the midsternum on the right side. The two light receiving sensors on either side of the spine box is illustrated. 10

Figure 11: Photograph of the test setup showing the dummy chest secured on an "x-y" cross table (C). A is the indenter attached to the piston of the eclectro-hydraulic testing device, and B is the left side fourth rib of the dummy. 11

Figure 12: Photograph showing the LED fixation method at the 9 cm position. An LED is attached to the left fourth rib (A). The slide arm of the internal chest potentiometer is shown (B). 12

Figure 13: Photograph showing the procedure used to measure the LED position along the curvilinear path of the rib. A: sternum midline, and B: cable tie for left sixth rib at 9 cm position from the midline....12

Figure 14: Schematic showing the cross section of a rib before loading and the positioning of LEDs at 6 and 11 cm on the right, and 9 cm on the left side. The deformed contour of the rib is shown in dashed lines. Both sensors can capture the light emitted by the LED positioned at 9 cm. In contrast, the positioning of the LED at the 6 and 11 cm locations may result is less than optimal light for the sensor(s), resulting in signal drop-out. 13

Figure 15: Deflection along the x-direction of the right fourth rib LED positioned at 6 cm. While the indenter continues to compress the chest, drop out occurs in the LED signal. The shape of the drop-out pulse is similar regardless of the positioning of the LED. 14

Figure 16: Deflections along the y-direction of the right and left fourth rib LEDs positioned at 6 cm. The drop-out occurs in both LEDs. The polarity reversal between the left and rib LEDs are discussed in the text. The shape of the drop-out pulse between the left and right LED is similar regardless of the positioning of the LED. 15

Figure 17: Plot showing drop-out from the lower sternum LED on the right side (deflection shown is along the x-direction) due to light interference from the presence of the slider arm of the internal chest potentiometer. Displacement data from the potentiometer is included. Data corresponds to 3-in chest compression test. 17

Figure 18: Photograph showing the test system with the wooden indenter (A) and LEDs positioned on the left sixth rib (C) at 11 cm. The dummy rights ribs are identified (B). 18

Figure 19: LED configurations in sternum-mounted evaluation tests. Note the placement of the four LEDs at the corners of the sternum plate on the dummy. The remaining eight LEDs are placed on both sides of ribs two through five. 18

Figure 20: Photograph showing the test system with the aluminum indenter (A) and LEDs positioned at 8 cm on the right 2-5 ribs (C). The PMMA leveler is identified (B).....19

Figure 21: Plot showing the peak chest compression before drop-out from LEDs positioned at locations shown on the x-axis. The 9 cm positioned LED did not have any drop-out and hence the maximum displacement achieved by the indenter was recorded. The sternum compression before drop-out exceeded the IARV of 63 mm in LEDs positioned at 10, 9, and 8 cm and sternum. Note the decreasing peak deflections before drop-out as LED positioning moves away from the 9 cm position. 20

Figure 22: Deflections of the left and right fifth and sixth ribs from LEDs positioned 13 cm along with the chest potentiometer and indenter displacements. Data corresponds to the 1-in chest compression test.....23

Figure 23: Deflections of the left and right fifth and sixth ribs from LEDs positioned 13 cm along with the chest potentiometer and indenter displacements. Data corresponds to the 2-in chest compression test.....23

Figure 24: Deflections of the left and right fifth and sixth ribs from LEDs positioned 13 cm along with the chest potentiometer and indenter displacements. Data corresponds to the 3-in chest compression test.....24

Figure 25: Deflections of the left and right fifth and sixth ribs from LEDs positioned 9 cm along with indenter displacements. Data corresponds to the 1-in chest compression test.....24

Figure 26: Deflections of the left and right fifth and sixth ribs from LEDs positioned 9 cm along with indenter displacements. Data corresponds to the 2-in chest compression test.....25

Figure 27: Deflections of the left and right fifth and sixth ribs from LEDs positioned 9 cm along with indenter displacements. Data corresponds to the 3-in chest compression test.....25

Figure 28: Deflections of the left and right fifth and sixth ribs from LEDs positioned 6 cm along with indenter displacements. Data corresponds to the 1-in chest compression test.....26

Figure 29: Deflections of the left and right fifth and sixth ribs from LEDs positioned 6 cm along with indenter displacements. Data corresponds to the 2-in chest compression test.....26

Figure 30: Deflections of the left and right fifth and sixth ribs from LEDs positioned 6 cm along with indenter displacements. Data corresponds to the 3-in chest compression test.....27

Figure 31: The test configuration for left side offset loading. A: Aluminum plate, B: frontend stiffener plate, and C: LED mounted to the left sixth rib at the 6 cm position. 28

Figure 32: LED configurations at 9 cm used in left offset loading evaluation tests. Dashed rectangle shows the outline of the aluminum indenter.....28

Figure 33: Deflections along the x-direction of ribs one and two as recorded by the LEDs positioned at 13 cm. Data corresponding to the 2.5-in chest compression test is shown. 29

Figure 34: Deflections along the x-direction of ribs one and two as recorded by the LEDs positioned at 9 cm. Data corresponding to the 2.5-in chest compression test is shown. Note no drop-outs. 29

Figure 35: Deflections along the x-direction of ribs one and two as recorded by the LEDs positioned at 6 cm. Data corresponding to the 2.5-in chest compression test is shown. 30

Figure 36: Test configuration for diagonal belt loading. A: Metal plate, B: LED mounted to the right sixth rib at the 9 cm position. 31

Figure 37: Deflections along the x-direction of ribs one and two as recorded by the LEDs positioned at 9 cm. Data corresponding to the 3-in diagonal belt loading compression test is shown. 31

Figure 38: Deflections along the x-direction of ribs three and four as recorded by the LEDs positioned at 9 cm. Data corresponding to the 3-in diagonal belt loading compression test is shown. 32

Figure 39: Deflections along the x-direction of ribs five and six as recorded by the LEDs positioned at 9 cm. Data corresponding to the 3-in diagonal belt loading compression test is shown. 32

Figure 40: Test configuration for sternum-mounted loading. A: Offset for the trigger system, B: the Aluminum plate indenter, and C: PMMA leveler. 34

Figure 41: LED configurations used in sternum-mounted loading tests. Dashed rectangle shows the outline of the indenter. 34

Figure 42: Deflections along the x-direction from sternum LEDs positioned at the four corners. Indenter and internal chest potentiometer data are also shown. 37

Figure 43: Comparison of deflection-time records from the chest potentiometer, indenter, and sternum LEDs. Data were averaged from LEDs positioned at the four corners of the sternum. 37

Figure 44: Deflections along the x-direction from sternum LEDs positioned at the four corners. Indenter and internal chest potentiometer data are also shown. 38

Figure 45: Comparison of deflection-time records from the chest potentiometer, indenter, and sternum LEDs. Data were averaged from LEDs positioned at the four corners of the sternum. 38

Figure 46: Test configuration for rib-mounted loading. A: indenter load cell, B: indenter, C: LED at right frontend stiffener plate at the fourth rib. 39

Figure 47: LED configurations used in rib-mounted LED tests. Dashed circle shows the outline of the indenter. 39

Figure 48: Deflection-time records from the LED positioned at the right fourth rib and indenter. 40

Figure 49: Test configuration for rib-mounted loading. A: indenter, B: right third rib. 41

Figure 50: LED configurations used in rib-mounted LED tests. Dashed circle shows the outline of the indenter centered at the interspace between ribs three and four. 42

Figure 51: Comparison of deflection data along the x-direction from LEDs positioned at the right 2-3 and 3-4 interspaces. Indenter displacements are also shown. 42

Figure 52: Photograph showing the setup for thorax rotated loading tests. A: indenter and B; right fourth rib. ..43

Figure 53: Schematic showing the setup for thorax rotated loading tests. Only one LED is shown in the illustration. 44

Figure 54: Comparison of deflection data along the vertical direction from the right fourth rib and indenter in rotated thorax tests. 44

Figure 55: Comparison of deflection data along the vertical direction from the right fourth rib and indenter in rotated thorax tests. 45

Figure 56: Schematic of the test with sternum modification with the indenter attached to the testing device. 46

Figure 57: Photograph of the setup used in indenter-mounted LED tests. Left: A: indenter extension, B: sternum modification, C: left 3-4 interspace, and D: RIbEye sensor head. Right: A: indenter extension, B and C: left third and fourth ribs, and D: sternum 47

Figure 58: Photograph of the setup used in indenter-mounted LED tests. Left: A: indenter extension, B: left third rib, C: left fourth rib, D: LED being evaluated, and E: LED on the fourth rib. Right: A: indenter extension, B: LED being evaluated. 47

Figure 59: Configuration for left third rib accuracy evaluation. 47

Figure 60: Configuration for right sixth rib accuracy evaluation. 48

Figure 61: Comparison of displacements from the indenter and LED mounted to the extension arm of the indenter for assessing the accuracy of an LED attached to the arm. The LED was positioned under the left third rib. 48

Figure 62: Comparison of displacements from the indenter and LED mounted to the extension arm of the indenter for assessing the accuracy of an LED attached to the arm. The LED was positioned under the right sixth rib. 49

Figure 63: LED configuration for dynamic test procedures. 49

Figure 64: Hybrid III dummy set-up for neutral position pendulum testing according to CFR § 572.34 51

Figure 65: Comparison of deflections in the x-direction from the internal chest potentiometer and LED positioned at 9 cm on ribs one and two during 6.6 m/s pendulum test. 51

Figure 66: Comparison of deflections in the x-direction from the internal chest potentiometer and LED positioned at 9 cm on ribs three and four during 6.6 m/s pendulum test. 52

Figure 67: Comparison of deflections in the x-direction from the internal chest potentiometer and LEDs positioned at 9 cm on ribs five and six during 6.6 m/s pendulum test. Drop-out occurred in three LEDs. 52

Figure 68: Deflections in the y-direction from LEDs positioned at 9 cm on all ribs during 6.6 m/s pendulum test. Drop-out occurred in three LEDs. 53

Figure 69: Deflections in the x-direction from LEDs positioned at 9 cm on ribs one and two during 6.6 m/s pendulum test.....53

Figure 70: Deflections in the x-direction from LEDs positioned at 9 cm on ribs three and four during 6.6 m/s pendulum test.....54

Figure 71: Deflections in the x-direction from LEDs positioned at 9 cm on ribs five and six during 6.6 m/s pendulum test.....54

Figure 72: Deflections in the y-direction from LEDs positioned at 9 cm on all ribs during 6.6 m/s pendulum test. 55

Figure 73: Deflections in the x-direction from LEDs positioned at 9 cm on ribs one and two during 4.8 m/s oblique pendulum test.....56

Figure 74: Deflections in the x-direction from LEDs positioned at 9 cm on ribs three and four during 4.8 m/s oblique pendulum test.....57

Figure 75: Deflections in the x-direction from LEDs positioned at 9 cm on ribs five and six during 4.8 m/s oblique pendulum test.....57

Figure 76: Deflections in the y-direction from LEDs positioned at 9 cm in all ribs during 4.8 m/s oblique pendulum test.....58

Figure 77: Photograph of pre-test position of Hybrid III/RibEye dummy in offset frontal crash test.....59

Figure 78: Deflections in the x-direction from LEDs mounted to ribs one and two as recorded by the LEDs positioned at 9 cm, during offset frontal pole test. Note that drop-outs occurred in left rib one at 175 and 220 ms. .60

Figure 79: Deflections in the x-direction from LEDs mounted to ribs three and four as recorded by the LEDs positioned at 9 cm, during offset frontal pole test. 60

Figure 80: Deflections in the x-direction from LEDs mounted to ribs five and six as recorded by the LEDs positioned at 9 cm, during offset frontal pole test. 61

Figure 81: Deflections in the y-direction from LEDs positioned at 9 cm on left ribs during frontal offset pole test. Note that drop-outs occurred in left rib one at 175ms and 220 ms.....61

Figure 82: Deflections in the y-direction from LEDs positioned at 9 cm on right ribs during frontal offset pole test. 62

Figure 83: Peak rib deflections (x direction) in left frontal offset crash test. Rib numbers are shown in the center. 63

Figure 84: Peak rib deflections (y direction) in left frontal offset crash test. Rib numbers are shown in the center. All deflections are positive, i.e., toward the right.....63

LIST OF TABLES

Table 1: RibEye accuracy with z-axis deflections (according to the manual) 8
Table 2: Power requirements based on the manual 8
Table 3: RibEye data demonstrating drop-out 16
Table 4: Number of LEDs deflecting out of sensor field (drop-outs) under central sternum loading 20
Table 5: Number of LEDs deflecting out of sensor field in left offset loading 29
Table 6: Number of LEDs deflecting out of sensor field with belt-type loading 32
Table 7: Accuracy description of tests 33
Table 8: Summary of data for accuracy evaluation 35
Table 9: Summary of data for accuracy evaluation (wrt: with respect to) 36
Table 10: Comparison of rib-mounted LED displacements 40
Table 11: Comparison of interspace LED displacements 41
Table 12: Right rib 4 LED deflections compared to indenter displacement in rotated thorax tests 43
Table 13: Summary of data 46
Table 14: Summary of pendulum test data 56
Table 15: Summary of peak deflections from frontal offset test 59

1.0 BACKGROUND

Hybrid III dummy is an anthropomorphic test device (ATD) used in crashworthiness assessments including the frontal impact Federal Motor Vehicle Safety Standard (FMVSS) No. 208 [3]. This dummy was developed in the 1970s through a contract between the National Highway Safety Administration (NHTSA) of the US Department of Transportation and General Motors [4]. From an instrumentation perspective, the dummy houses a triaxial accelerometer at the center of gravity of the head to determine the head injury criterion, a triaxial load cell on the upper neck to compute the neck injury criterion, uniaxial load cell at the center of the upper legs to record the compressive force on the femur, a triaxial accelerometer on the spine to record the chest acceleration, and an internal deflection potentiometer to measure the ribcage deflection.

The thorax body region in the dummy consists of a welded steel spine and rib cage covered by a removable chest jacket. The dorsal spine serves as an attachment to the neck and collar bone superiorly, ribcage anteriorly, and the molded poly-acrylate elastomer lumbar spine inferiorly. The six steel ribs are posteriorly attached to the thoracic spine and bonded to the internal surface by a poly-viscous material to ensure appropriate dynamic response. The urethane bib attached to the anterior surface of the ribcage distributes frontal impact loads, the intended primary dummy application. The sternum, made of Delrin material, has aluminum backing. The internal rotary deflection potentiometer attached to the top of a bracket behind the sternum extends over the lumbar spine, and a rod extends from the transducer to the sternum to provide input to the potentiometer. The potentiometer measures the compression of the sternum towards the spine, and the design of the dummy is such that the chest can be deflected up to 90 mm. The injury assessment reference value (IARV) for the chest deflection criterion for the 50^{th} percentile male dummy falls within this limit [10]. The measurement is made at the middle of the sternum, i.e., one location in the chest of the dummy.

The chest force-deflection responses are applicable to blunt frontal impacts and are based on tests to the mid-sternum impacts using a 23.4 kg pendulum at velocities of 4.3 and 6.7 m/s [7,8,12]. As described, the peak chest deflection is obtained from the potentiometer measuring the longitudinal displacement (along the x-axis, antero-posterior direction) of the sternum with

respect to the thoracic spine, and the force is recorded from a load cell attached to the pendulum impactor. Data are gathered and processed according to the Society of Automotive Engineers SAE J211 specifications [1].

With increasing awareness for safety in vehicular environments and technological advancements such as dual stage frontal air bags and pre-tensioners and load limiters in belt restraints, measuring chest deflection at multiple points facilitates an assessment of non-uniform, asymmetric thorax loading. Occupant out-of-position may also contribute to the asymmetrical chest deformations even in pure frontal impacts. NHTSA developed an dedicated instrument for such deformation measurements [5]. The device, commonly termed as chestband, is a noninvasive high carbon steel alloy strip with strain gauges bonded at 59 locations, and is placed on the external periphery of the human surrogate. Strain signals are processed using NHTSA-developed software to obtain temporal deformation contours of the chest, from which peak deflections are determined. Deflections at multiple levels have been obtained using more than one chestband. As the instrument is not fixed to a specific ribcage/sternum component, deflections can be captured along with its location. This instrument has been used to compare chest deflections in frontal impacts with different restraint systems: three-point belt, only lap belt, only air bag, and air bag and three-point belted using post mortem human surrogates and the Hybrid III dummy [14,15]. Differences in chest deflection patterns between the dummy and post mortem human surrogates have been reported [15]. Mechanisms of injury in frontal impact under different restraint systems have been derived using chest deformation patterns [13]. In an analysis of thoracic trauma from restrained occupants in frontal impact, it has been shown that peak chest deflections do not always occur at the center of the chest (location of the internal potentiometer in the Hybrid III dummy), and furthermore, the metric is dependent on the type of restraint; air bag and/or belt [11]. As thoracic injury is correlated to peak chest deflections, it would be an improvement to determine the global maximum deflection under any restraint condition for crashworthiness applications. Because the existing potentiometer in this dummy is specific to the sternum, it does not necessarily capture peak deflections that may occur at other locations within the ribcage. Therefore, more advanced instrumentation techniques have been developed.

While the chestband is an effective instrument to measure chest deflections, as it is externally wrapped to the chest, computed deflections include the deformation of the skin/flesh and rib cage. To obtain the actual rib deflections, considered to be a more appropriate injury predictor than the total deflection, researchers have accounted for the skin/flesh thickness by subtracting 10 mm from the total deflections [9]. Recently, an optically-based instrument, termed RibEye, has been developed by Robert A. Denton, Inc., to measure internal chest deflection of devices such as the Hybrid III dummy [6]. This report describes results from tests conducted to evaluate the RibEye system incorporated in the 50th percentile Hybrid III dummy. Test protocols and results follow a brief description of the RibEye system.

2.0 RIBEYE SYSTEM

The underlying concept is that an optically-based system, being not affixed to a specific mechanical linkage such as the internal chest potentiometer connecting the spine and sternum, can enhance the number of deflection measurements. Briefly, the RibEye system is comprised of up to 12 light emitting diodes (LEDs) mounted to the ribs of the dummy internally, two incident light detectors (sensors) that receive light from the LEDs, a controller, and an interface box (Figures 1-7). The current version of the system is capable of obtaining deflection data along the x- and y-directions, fore-aft and side to side. The sensors are mounted laterally to each side of the thoracic spine of the dummy, and the controller is located within the spine box at its uppermost location. LEDs connect to the controller via a block mounted superior to the sensor heads. The interface box can be secured in the trunk of the test vehicle.

LEDs can be mounted at various positions on the inside surface of the ribs or sternum and secured by attaching nylon zip-ties. The default LED locations are placed one on each rib on either side. However, the RibEye allows the user to override the default condition and position multiple LEDs on the same rib or sternum as long as proper z-axis location is maintained. All LEDs are connected via a cable to the dedicated data acquisition system housed within the thoracic spine of the dummy.

Figure 1: RibEye system showing the LEDs (A), two sensor heads located on either side of the dummy thoracic spine (B), interface box (C and E), dummy thoracic spine box (D), and LED connector block (F).

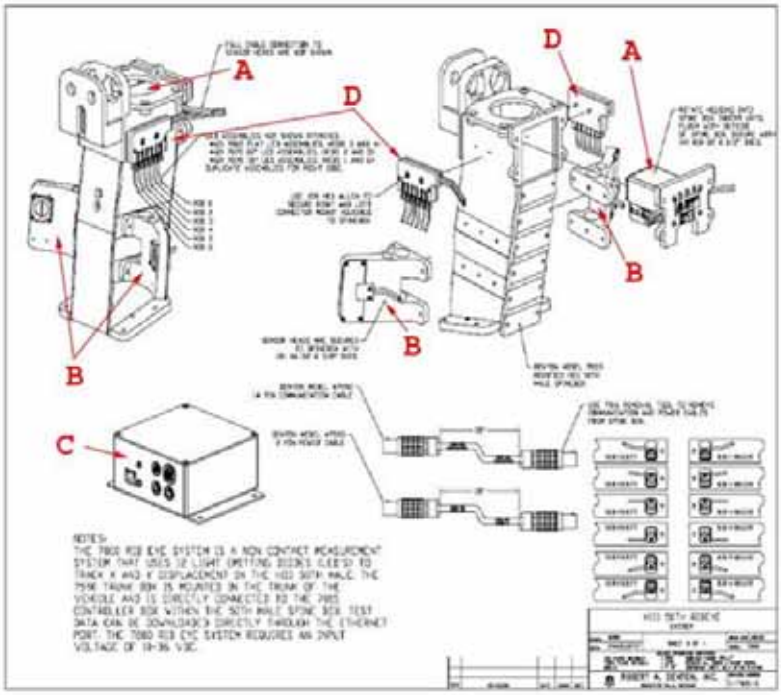

Figure 2: RibEye system components showing the controller (A), sensor heads (B), interface box (C), and LED connector block (D).

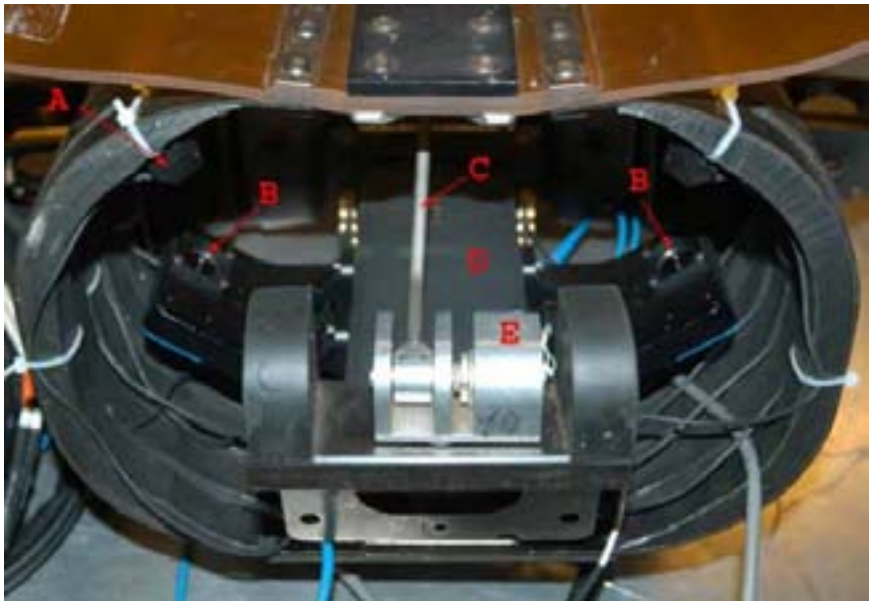

Figure 3: RibEye system shown installed in the 50th percentile male Hybrid III dummy. The photo shows an LED fixed to right sixth rib (A), sensors (B). The standard Hybrid III sternum displacement slider arm (C), dummy thoracic spine box (D), and internal chest potentiometer assembly (E) are also shown.

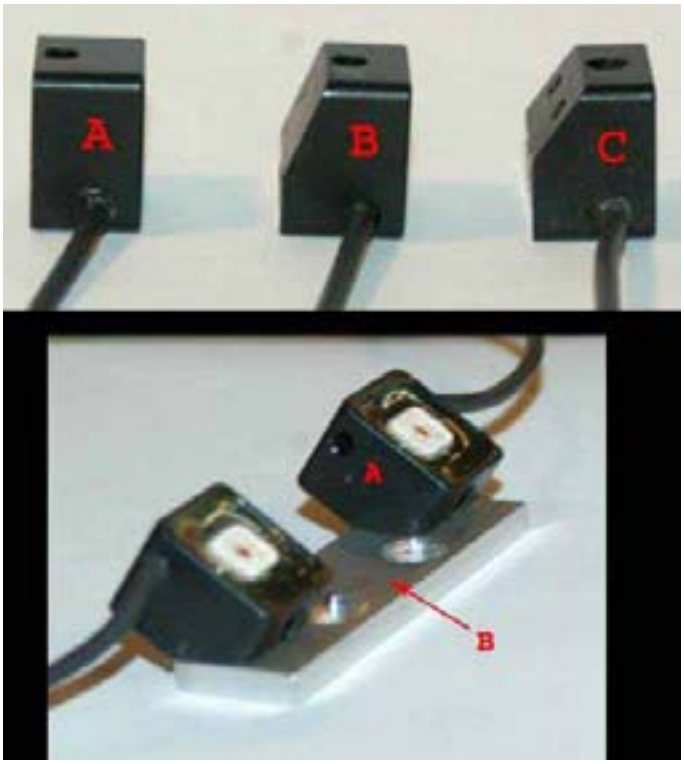

Figure 4: The top illustration shows the LED case design: flat back LED (A), 20-deg angled back LED (B), and 35-deg angled back LED (C). The bottom illustration shows the 35-deg angled back LED (A) and the sternum mounting plate (B).

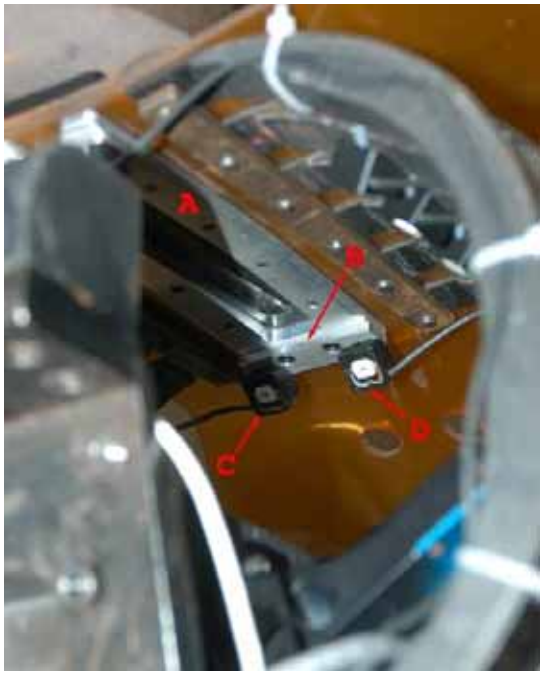

Figure 5: Hybrid III dummy chest showing the sternum assembly (A), sternum mounting plate (B), upper right and left sternum LEDs (C and D).

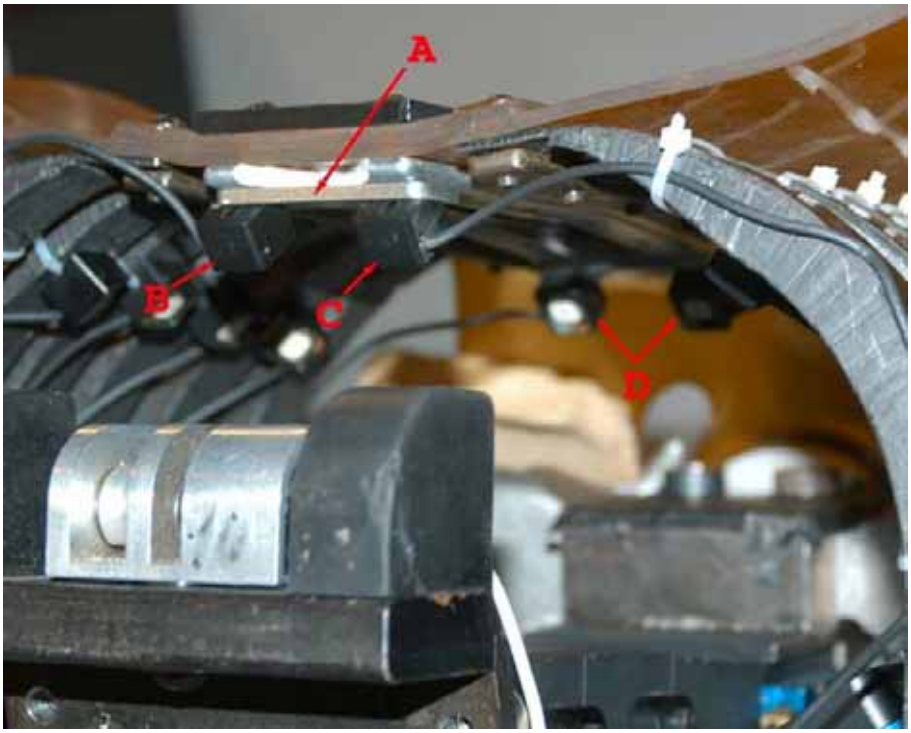

Figure 6: Inferior view of the sternum-mounted LED: sternum mounting plate (A), lower right and left sternum LEDs (B and C), and upper sternum LED (D).

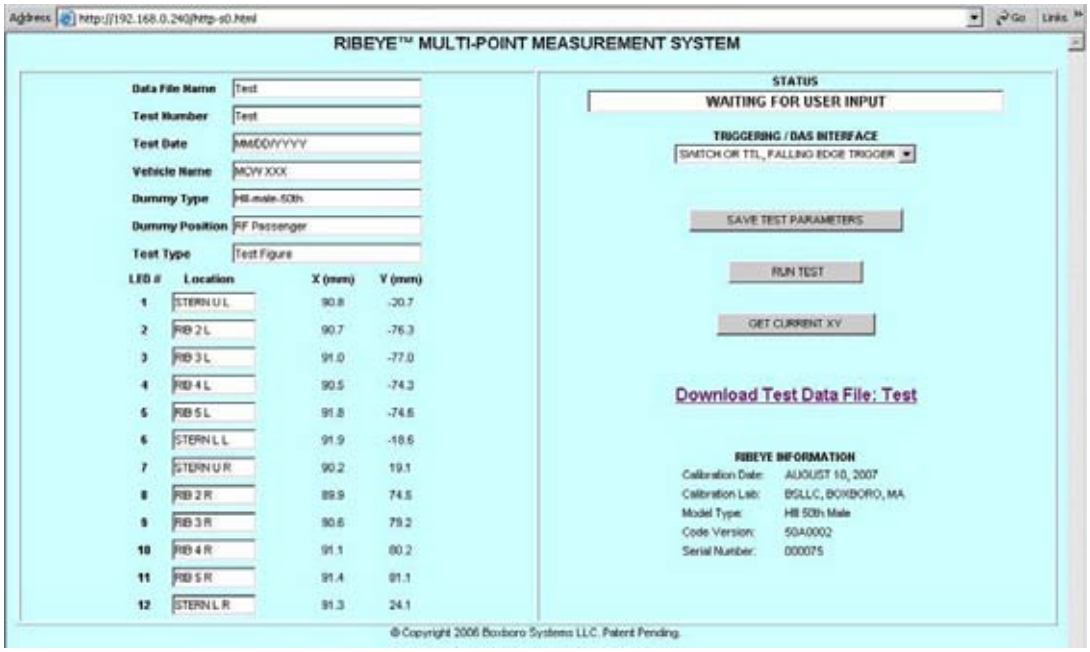

Figure 7: RibEye use interface.

The user indicates the position of the LED in the "Location" field of the user-interface. Three LED case designs exist: with different back angles that direct light toward the RibEye sensors (Figure 4). The flat back LEDs are designed for positioning on ribs three and four, the 20-deg angled back LEDs are designed for positioning on ribs two and five, and the 35-deg angled back LEDs are designed for positioning on ribs one and six. Optionally, the 35-degree angled back LEDs may be positioned on the upper and lower sternum using the mounting plates (Figures 5-7).

During testing each LED is powered sequentially and sampled at 10,000 Hz, while two sensors detect the angle of the LED with respect to frontal (xy) and lateral (xz) planes. The resulting digital data are stored in memory. This constitutes the "raw data" from the RibEye system. These data are then corrected for ambient light conditions and adjusted using calibration curves housed within the software of the data acquisition system. In other words, the light intensity data collected based on the incident angle is converted by an embedded microprocessor using optical triangulation techniques to compute deflection records at each LED position. These processed data are then stored in the RibEye flash memory. Data are downloaded to an external computer and saved as a text file using the RibEye interface within a web browser (Figure 7). Thus, it is possible to obtain antero-posterior (x) and lateral (y) coordinates of deflection of the rib or sternum at the positioned LED location during loading. Using 12 sensors, deflections can

be determined at 12 locations. The system also allows the user to download the "raw data" using the provided Hyperterminal software subsequent to each test. However, processing of this "raw data" to provide LED deflections can be only be done by the manufacturer, Robert A. Denton, Inc.

2.1 RibEye specifications

The following RibEye multi-point deflection measurement system specifications were extracted from the User's Manual. The measurement ranges in the x-y and x-z planes are demonstrated in Figures 8-9. For Figures 8 and 9, the x=0, y=0, z=0, i.e., origin, is the midpoint of the line segment connecting the two sensors. With respect to the dummy, this is approximately on the front surface of the spine mount box in the center of the chest. Thus, the absolute location of the midsternum is approximately x=87, y=0, z=0 mm. The system does not account for out-of-plane movements. Thus, any z-axis movement of an LED will produce measurement inaccuracies. Tables 1 and 2 list the accuracy associated with z-direction deflection ranges. The power supply to the system should be 12 to 36 volts DC. Fuse protection is an internal self-resetting polymer fuse in the interface box. RibEye's self-contained data system has a sampling rate of 10,000 Hz per LED and an acquisition time of 90 milliseconds pre-trigger, 910 milliseconds post-trigger (1 second total). All data are collected in RAM and stored post-test in flash memory.

Table 1: RibEye accuracy with z-axis deflections (according to the manual)

z-deflection	x-accuracy	y-accuracy
mm	mm	mm
0	1.0	1.0
± 12.5	1.0	2.0
12.5 to 25.0	2.0	2.0
-12.5 to -25.0	2.0	2.0

Table 2: Power requirements based on the manual

Operating conditions	Interface box (W)	Controller and LEDs (W)	Total (W)
On or idle	3.3	2.0	5.3
Collecting data	3.3	5.0	8.3
Maximum*	3.3	9.0	12.3

*: when all LEDS are out of view of both sensors and are driven to full power

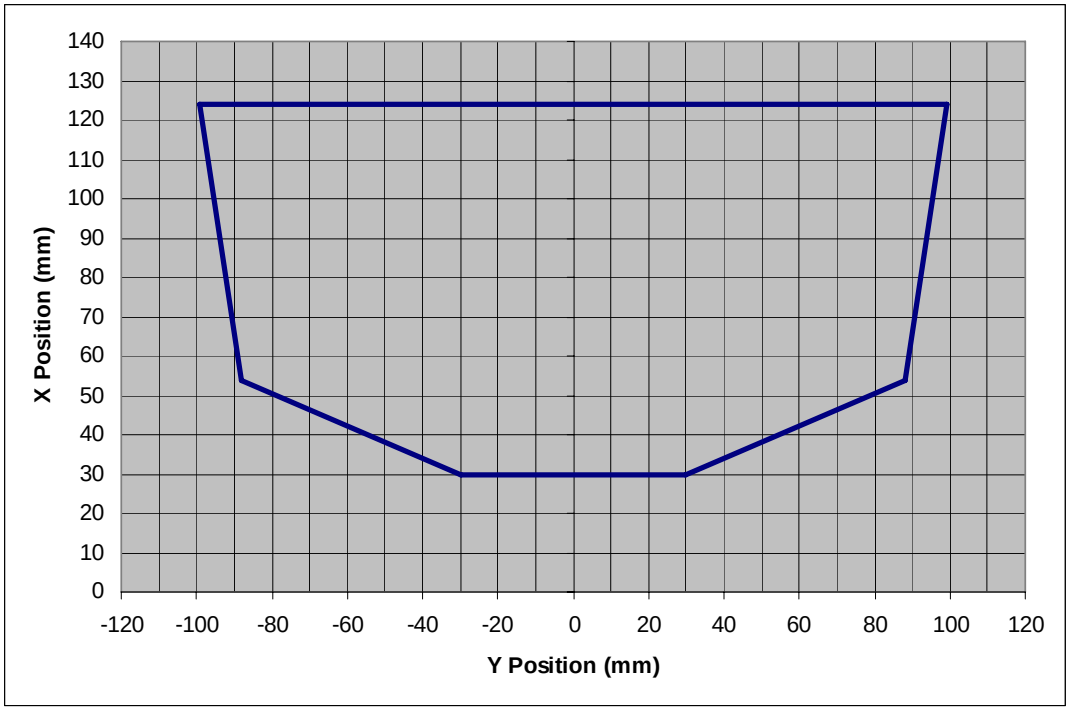

Figure 8: The specified range LED x-y positions for the Hybrid III dummy.

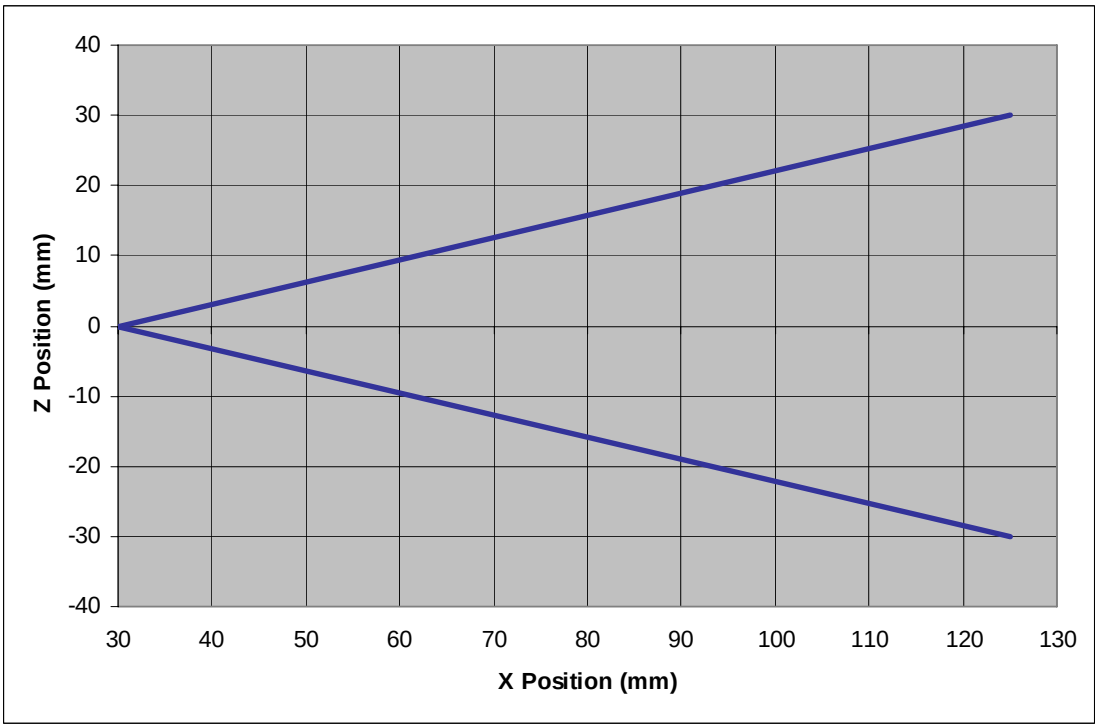

Figure 9: The specified range LED x-z positions for the Hybrid III dummy.

3.0 EVALUATIONS BASED ON QUASI-STATIC LOADING

The evaluation of the RibEye system consisted of quasi-static and dynamic tests using pendulum impacts and full-scale vehicle crash tests. LED positions are referred based on the rib number (one through six) and side (left or right), and the distance (in cm) from the center of the sternum (Figure 10). It should be noted that LED positioning is flexible with possible placements at different locations on the same rib and multiple LEDs on the rib or sternum. A figure is included for each test setup to identify LED positioning, whether on the sternum or rib.

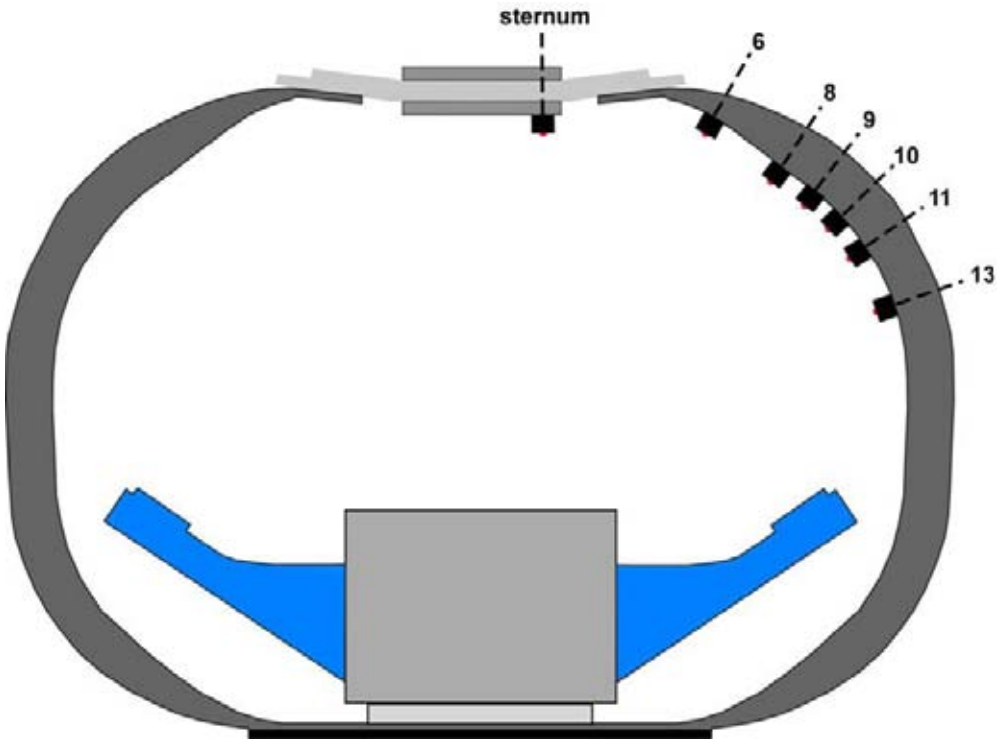

Figure 10: RibEye system showing LED positions on the sternum and at 6, 8, 9, 10, 11, and 13 cm along the rib path measured from the midsternum on the right side. The two light receiving sensors on either side of the spine box is illustrated.

3.1 LED positioning and drop-out

The purpose of the quasi-static tests was to determine the accuracy of RibEye-based deflection measurements under controlled laboratory conditions using an electro-hydraulic testing apparatus and evaluate the overall performance of the system as installed in the 50th percentile Hybrid III dummy. All quasi-static tests were designed such that deflections from the RibEye system were obtained in addition to the input displacement records from the indenter of the electro-hydraulic testing device. The internal potentiometer was used in approximately one-

half of these tests to compare RibEye and sternum deflections. These tests with the internal chest potentiometer determined the effects of interference in the light path for optimum performance.

3.1.1 LED positioning:

The thorax of the dummy was isolated and mounted on an "x-y" cross table secured to the frame of the electro-hydraulic testing device. The lower thorax of the dummy and the table were shimmed such that the RibEye sensor heads attached to the spine box were level with respect to the horizontal and orthogonal to the indenter of the testing device (Figure 11). LEDs were positioned on the inside surface of the ribs using double-sided tape and nylon cable ties (Figure 12). Position measurements were made from the midline of the sternum along the outer surface of the ribs, i.e., following the curvilinear path of the ribcage (Figure 13). The measurement methodology was chosen for its practicality, although it may introduce small variation in LED position.

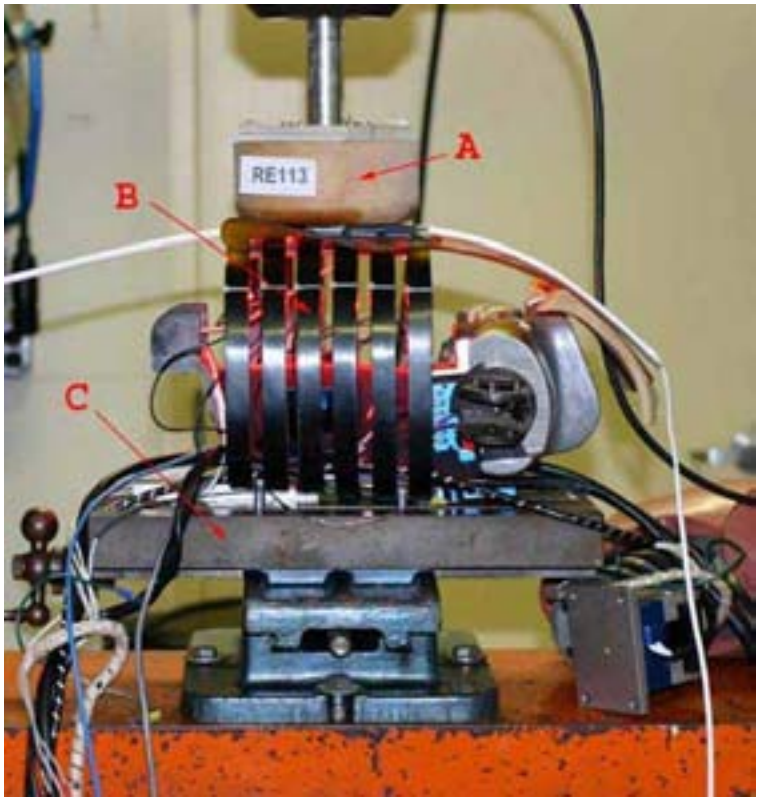

Figure 11: Photograph of the test setup showing the dummy chest secured on an "x-y" cross table (C). A is the indenter attached to the piston of the electro-hydraulic testing device, and B is the left side fourth rib of the dummy.

Figure 12: Photograph showing the LED fixation method at the 9 cm position. An LED is attached to the left fourth rib (A). The slide arm of the internal chest potentiometer is shown (B).

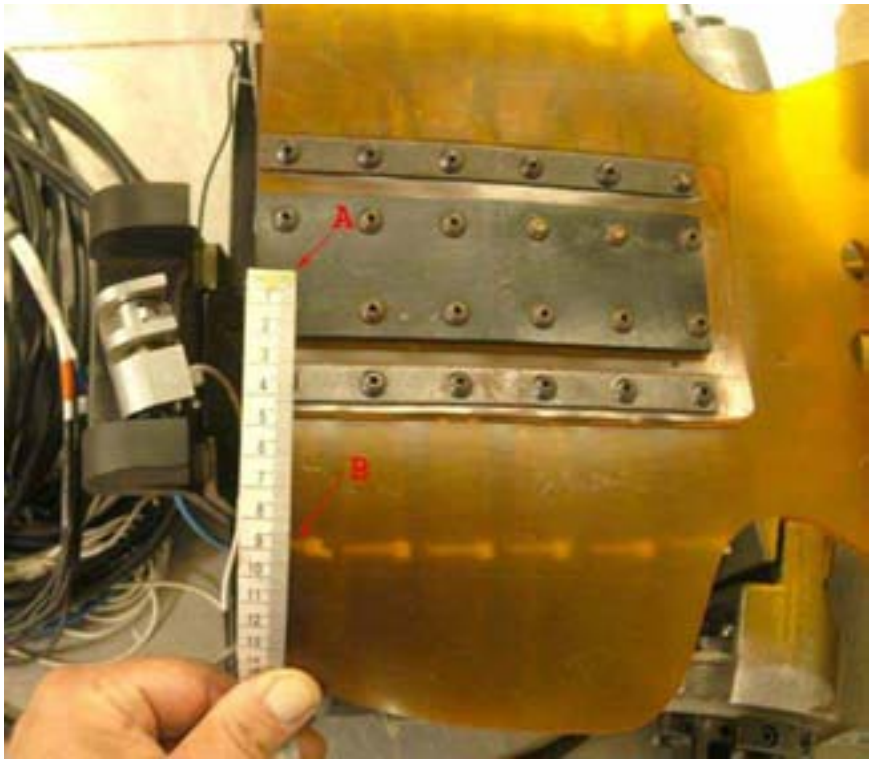

Figure 13: Photograph showing the procedure used to measure the LED position along the curvilinear path of the rib. A: sternum midline, and B: cable tie for left sixth rib at 9 cm position from the midline.

"Shake-down" tests were performed to ensure the stability of the thorax mounted on the "x-y" cross table and satisfactory LED fixation by displacing the actuator of the electro-hydraulic testing device (indenter) in a single cycle compressive haversine waveform at a velocity of 0.15 m/s. All five tests indicated that the testing configuration was stable and deemed to be appropriate for additional experiments, described below.

3.1.2 LED signal drop-out assessment tests:

In order for the RibEye system to optically track the position of the LEDs, there must be sufficient light projected from each LED onto the spine box-mounted sensors. If either or both sensors detect inadequate light intensity, data from that particular LED will be "forced out of range" and the system will not track the LED motion until the light intensity requirement is again satisfied. This light intensity requirement can also be affected by extraneous light such as those resulting from high intensity lighting systems, typically used in crashworthiness studies to capture the overall kinematics. However, the dummy chest jacket use minimizes the extraneous light interference. When the sensors detect inadequate light intensity, signal "drop-out" occurs, resulting in gaps within the RibEye deflection records. A schematic representation of the drop-out phenomena is shown in figure 14.

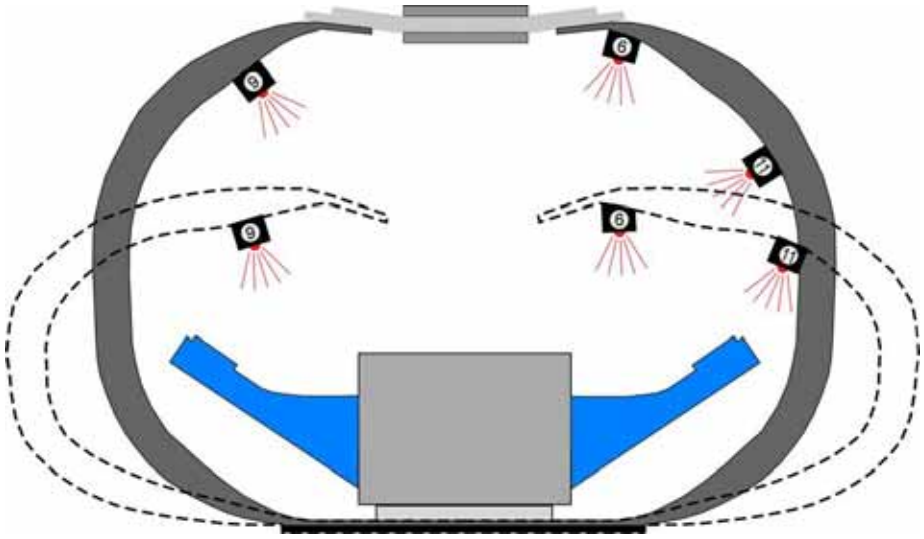

Figure 14: Schematic showing the cross section of a rib before loading and the positioning of LEDs at 6 and 11 cm on the right, and 9 cm on the left side. The deformed contour of the rib is shown in dashed lines. Both sensors can capture the light emitted by the LED positioned at 9 cm. In contrast, the positioning of the LED at the 6 and 11 cm locations may result is less than optimal light for the sensor(s), resulting in signal drop-out.

In the x-direction deflection plot, drop-out appears an instantaneous negative change in the LED displacement followed by a horizontal interval (Figure 15). The displacement magnitude of the horizontal interval indicates the initial absolute position of the LED prior to compression, and any association with the indenter and chest potentiometer traces is coincidental. At the end of the drop-out period, there is an instantaneous positive change in the displacement as normal LED tracking resumes. In the y-direction deflection plot, signal drop-out pattern is similar to the x-direction, but in right-sided LEDs the deviation is negative and in left-sided LEDs it is positive (Figure 16).

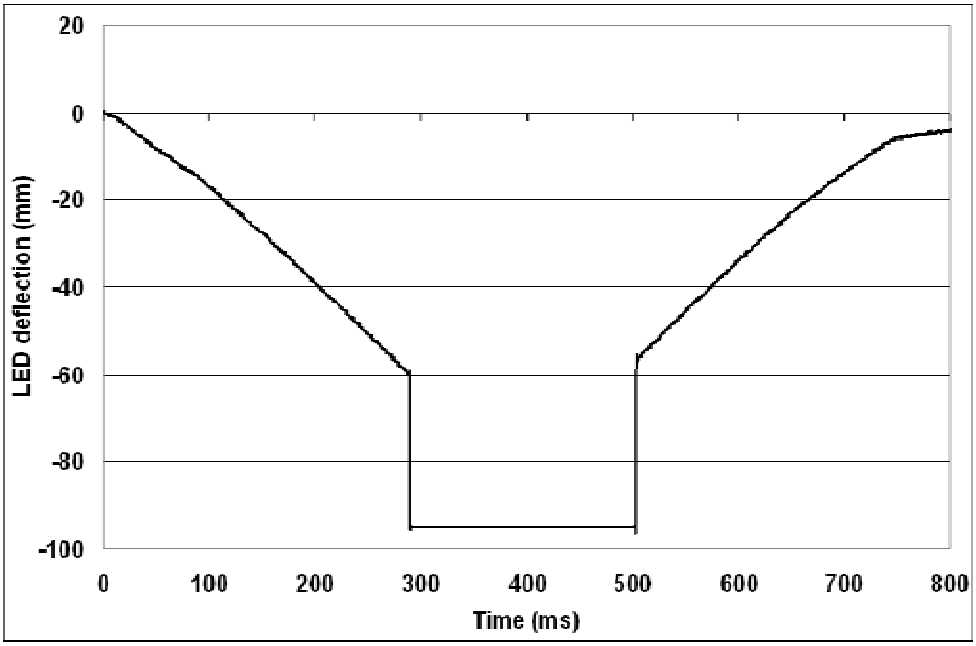

Figure 15: Deflection along the x-direction of the right fourth rib LED positioned at 6 cm. While the indenter continues to compress the chest, drop out occurs in the LED signal. The shape of the drop-out pulse is similar regardless of the positioning of the LED.

Therefore, the graphical appearance of LED signal drop-out is a consequence of the RibEye methodology in data processing under inadequate signal conditions. If inadequate light from a particular LED is provided to the left sensor, all data for that LED during the period of diminished optical signal is assigned an integer value, "1." On the other hand, if inadequate

light is provided to the right sensor, all data for that particular LED is assigned an integer value, "2." However, if inadequate light is provided to both sensors, all data for that LED is assigned an integer value, "3." These values do not appear to be in the "raw data", but is most likely included in the output from the microprocessor which feeds into the flash memory.

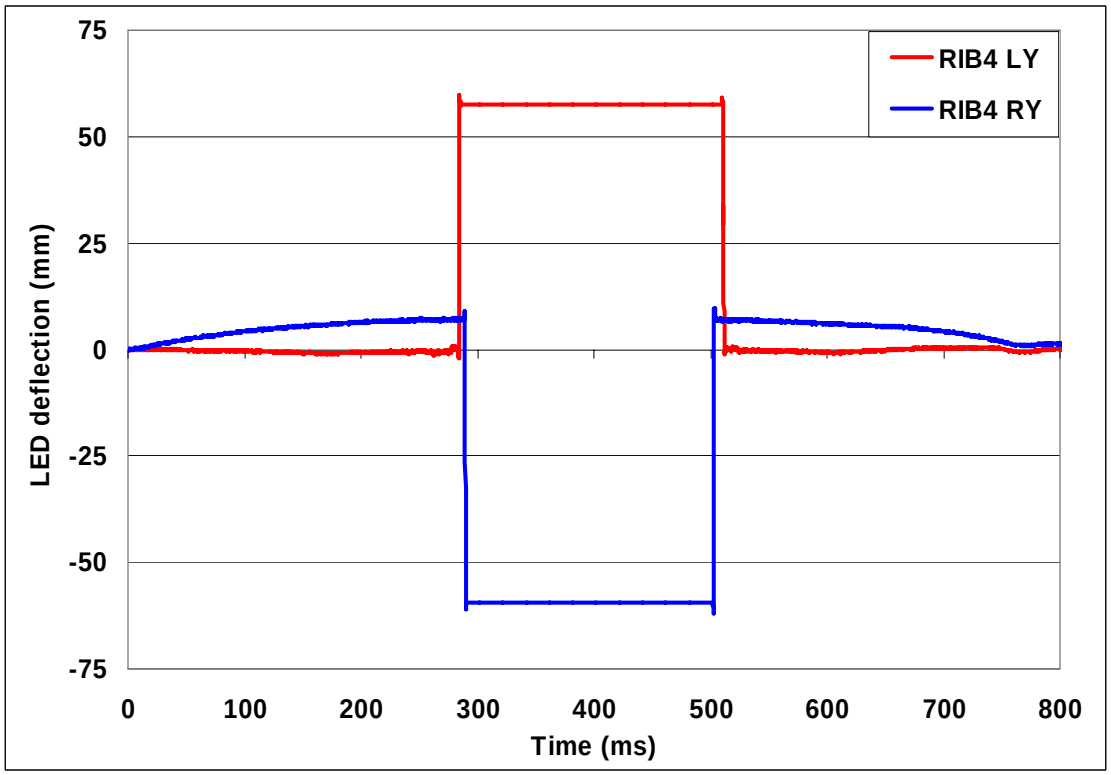

Figure 16: Deflections along the y-direction of the right and left fourth rib LEDs positioned at 6 cm. The drop-out occurs in both LEDs. The polarity reversal between the left and rib LEDs are discussed in the text. The shape of the drop-out pulse between the left and right LED is similar regardless of the positioning of the LED.

Table 3 contains a portion of the text output from the RibEye web interface software. The output provides absolute xy location information for each LED. Note that data demonstrating insufficient light detection by the left sensor from the LED affixed to left rib six (RIB6 LX and RIB6 LY) at 100.3 milliseconds are assigned the integer value, "1". The right sensor detected inadequate light projected from LEDs attached to right ribs one and two during the 99.3 – 100.9 millisecond interval shows the integer value, "2". In this example, at no time were the LED

light signals undetectable by both sensors. In subsequent plots the absolute position data are filtered and converted to relative data such that all sensors begin at zero. In other words, the initial absolute position value is subtracted from all values to establish zero baseline. This process results in converting integer values indicating drop-out to relative deflection magnitudes.

LED signal drop-out may occur from rib or sternum bending that directs the light beam away from the sensor(s), or, obstruction of the beam by another component of the dummy such as the slider arm of the internal chest potentiometer. Signal drop-out secondary to the bending path appears as a horizontal interval symmetric about the center of the indenter trace corresponding to maximal compression. In contrast, signal drop-out due to the slider arm obstruction appears as two shorter intervals. The initial drop-out interval occurs during compression while the second interval occurs symmetrically during release (Figure 17).

Table 3: RibEye data demonstrating drop-out

Time (ms)	RIB5 LX	RIB5 LY	RIB6 LX	RIB6 LY	RIB1 RX	RIB1 RY	RIB2 RX	RIB2 RY
99.3	47.5	-118.6	46.3	-103.8	2	2	2	2
99.4	47.2	-118.5	47.1	-103.2	2	2	2	2
99.5	47.4	-119.0	46.7	-103.0	2	2	2	2
99.6	47.8	-119.2	46.6	-102.6	2	2	2	2
99.7	47.6	-119.2	46.1	-102.4	2	2	2	2
99.8	47.4	-119.3	45.8	-102.6	2	2	2	2
99.9	46.9	-119.4	45.5	-102.0	2	2	2	2
100	47.4	-118.8	46.2	-101.7	2	2	2	2
100.1	47.7	-118.9	45.9	-101.3	2	2	2	2
100.2	47.5	-119.4	46.0	-100.7	2	2	2	2
100.3	47.8	-119.4	1	1	2	2	2	2
100.4	47.0	-120.0	1	1	2	2	2	2
100.5	47.7	-119.0	1	1	2	2	2	2
100.6	47.8	-118.9	1	1	2	2	2	2
100.7	47.1	-119.7	1	1	2	2	2	2
100.8	47.0	-120.1	1	1	2	2	2	2
100.9	46.9	-120.4	1	1	2	2	2	2

Note: “1”: left sensor drop-out; “2”: right sensor drop-out; and “3”: would indicate drop-out from both sensors

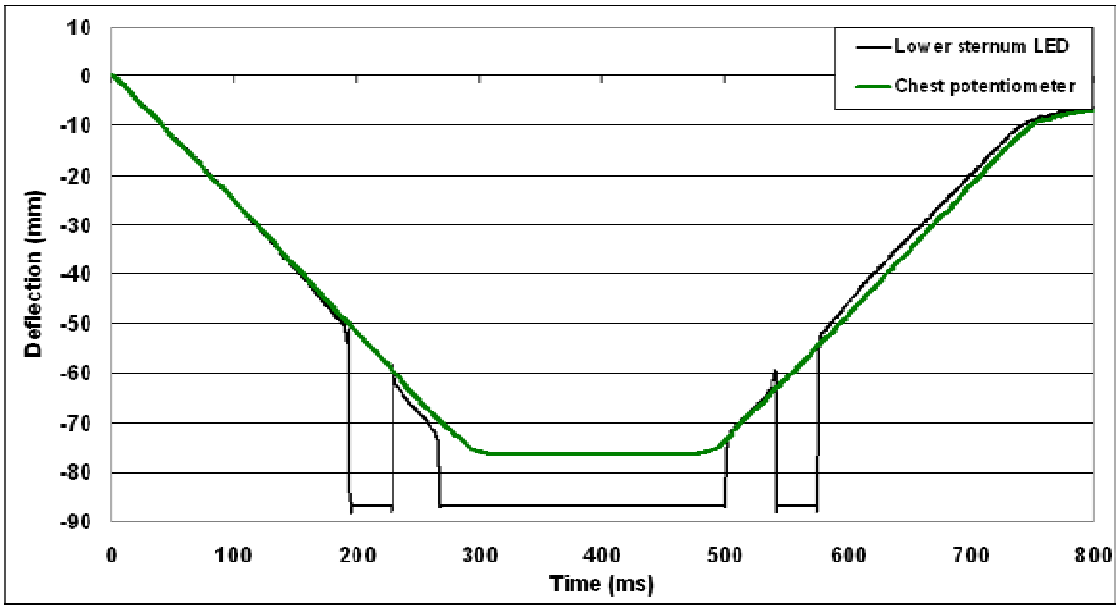

Figure 17: Plot showing drop-out from the lower sternum LED on the right side (deflection shown is along the x-direction) due to light interference from the presence of the slider arm of the internal chest potentiometer. Displacement data from the potentiometer is included. Data corresponds to 3-in chest compression test.

Drop-out assessment tests were conducted using a ramp waveform with a 200 ms hold at maximal compression. Indenter displacements ranged from 1-in to 3-in. Note the maximum sternum deflection specified FMVSS No. 208 is 2.5 inches [2]. Indenter velocities were 0.25 or 0.50 m/s. All tests, except with LEDs at the 11 cm position, were performed with and without the internal chest potentiometer slider arm. RibEye data were separated into individual channels and a CFC600 filter was used according to SAE J211-1 2003 specifications for filtration of thorax deflections.

3.1.3 Mid-Sternum compression tests:

3.1.3.1 Round indenter loading:

A wood cylinder (dia. 15 cm) attached to the actuator of the electro-hydraulic testing device was used to determine the drop-out with varying LED positions and sternum compression parameters. The loading parallels the Hybrid III dummy evaluation criterion. Compression tests were performed with LEDs affixed to ribs one through six bilaterally in each of the following LED configurations: 6, 8, 9, 10, 11, or 13 cm from the sternum midline. The center of the indenter contacted the thorax at mid-sternum (Figures 18 and 19). Results are summarized in Table 4.

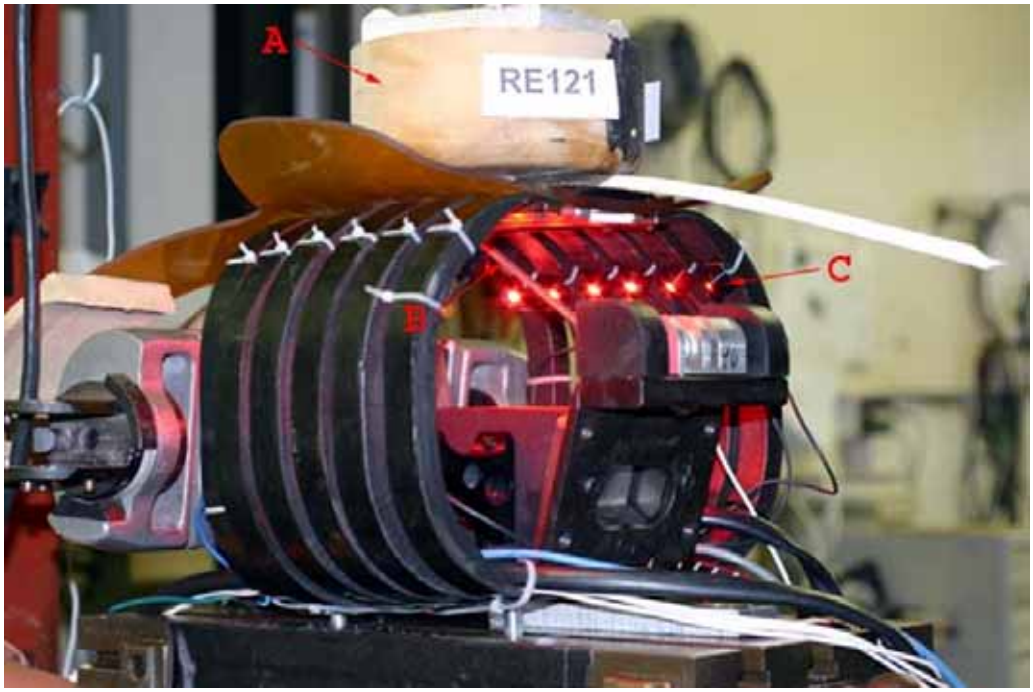

Figure 18: Photograph showing the test system with the wooden indenter (A) and LEDs positioned on the left sixth rib (C) at 11 cm. The dummy rights ribs are identified (B).

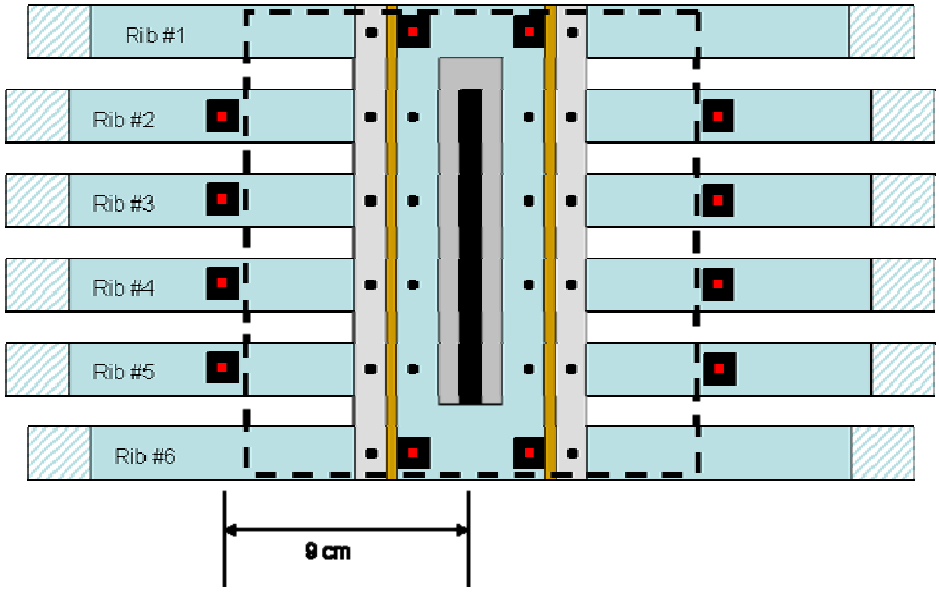

Figure 19: LED configurations in sternum-mounted evaluation tests. Note the placement of the four LEDs at the corners of the sternum plate on the dummy. The remaining eight LEDs are placed on both sides of ribs two through five.

3.1.3.2 Plate indenter loading:

The sternum attachment option was evaluated with four LEDs mounted to the upper and lower corners of the sternum plate via screws. The remaining LEDs were mounted to ribs two through five bilaterally at either 8 or 9 cm from the midline (Figure 20). The RibEye system was compressed using a 15 cm square aluminum plate indenter. A polymethylmethacrylate leveling plate was used to compensate for the convexity of the sternum plate and provide level contact surface (Figure 21).

Seventy-three tests were conducted in this drop-out evaluation series. Table 4 summarizes the LED signal drop-out from the RibEye system. The reported number of LED drop-outs is based on the mean number of drop-outs from tests at two velocities under each condition: with and without the internal chest potentiometer. It was increasingly evident, as testing proceeded, that the indenter velocity was not a factor in LED drop-out. Therefore, the final nine tests in this series were performed at the lower indenter velocity only. The presence of the linkage arm of the internal chest potentiometer appeared to increase the likelihood of interference as the location of LEDs moved away (towards left or right) from the 9 cm position. As expected, increasing the magnitude of the chest compression increased the likelihood of drop-out.

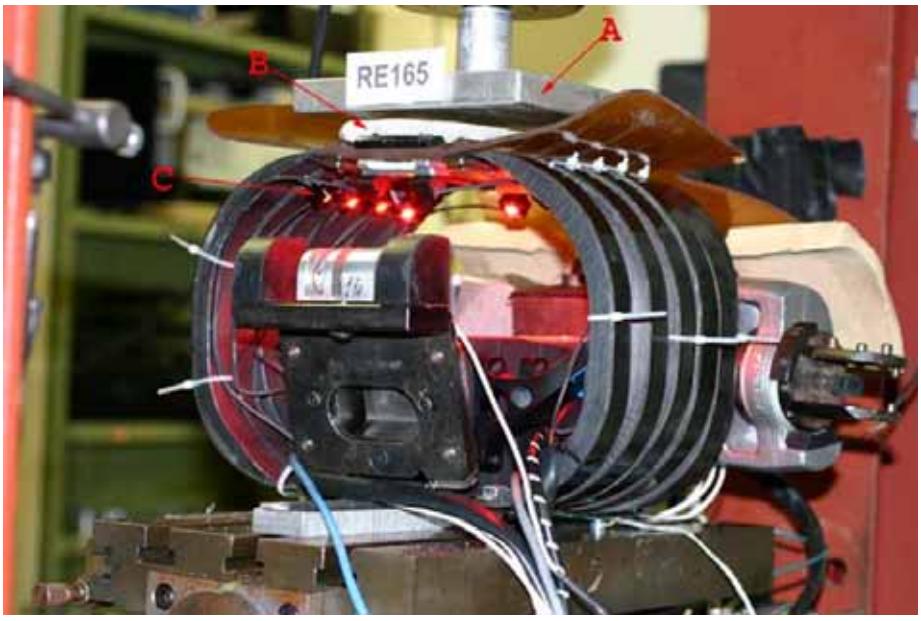

Figure 20: Photograph showing the test system with the aluminum indenter (A) and LEDs positioned at 8 cm on the right 2-5 ribs (C). The PMMA leveler is identified (B).

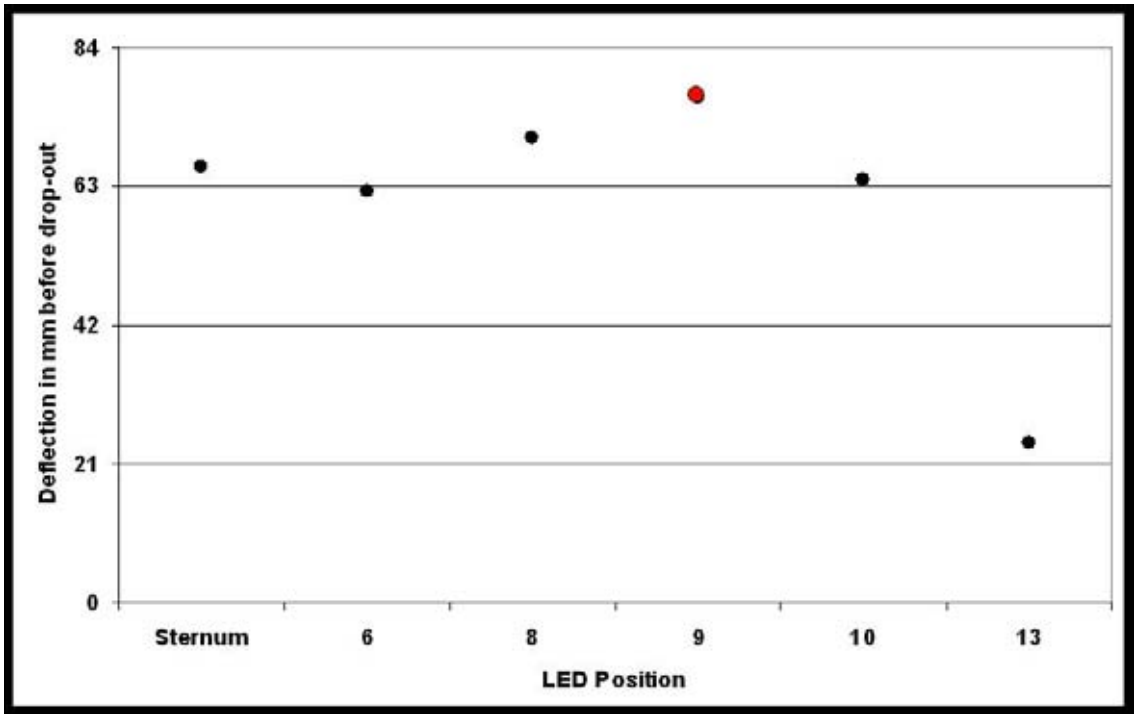

Figure 21: Plot showing the peak chest compression before drop-out from LEDs positioned at locations shown on the x-axis. The 9 cm positioned LED did not have any drop-out and hence the maximum displacement achieved by the indenter was recorded. The sternum compression before drop-out exceeded the IARV of 63 mm in LEDs positioned at 10, 9, and 8 cm and sternum. Note the decreasing peak deflections before drop-out as LED positioning moves away from the 9 cm position.

Table 4: Number of LEDs deflecting out of sensor field (drop-outs) under central sternum loading

LED Position	Test with internal chest potentiometer				Test without internal chest potentiometer			
	1-in	2-in	2.5–in	3-in	1-in	2-in	2.5–in	3-in
13 cm	0/12	8/12	11/12	12/12	0/12	8/12	N/T	12/12
11 cm	0/12	0/12	N/T	9/12	N/T	N/T	N/T	N/T
10 cm	0/12	0/12	N/T	4/12	0/12	0/12	N/T	5/12
9 cm	0/12	0/12	N/T	3/12	0/12	0/12	N/T	0/12
8 cm	0/12	1/12	N/T	4/12	0/12	0/12	N/T	3/12
6 cm	0/12	2/12	N/T	12/12	0/12	0/12	N/T	11/12
Sternum	0/4	2/4	N/T	4/4	0/4	0/4	0/4	4/4

Note: Denominator indicates the total number of LEDs used in the test. Sternum tests were conducted with the plate indenter and rib tests were conducted with the round indenter. N/T: not tested

The percentage of LED drop-out was sensitive to positioning, magnitude of sternum compression (1-in test), and the presence of the internal chest potentiometer (Table 4). No drop-out occurred in tests with 1-in sternum compression, and this was independent of the presence or absence of internal chest potentiometer. In the 2-in compression test without the presence of the potentiometer, the drop-out occurred only at the 13 cm position. However, the presence of the potentiometer at this compression magnitude produced drop-out at the following positions: 6 cm; 8 cm; 13 cm; and the sternum. The 3-in sternum test without the chest potentiometer produced dropout at all LED positions except the 9 cm position. Inclusion of the potentiometer in the 3-in compression test resulted in LED dropout in all configurations.

These findings indicate that the mechanism of signal drop-out can be influenced by obstruction within the light field (presence of internal chest potentiometer slider arm), initial position of the LED, and orientation of the LED deflection path.

Peak chest compressions before drop-out depended on the position of the LED, with the 9 cm position showing no drop-out (3-in compression test) and increasing drop-outs with positions medially and laterally, i.e., away from the 9 cm position. As shown in Figure 21, at the 6 cm LED position, the peak compression before drop-out was 62.3 mm, followed by 70.3 mm at the 8 cm, 63.8 mm at the 10 cm, and 24.3 mm at the 13 cm LED positions. At the sternum, the peak chest compression occurred at 65.8 mm.

These findings indicate that the 9 cm position is the most optimal. Because the peak sternum compression exceeded the injury assessment reference value (IARV) of 63 mm, according to FMVSS No. 208, (section S6.4, Code of Federal Regulations, 10/1/2006 edition) with LEDs positioned at 8 cm, 9 cm, and 10 cm, and on the sternum, it may be appropriate to use these positions when the symmetrical load is on the center of the sternum.

Figures 22-30 show representative lower rib deflection-time plots for LED positions of 13 cm, 9 cm, and 6 cm during 1-in, 2-in, and 3-in tests, at 0.5 m/s velocity. The deflection plots indicate

the relative motion of the LEDs. The 1-in compression test produced 10 to 15 mm of rib deflection at 13 cm from the midline without LED drop-out. However, LED drop-out was produced in three of the lower four ribs in the 2-in compression tests. Drop-out occurred in all lower ribs in the 3-in compression tests. It should be noted that the relative value of deflection indicating drop-out is coincidently of similar magnitude as the maximum actuator/indenter displacement. Moving the placement of the LEDs medially, i.e., towards the sternum, to the 9 cm position, reduced the sensitivity to drop-out such that LEDs were adequately visualized by both sensors in all 1-in, 2-in, and 3-in compression tests. Lower rib and indenter displacements for the 9 cm LED position are illustrated (Figures 25-27). At the 6 cm position, there was increased sensitivity to drop-out in the 3-in compression tests (Figure 30). However, 1- and 2-in compression tests resulted in no drop-out (Figures 28 and 29).

Despite demonstrating lower magnitudes, these findings indicate that the displacements of all LEDs within the sensor fields mimicked the shape of the input compressive deflection-time waveform. The electro-hydraulic piston traveled purely along the x-axis. Because of the three-dimensional nature of the ribcage and off-central locations of the LEDs, input piston-measured displacements were greater than the displacements recorded by the LEDs at various locations along the ribcage. LED deflection responses did not always return to zero because the RibEye data acquisition system is limited to 910 msec after trigger (total 1000 msec recording time) and the dummy ribcage did not fully relax within this period. Response: The following replaces the current text in the report.

Discrepancies may arise due to the recording system, asymmetric kinematics induced because of the loading bias, or both. Bilateral accuracy bench tests removing the dummy ribs from the system, evaluated LED on the indenter, demonstrated -3.7 to 2.2% disagreement between the RibEye and the indenter LED. These were not dynamic tests, however. While no repeat or other types of tests were conducted in the current evaluation study, given the symmetric nature of the recording system, the authors feel that the discrepancies between the left and right responses of the same rib may be more due to the mechanical response of the dummy during the loading scenario. This issue may need to be explored.

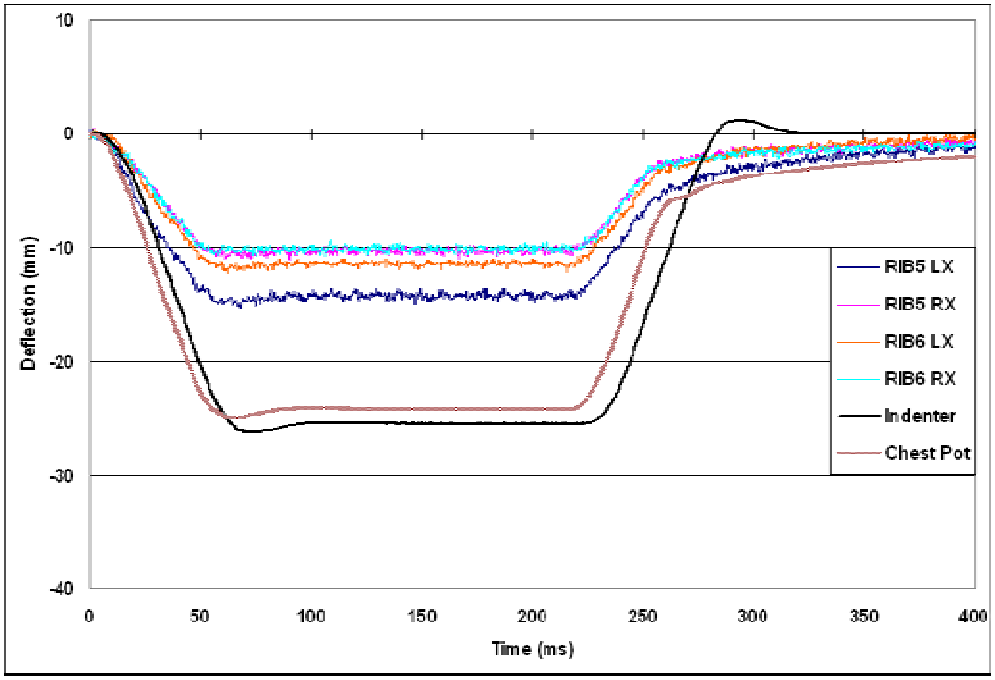

Figure 22: Deflections of the left and right fifth and sixth ribs from LEDs positioned 13 cm along with the chest potentiometer and indenter displacements. Data corresponds to the 1-in chest compression test.

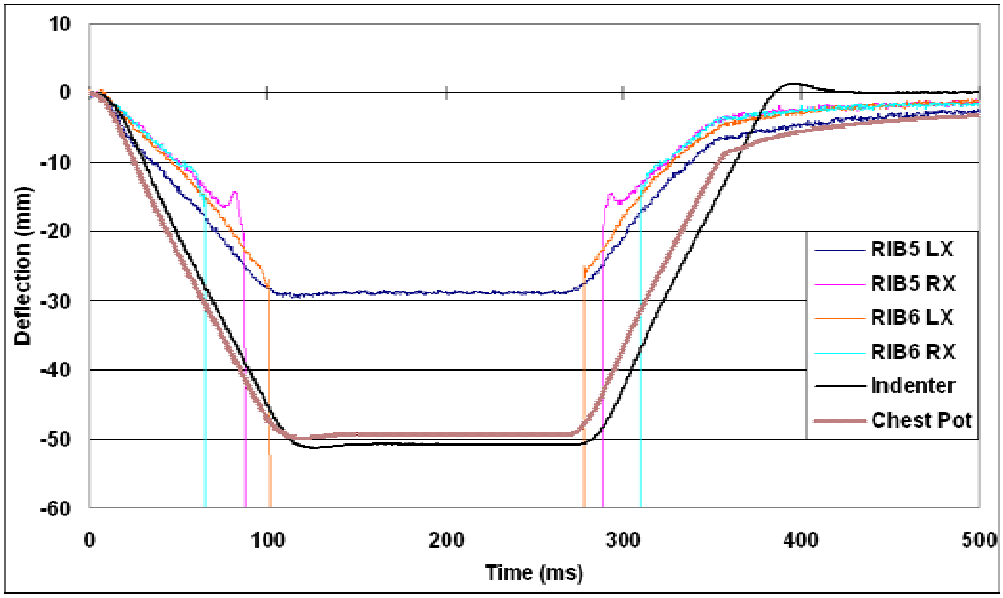

Figure 23: Deflections of the left and right fifth and sixth ribs from LEDs positioned 13 cm along with the chest potentiometer and indenter displacements. Data corresponds to the 2-in chest compression test.

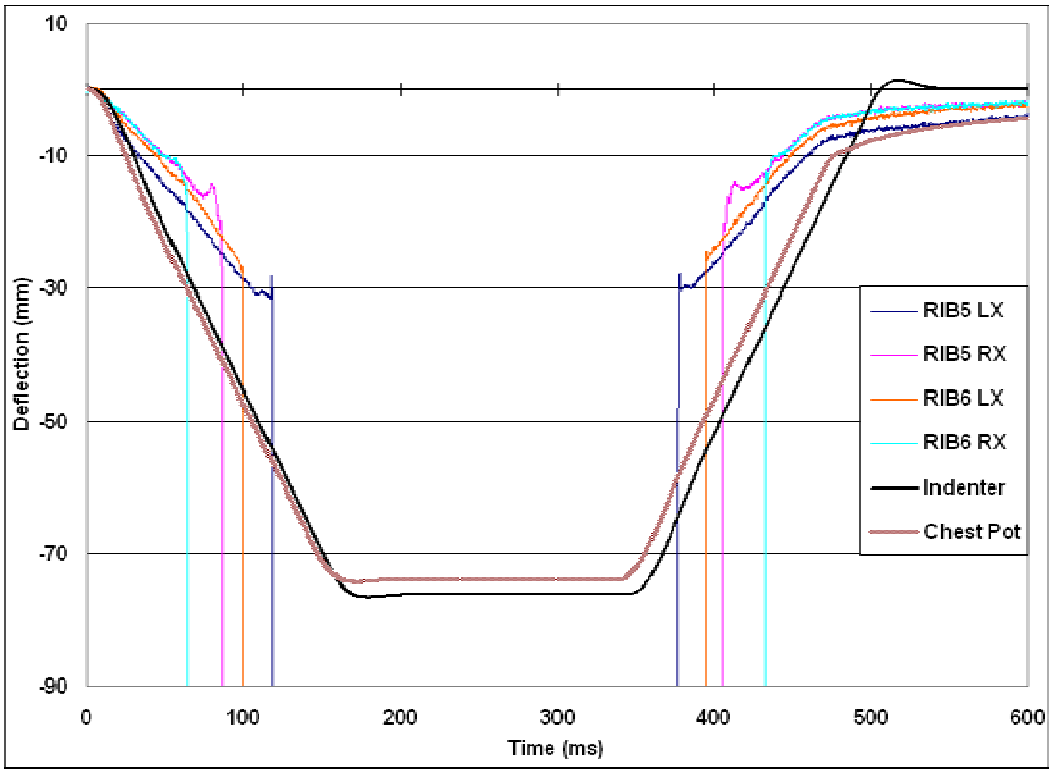

Figure 24: Deflections of the left and right fifth and sixth ribs from LEDs positioned 13 cm along with the chest potentiometer and indenter displacements. Data corresponds to the 3-in chest compression test.

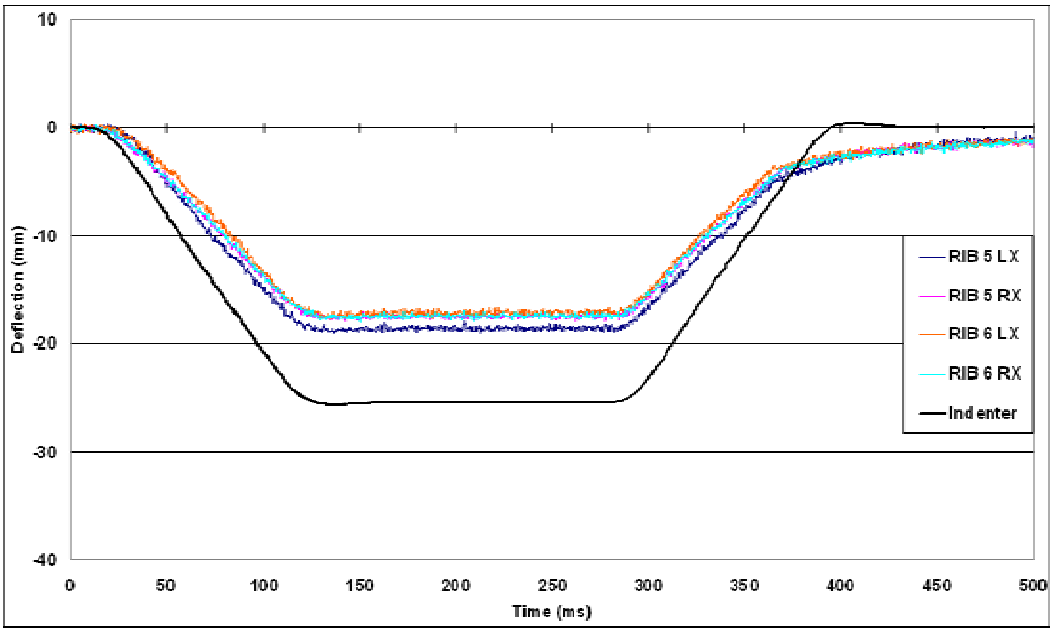

Figure 25: Deflections of the left and right fifth and sixth ribs from LEDs positioned 9 cm along with indenter displacements. Data corresponds to the 1-in chest compression test.

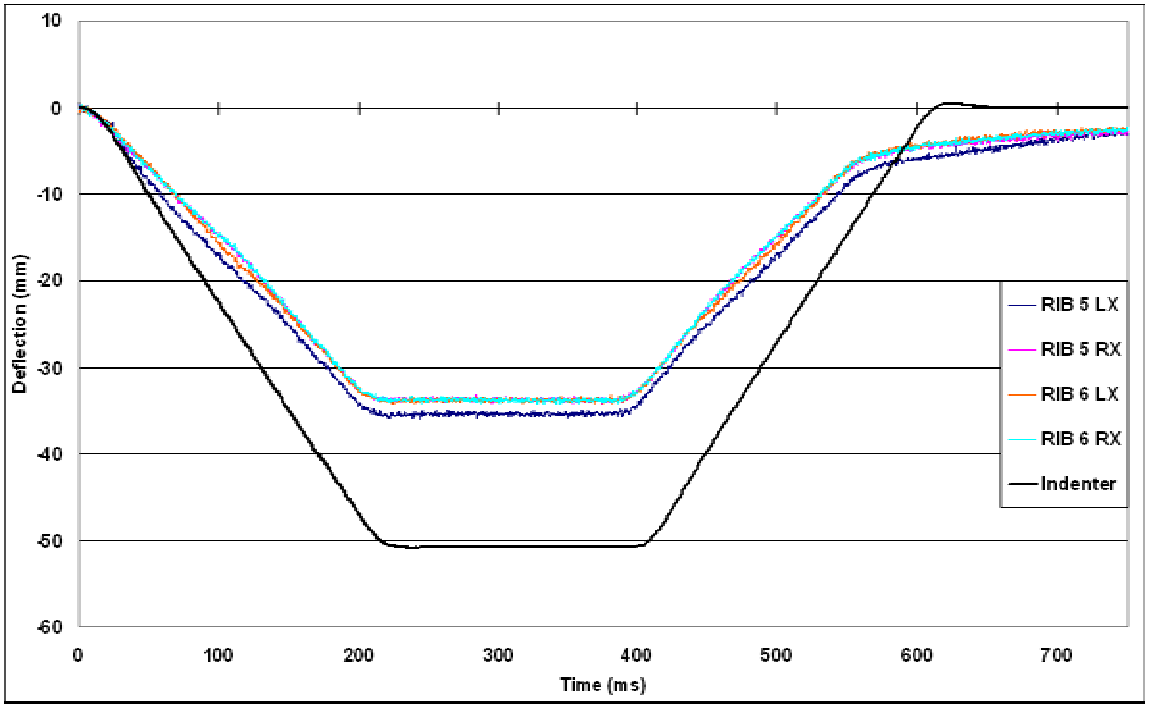

Figure 26: Deflections of the left and right fifth and sixth ribs from LEDs positioned 9 cm along with indenter displacements. Data corresponds to the 2-in chest compression test.

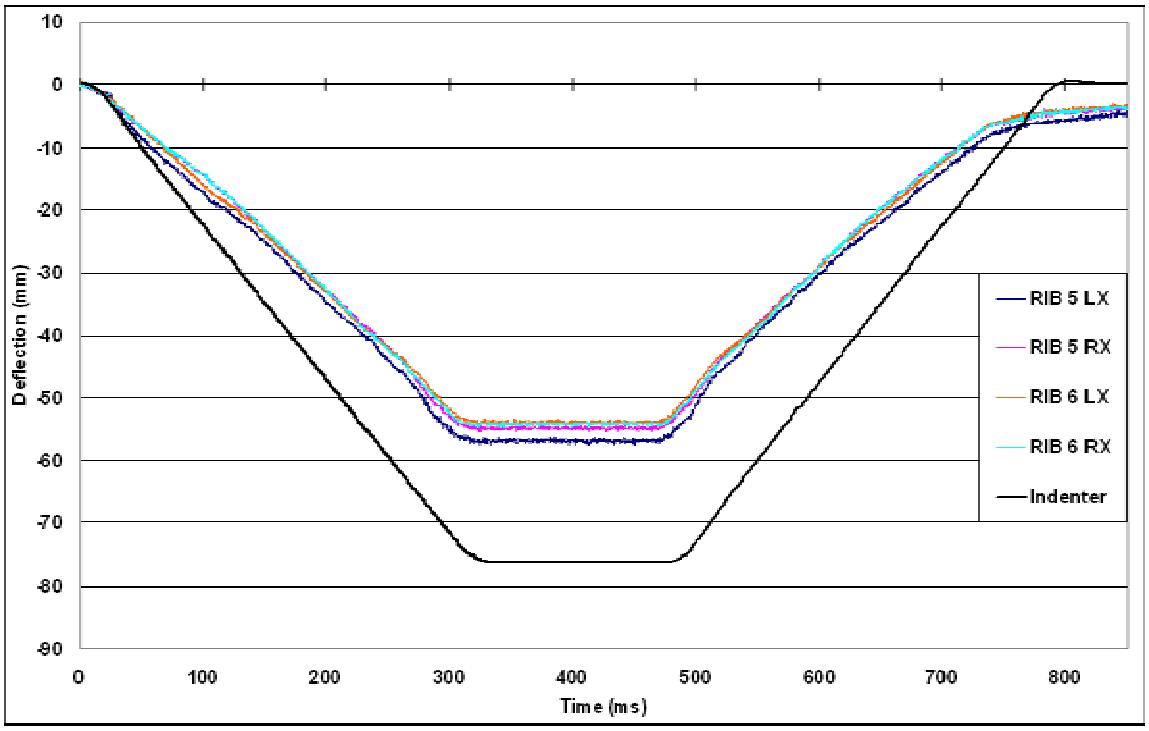

Figure 27: Deflections of the left and right fifth and sixth ribs from LEDs positioned 9 cm along with indenter displacements. Data corresponds to the 3-in chest compression test.

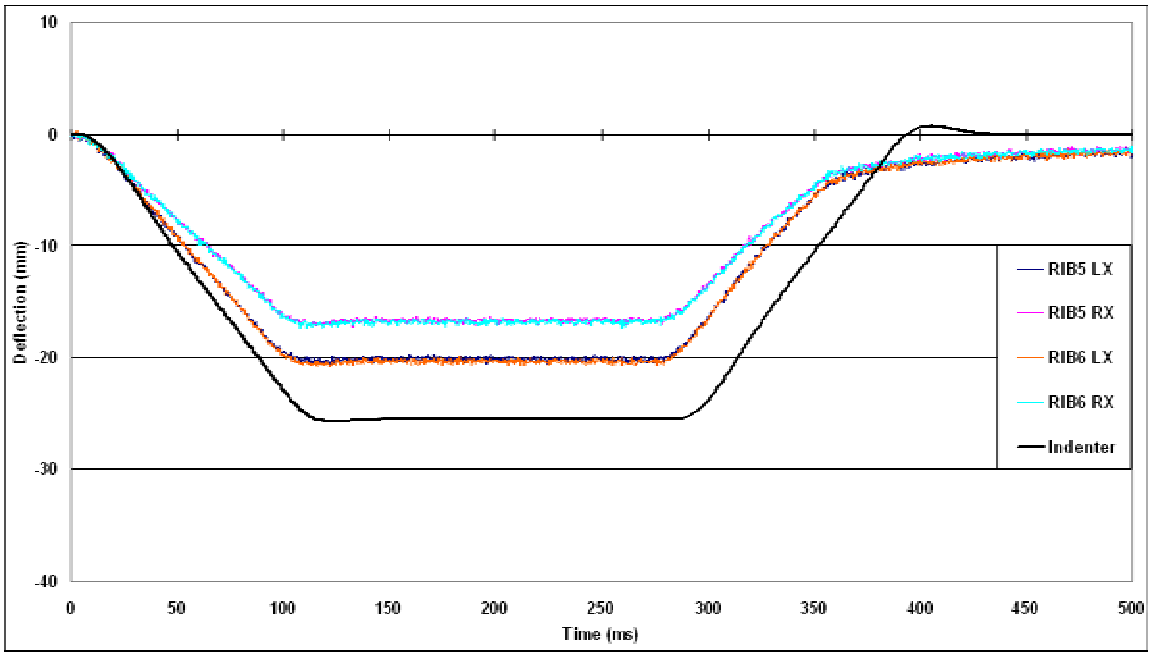

Figure 28: Deflections of the left and right fifth and sixth ribs from LEDs positioned 6 cm along with indenter displacements. Data corresponds to the 1-in chest compression test.

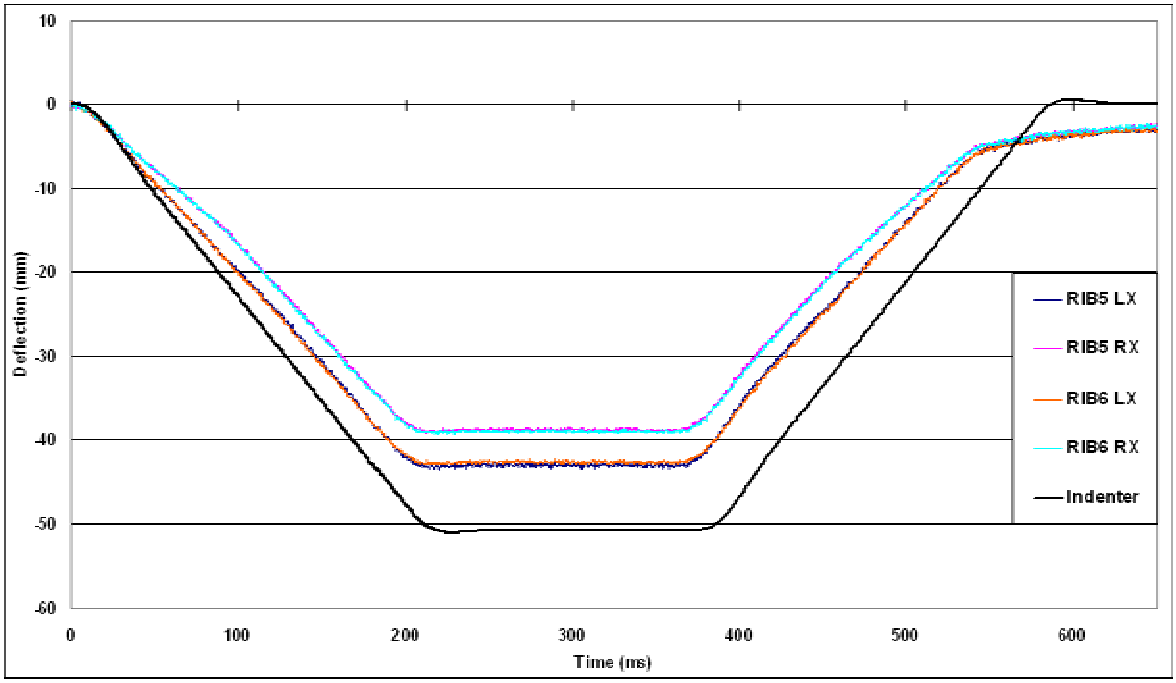

Figure 29: Deflections of the left and right fifth and sixth ribs from LEDs positioned 6 cm along with indenter displacements. Data corresponds to the 2-in chest compression test.

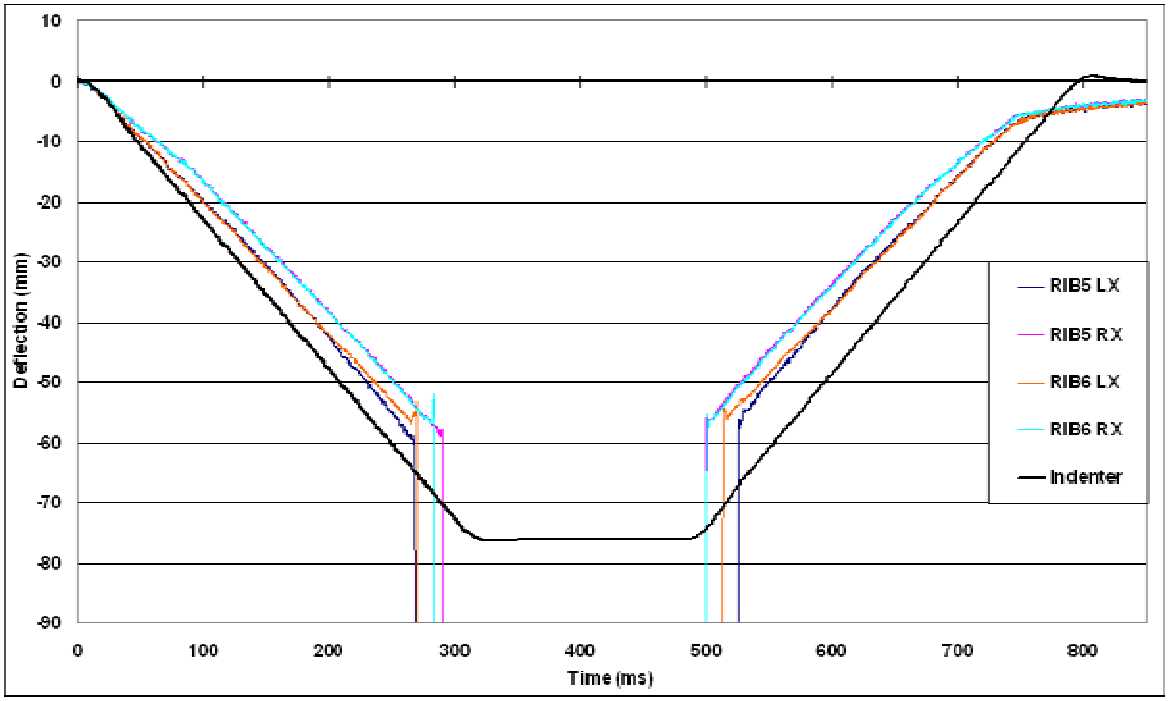

Figure 30: Deflections of the left and right fifth and sixth ribs from LEDs positioned 6 cm along with indenter displacements. Data corresponds to the 3-in chest compression test.

3.1.4 Left side offset tests:

The purpose of this series of tests was to determine the drop-out characteristics with offset loading to the left side of the ribcage. The longitudinal edge of the indenter, 51 mm x 102 mm, was aligned with the front end stiffener plate of the left side ribs two through five (Figures 31 and 32). The performance was evaluated in 1-, 2-, and 2.5-in compression tests, with LEDs mounted at the 6 cm, 9 cm, and 13 cm positions, resulting in nine tests. The extreme case of the 3-in compression test was not considered because subjecting the Hybrid III dummy thorax to this magnitude may exceed its capacity. The peak deflection magnitudes before LED signal drop-out were 57.0, 63.7, and 25 mm for the 6, 9, and 13 cm LED positions. Similar to the case of mid-sternum loading, the 9 cm position was found to be the most optimal. The plots of deflections of ribs one and two, shown in Figures 33-35 for the three LED positions, reflect the asymmetric loading associated with these offset tests. Independent of drop-out, increased deflection of the left side ribs is evident relative to the right side. Drop-out was produced with LEDs positioned in the 13 cm configuration at all three indenter compression magnitudes (Table 5). However, no drop-out occurred at the 9 cm position, independent of compression

magnitude. At the 6 cm position, drop-out occurred in the 2.5 in chest compression test. These findings indicate that, again, the mechanism of signal drop-out is influenced by the initial position of the LED and its orientation secondary to its deflection path. Further, the RibEye system appears to be capable of responding to asymmetric loading.

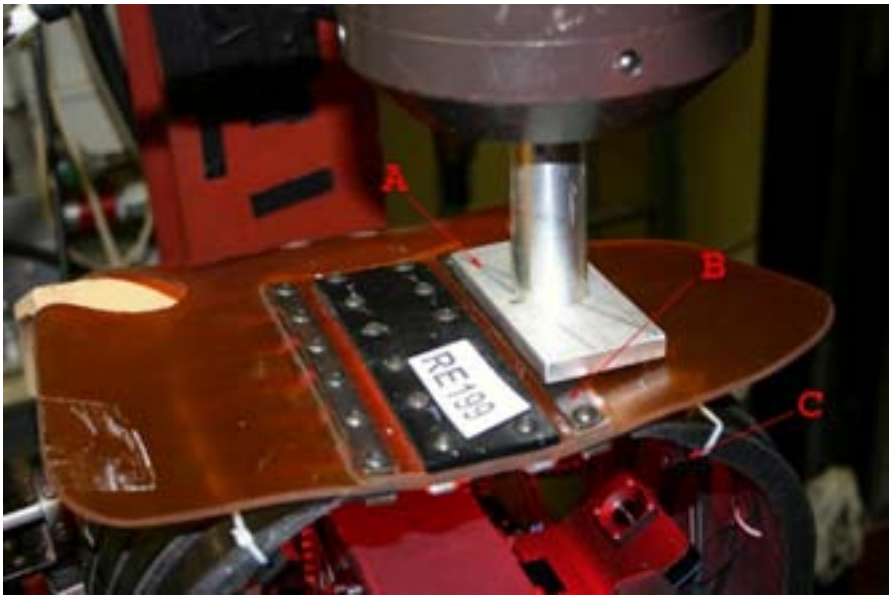

Figure 31: The test configuration for left side offset loading. A: Aluminum plate, B: frontend stiffener plate, and C: LED mounted to the left sixth rib at the 6 cm position.

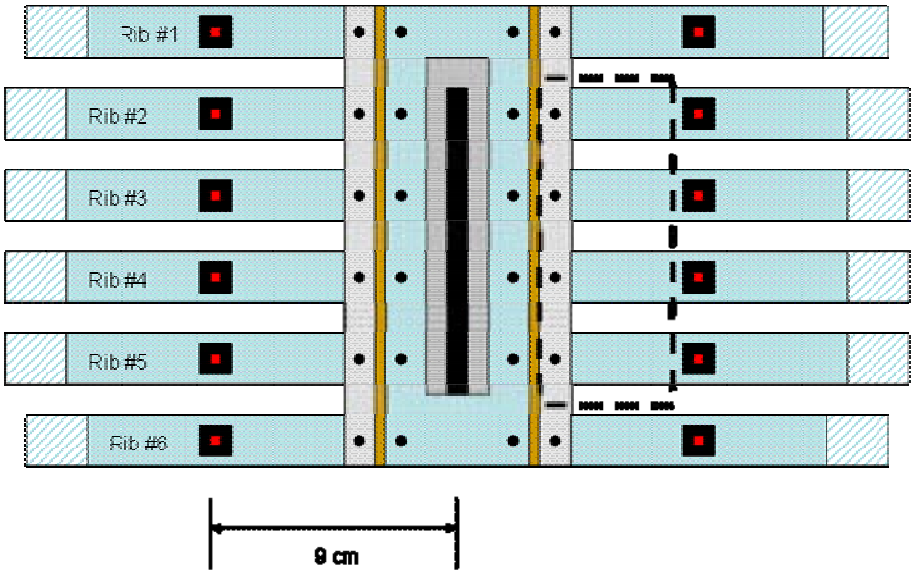

Figure 32: LED configurations at 9 cm used in left offset loading evaluation tests. Dashed rectangle shows the outline of the aluminum indenter.

Table 5: Number of LEDs deflecting out of sensor field in left offset loading

LED Position	Chest compression tests without Chest Potentiometer		
	1-in	2-in	2.5-in
13 cm	1/12	6/12	6/12
9 cm	0/12	0/12	0/12
6 cm	0/12	0/12	7/12

Note: Denominator indicates the total number of LEDs used in the test.

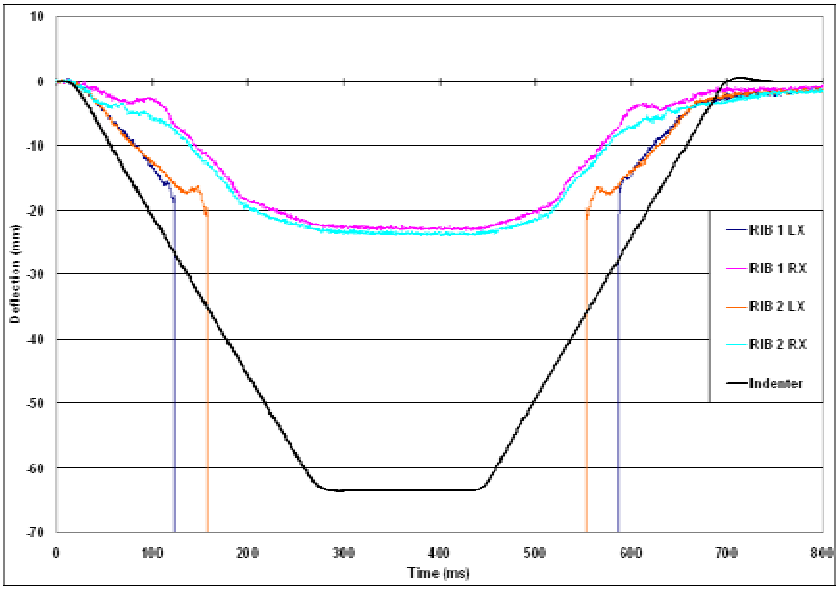

Figure 33: Deflections along the x-direction of ribs one and two as recorded by the LEDs positioned at 13 cm. Data corresponding to the 2.5-in chest compression test is shown.

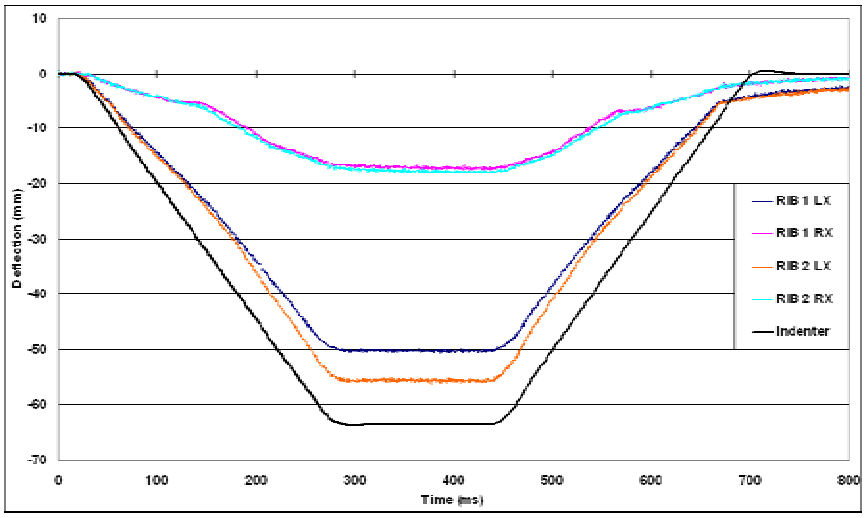

Figure 34: Deflections along the x-direction of ribs one and two as recorded by the LEDs positioned at 9 cm. Data corresponding to the 2.5-in chest compression test is shown. Note no drop-outs.

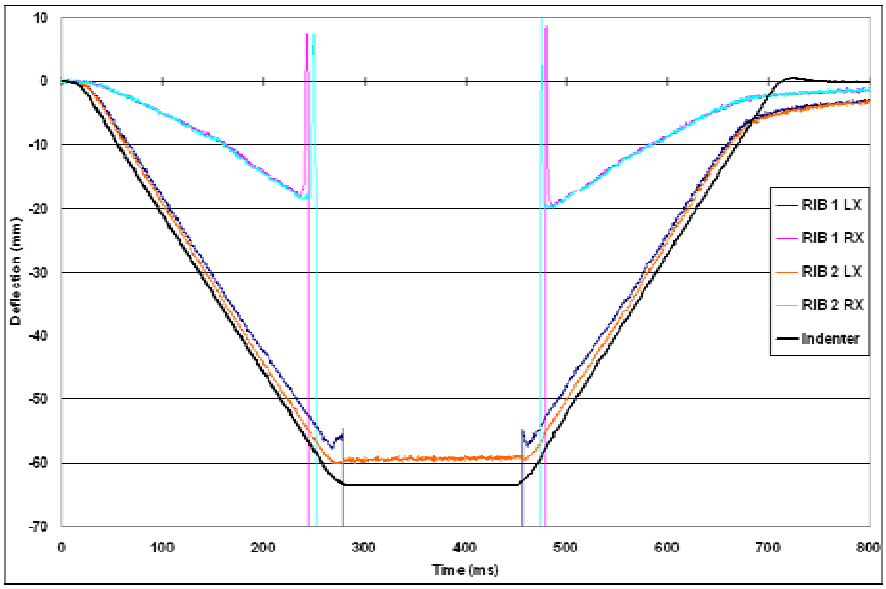

Figure 35: Deflections along the x-direction of ribs one and two as recorded by the LEDs positioned at 6 cm. Data corresponding to the 2.5-in chest compression test is shown.

3.1.5 Diagonal belt loading tests:

The purpose of this series of tests was to determine the drop-out characteristics with asymmetric loading generated by a typical diagonal shoulder belt. Loading was accomplished using a 51 mm wide metal plate angled at approximately 45 deg in the frontal (yz) plane and positioned with its center at mid-sternum (Figure 36). LEDs were positioned at the 9 cm location, and the plate was displaced to compress the dummy chest to 1-in, 2-in, and 3-in. Two tests at each of the two lower compressions were conducted successfully. However, when the fifth test was conducted at the greatest displacement, the plate contacted the molded stop assembly (Hybrid III drawing 78051-85). As data were not usable, the plate was shortened and a sixth test was run. Figures 37-39 show deflection-time plots for the 3-in test with LEDs positioned at 9 cm. As expected, upper ribs one and two responded with greater displacement on the right side and lower ribs five and six responded with greater displacements on the left side, and the middle ribs three and four responded with similar magnitudes of deflection. The upper- and lower-most LEDs appear to be sensitive to drop-out in the diagonal belt-type loading, with no drop-outs occurring in the middle ribs. The left third rib exhibited paradoxical outward motion at maximal compression. The response of this is not indicative of drop-out. This LED is just below the edge of the indenter plate, and the LED mounting bolt slipped out from underneath the indenter. When this occurred, the rib (and LED) exhibited a sudden but small "bounce back"

effect. Drop-out only occurred in the most severe, 3-in compression test (Table 6), and the first LED dropped out at an indenter displacement of 63.7 mm, exceeding the IARV for sternum compression. Because drop-outs occurred in multiple LEDs, the system may not fully capture the ribcage motion at this severe magnitude of chest compression.

Figure 36: Test configuration for diagonal belt loading. A: Metal plate, B: LED mounted to the right sixth rib at the 9 cm position.

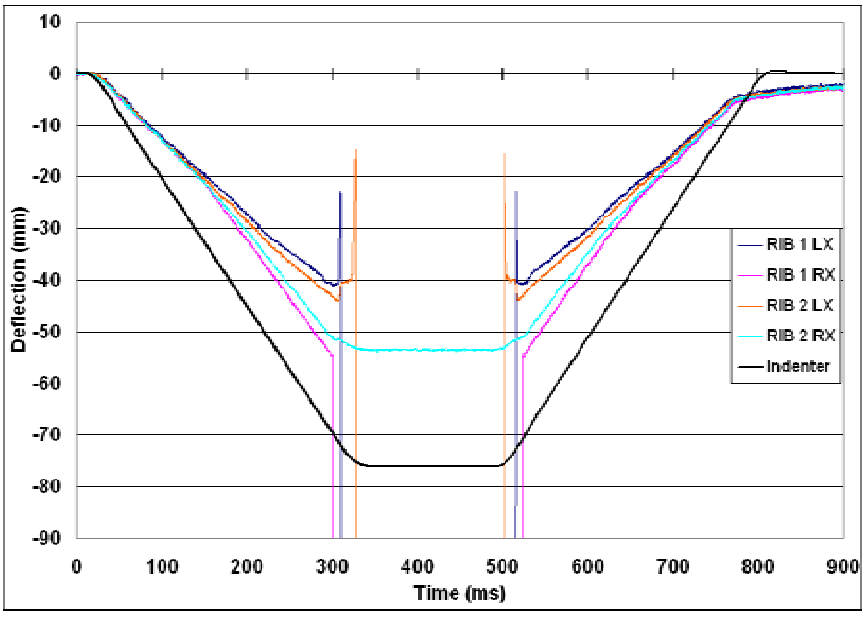

Figure 37: Deflections along the x-direction of ribs one and two as recorded by the LEDs positioned at 9 cm. Data corresponding to the 3-in diagonal belt loading compression test is shown.

Table 6: Number of LEDs deflecting out of sensor field with belt-type loading

LED Position	Indenter Displacement (mm) without Chest Potentiometer		
	1-in	2-in	3-in
9 cm	0/12	0/12	6/12

Note: Denominator indicates the total number of LEDs used in the test.

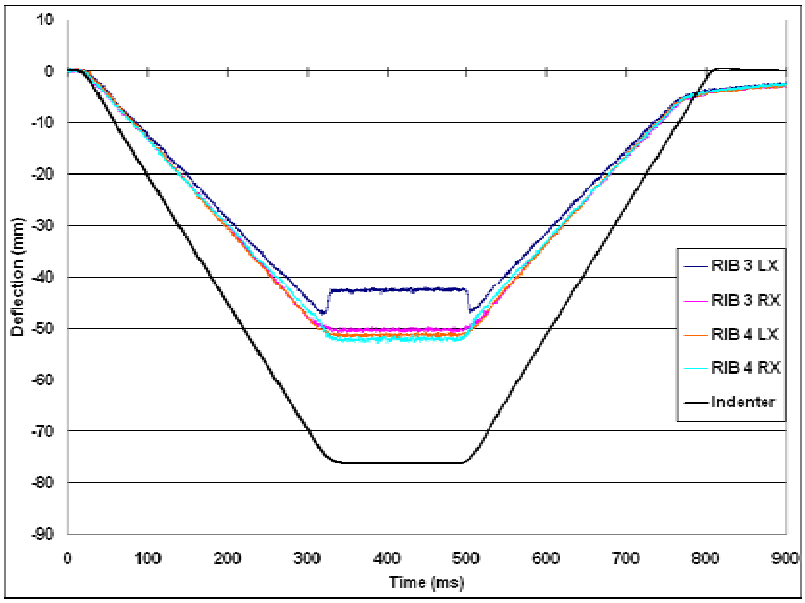

Figure 38: Deflections along the x-direction of ribs three and four as recorded by the LEDs positioned at 9 cm. Data corresponding to the 3-in diagonal belt loading compression test is shown.

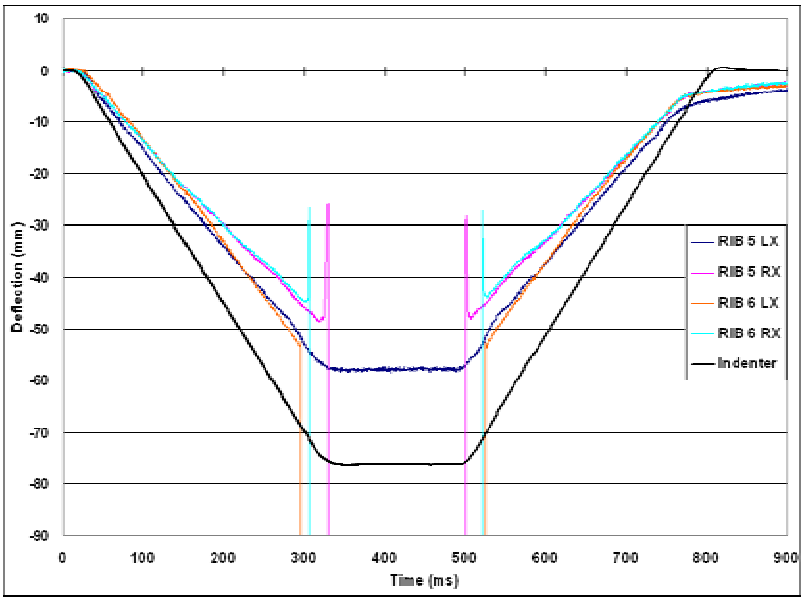

Figure 39: Deflections along the x-direction of ribs five and six as recorded by the LEDs positioned at 9 cm. Data corresponding to the 3-in diagonal belt loading compression test is shown.

3.2 Accuracy assessment

The purpose of the next series of tests was to directly compare the deflection measuring capability of the RibEye system with the current deflection measuring standard (internal chest potentiometer) and/or with the actuator/indenter deflection. As described, the potentiometer measures sternum compression via a transducer arm whose end travels in a midline track within the dummy sternum. The transducer arm induces rotation in a potentiometer during compression and the resulting electrical signal is converted to linear displacement.

Forty-five tests were conducted in this series which consisted of four subseries (Sections 3.2.1 to 3.2.4). Six tests demonstrated dropout and were therefore excluded, leaving thirty-nine reportable tests (Table 7). These tests were designed to evaluate the accuracy of deflection records along the x-, or both x- and y-directions (Table 7). The first three subseries involved test configurations that maintained the integrity of the dummy thorax such that LEDs were mounted to the sternum, rib, or rib inter-space while the chest compression was induced by the indenter. The fourth subseries entailed mounting an LED directly to the electro-hydraulic piston/actuator and tracking its displacement. Indenter displacement and velocity were varied with each subseries. Following each test the RibEye data was separated into individual channels and a CFC60 filter was applied. RibEye deflection data were compared to the displacement of the indenter and with the chest displacement potentiometer data in the sternum-mounted subseries of tests.

Table 7: Accuracy description of tests

LED Mounting Location	# of Tests	Loading Location	Comparison	Evaluation Parameter
Sternum	16	central sternum	chest pot and Indenter	x-direction accuracy
Right rib 4 (antero-medial)	7	over LED	Indenter	x-direction accuracy with and without z-deviation
Right rib 4 (8 cm with rotated thorax)	4	over LED	Indenter	x- and y-direction accuracy
Indenter extension	18	None	Indenter	x-direction accuracy

3.2.1 Sternum-mounted LED tests:

This subseries consisted of 11 tests to evaluate the accuracy of RibEye detection of four LEDs mounted on the upper and lower corners of the sternum (Figure 40). The remaining eight LEDs were considered secondary and mounted on the sternum (Figure 41) or, onto ribs two through five bilaterally at either 8 or 9 cm from the midline (Figure 19). These are the same tests discussed above in the sternum mounted LED drop-out tests (Section 3.1.2). It was expected that the deflections from the corner mounted LEDs will match the internal chest potentiometer deflection. However, because of the flexibility of the sternum material (bib), a slight mismatch is expected between the internal chest potentiometer and the indenter.

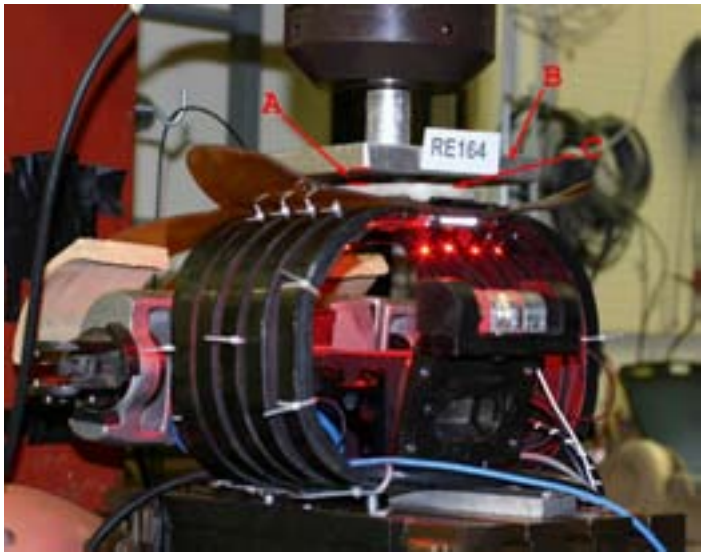

Figure 40: Test configuration for sternum-mounted loading. A: Offset for the trigger system, B: the Aluminum plate indenter, and C: PMMA leveler.

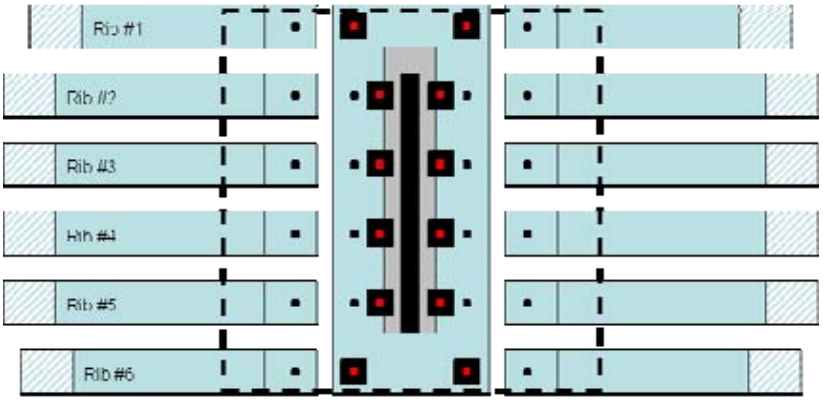

Figure 41: LED configurations used in sternum-mounted loading tests. Dashed rectangle shows the outline of the indenter.

Chest compression tests were conducted using a 15 cm square aluminum plate indenter. A leveling plate of polymethylmethacrylate (PMMA) was devised to compensate for the convexity of the sternum plate and provide a level surface for indenter contact. This ensured that the dummy sternum deflected uniformly without rotation which validates the RibEye comparison with the internal chest displacement potentiometer. These tests were designed to evaluate the accuracy of deflection records along the x-direction (Table 7). The 1- to 3-in compression tests were conducted at 0.25 m/s, with and without inclusion of the internal chest potentiometer. Four tests resulted in drop-out of the critical sternum mounted LEDs and one test resulted in questionable data. These tests were excluded from analysis. The mean sternum deflection was calculated using the displacements of the four LEDs. Table 8 lists the peak indenter displacement, and data from the four LEDs, along with mean and one standard deviation.

Table 8: Summary of data for accuracy evaluation

Test ID	Chest Pot	Peak UL Sternum Deflection CFC60 (mm)	Peak UR Sternum Deflection CFC60 (mm)	Peak LL Sternum Deflection CFC60 (mm)	Peak LR Sternum Deflection CFC60 (mm)	Mean Sternum Deflection ± SD (mm)
183	Y	-26.2	-25.9	-25.5	-25.6	-25.8 ± 0.3
161	Y	-26.0	-25.8	-25.3	-25.5	-25.6 ± 0.3
167	N	-26.8	-26.3	-26.1	-25.8	-26.2 ± 0.4
171	Y	-27.9	-27.8	-26.9	-26.9	-27.4 ± 0.6
172	Y	-27.7	-27.6	-26.5	-26.7	-27.1 ± 0.6
164	N	-25.6	-25.1	-24.7	-24.6	-25.0 ± 0.5
184	Y	-27.8	-27.2	-27.0	-27.0	-27.5 ± 0.4
173	Y	-41.1	-40.7	-40.8	-39.5	-40.5 ± 0.7
165	N	-52.8	-53.3	-52.4	-53.1	-52.9 ± 0.4
168	N	-55.5	-55.3	-54.5	-54.9	-55.0 ± 0.4
170	N	-66.8	-68.4	-68.6	-69.7	-68.4 ± 1.2

Table 9 shows the comparison of the peak indenter deflections with mean deflections from the four LEDs, and in certain cases, mean deflection data are also compared with peak internal chest potentiometer displacements. Determination of the mean deflections from the four corners provides a realistic estimate of the central compression of the sternum with respect to the spine. The difference in mean sternum deflection compared to the indenter displacement ranged from -

3.3 mm to 2.4 mm (-11.5% to 3.7%). The difference in mean sternum deflection compared to the chest potentiometer ranged from -0.1 mm to 0.7 mm (-0.5% to 1.8%). Figures 42-45 show representative deflection plots in this subseries of accuracy tests. These results indicate that the LEDs can be effectively positioned at any corner(s) of the sternum to record deflections at this region of the chest. It should be noted that the mounting hardware is (already) provided by the manufacturer. Because of the current limit of 12 LEDs on the RibEye system, use of LED(s) on the sternum reduces the number of possible rib deflection measurements.

Table 9: Summary of data for accuracy evaluation (wrt: with respect to)

Peak Chest Pot Deflection CFC600 (mm)	Mean Sternum Deflection (see table 8) (mm)	Difference Mean Peak wrt Indenter (mm)	% Difference Mean wrt Indenter	Difference Mean Peak wrt Chest Pot (mm)	% Difference Mean wrt Chest Pot
-25.9	-25.8	-1.6	-5.7	-0.1	-0.5
-25.6	-25.6	-2.1	-7.6	0.1	0.2
N/A	-26.2	-1.6	-5.6	N/A	N/A
-26.9	-27.4	-0.7	-2.4	0.5	1.8
-26.7	-27.1	-0.9	-3.2	0.4	1.5
N/A	-25.0	-3.3	-11.5	N/A	N/A
-27.2	-27.2	-2.3	-7.9	0.1	0.2
-39.9	-40.5	-0.2	-0.4	0.7	1.7
N/A	-52.9	0.4	0.7	N/A	N/A
N/A	-55.0	1.7	3.2	N/A	N/A
N/A	-68.4	2.4	3.7	N/A	N/A

3.2.2 Rib-mounted LED tests:

The RibEye system requires that LEDs be mounted at standard locations on the dummy ribs or at the corners of the sternum relative to the vertical (z) axis so that appropriate corrections can be applied to achieve the specified accuracy of 1 mm, described earlier. It was expected that any z-direction LED displacement would adversely affect the system accuracy. This was investigated by conducting tests for two LED positions: the standard z-location at the center of each rib, i.e., 0 cm z-component, and at a z-direction offset position of 1.5 cm from the center of each rib, i.e., 1.5 cm z-component. The 1.5 cm z-direction offset position corresponds to the interspace between adjacent ribs. The 0 cm z-component test was conducted as follows. An LED was mounted at the antero-medial rib margin of the right fourth rib (Figures 46-47). Two tests were conducted in this subseries with chest compression set at 1/2 in and directed over the

LED. Although the peak indenter displacement was greater than LED deflection, the difference was within the accuracy of the RibEye system specified by the manufacturer; a representative plot from one of the two tests is shown (Figure 48). For the two tests, differences between LED deflections and indenter displacements were -0.78 mm and -0.84 mm (-6.1% and -6.5%, Table 10).

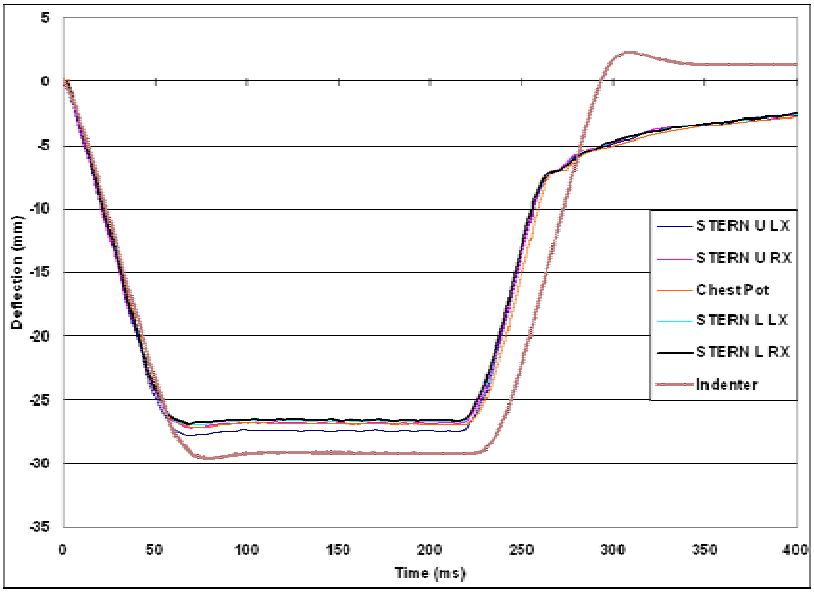

Figure 42: Deflections along the x-direction from sternum LEDs positioned at the four corners. Indenter and internal chest potentiometer data are also shown.

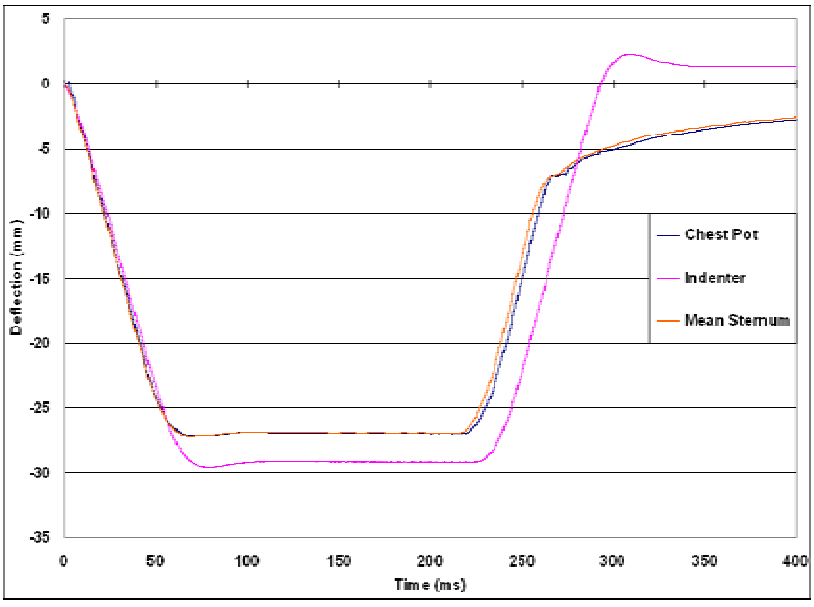

Figure 43: Comparison of deflection-time records from the chest potentiometer, indenter, and sternum LEDs. Data were averaged from LEDs positioned at the four corners of the sternum.

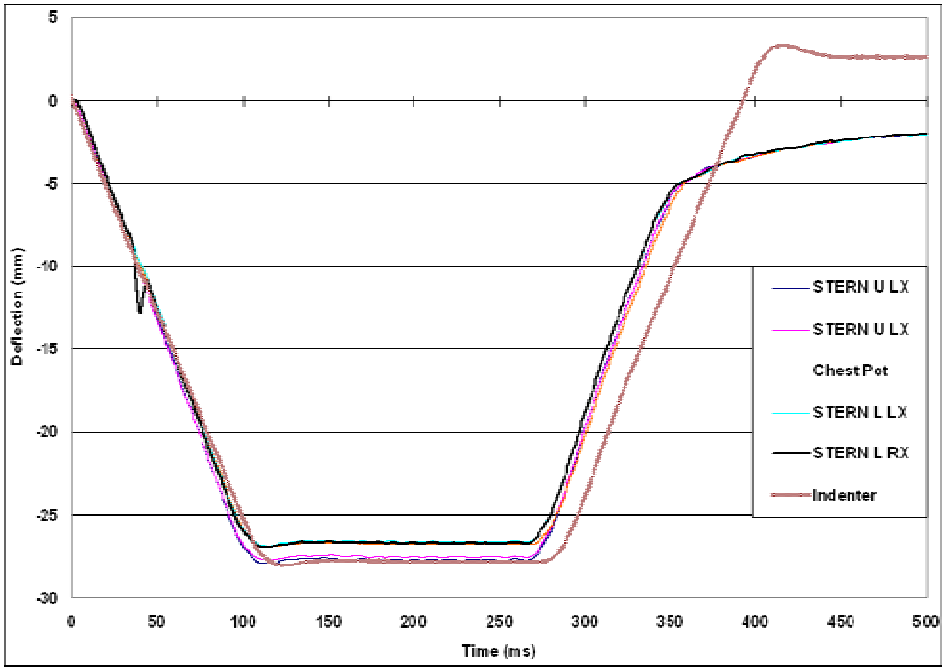

Figure 44: Deflections along the x-direction from sternum LEDs positioned at the four corners. Indenter and internal chest potentiometer data are also shown.

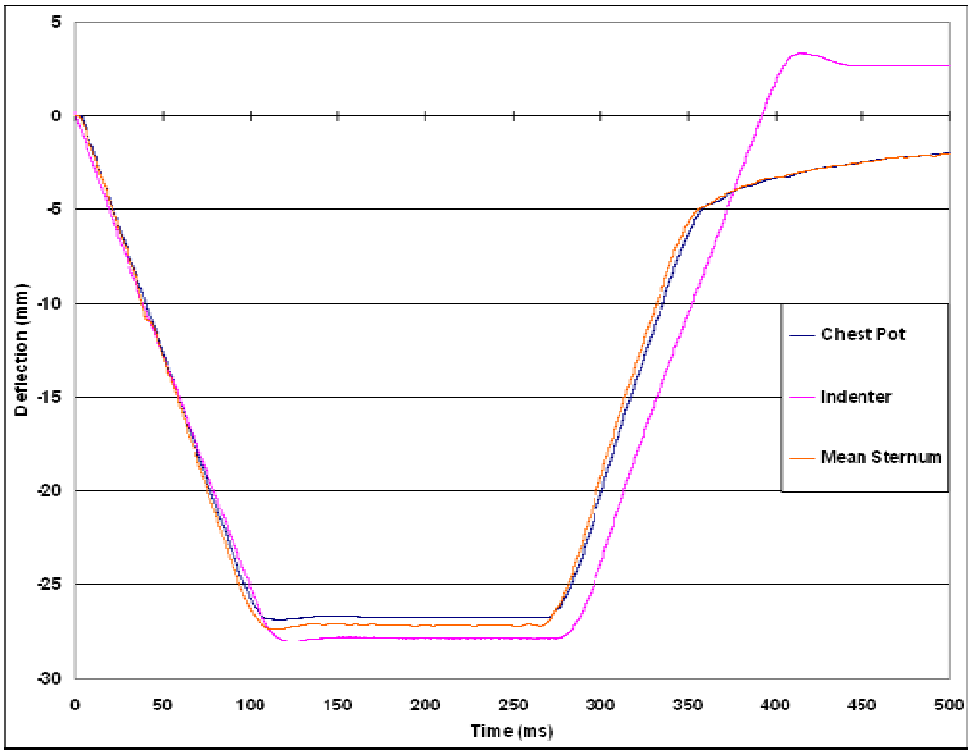

Figure 45: Comparison of deflection-time records from the chest potentiometer, indenter, and sternum LEDs. Data were averaged from LEDs positioned at the four corners of the sternum.

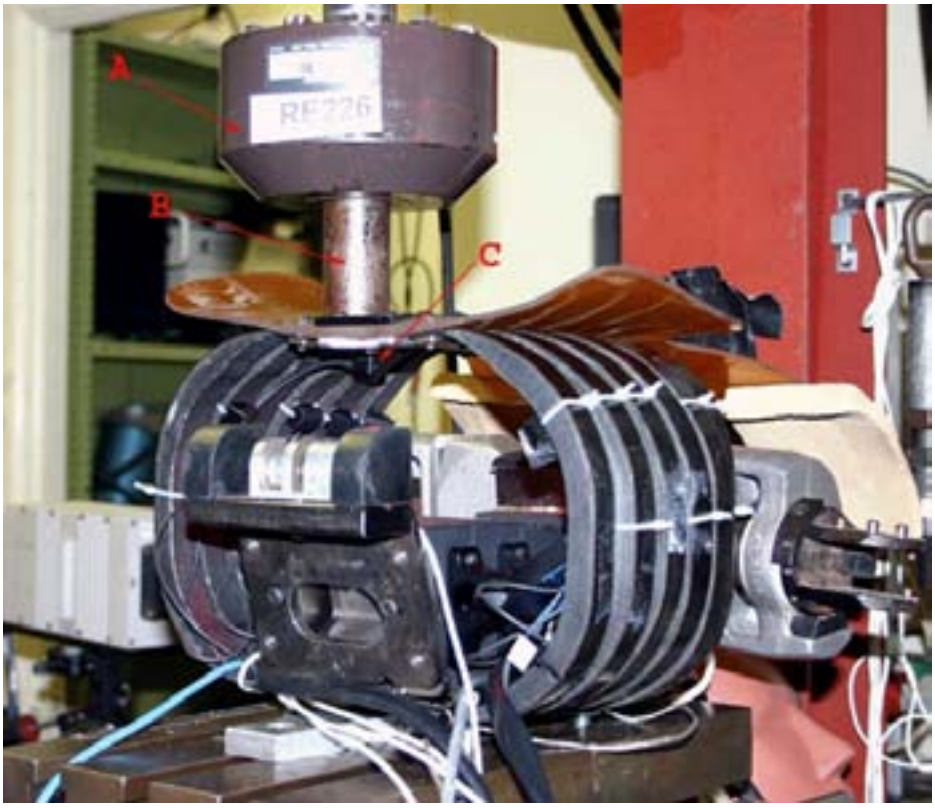

Figure 46: Test configuration for rib-mounted loading. A: indenter load cell, B: indenter, C: LED at right frontend stiffener plate at the fourth rib.

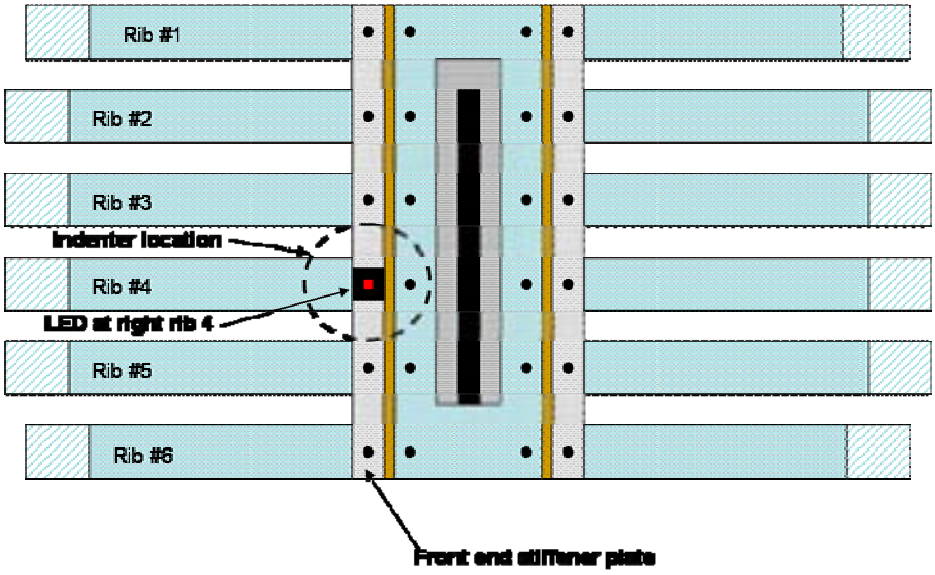

Figure 47: LED configurations used in rib-mounted LED tests. Dashed circle shows the outline of the indenter.

Table 10: Comparison of rib-mounted LED displacements

Test	LED Placement	Peak Indenter Disp	Peak LED Displacement	Indenter LED Difference	Percent Difference
226	R Rib 4	-12.8	-12.0	-0.8	-6.1
227	R Rib 4	-13.0	-12.1	-0.8	-6.5

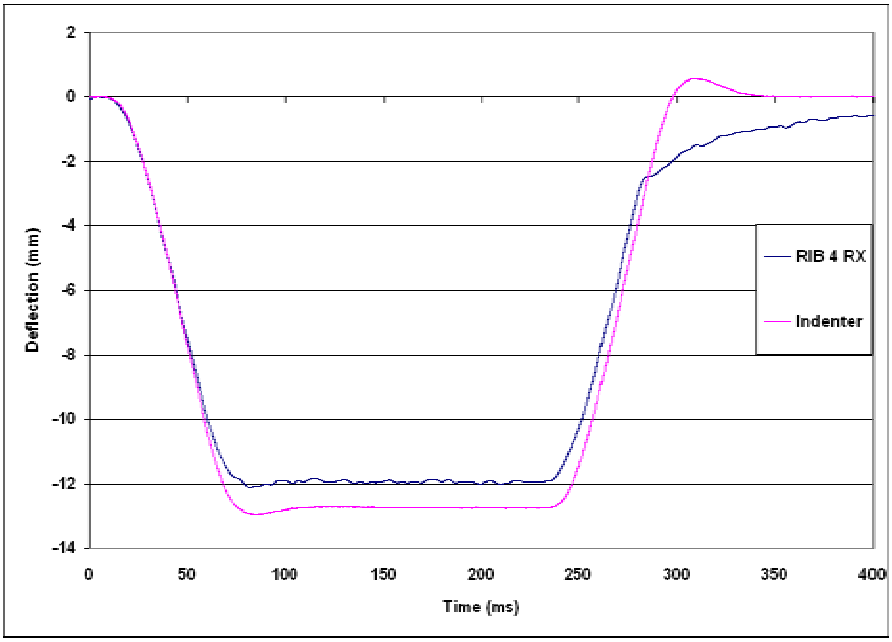

Figure 48: Deflection-time records from the LED positioned at the right fourth rib and indenter.

The 1.5 cm z-component test was conducted as follows. Two LEDs, originally intended for mounting on right ribs 3 and 4, were mounted on the frontend stiffener plate at the interspaces of right ribs 2-3 and 3-4 (Figures 49-50). These mounting positions provided secure and repeatable LED fixation with 1.5 cm z-axis deviation. For this subseries of tests, chest compressions of 1/2 in and 1-in were directed over the right 3-4 rib interspace. The 1-in test resulted in signal drop-out of both LEDs and was excluded from the accuracy analysis. Figure 51 compares LED deflections with indenter displacements after correction for the indenter offset at the initiation of loading. As can be seen, data from the two LEDs are very similar, but indenter displacements are greater than LED-measured deflections. The discrepancy between the LED and indenter displacements can be attributed to the z-location of the LED. Table 11 compares the interspace mounted LED deflections with the indenter displacements: differences

ranged from 2.8 to 3.7 mm (15 to 18%). These results indicate that the z-location of the LED affects the system response and accuracy.

Table 11: Comparison of interspace LED displacements

Test ID	Peak Indenter Displacement CFC1000	Peak R2-3 Disp	% R2-3 Difference	Peak R3-4 Disp	% R3-4 Difference	Mean R2-3 & R3-4 Displacement	% Mean Difference
174	-16.0	-13.2	17.7	-13.2	17.7	-13.2	17.7
175	-15.7	-12.7	18.9	-12.9	18.0	-12.8	18.4
177	-21.9	-18.6	15.2	-18.6	15.0	-18.6	15.1
178	-24.1	-20.1	16.4	-20.5	14.7	-20.3	15.6

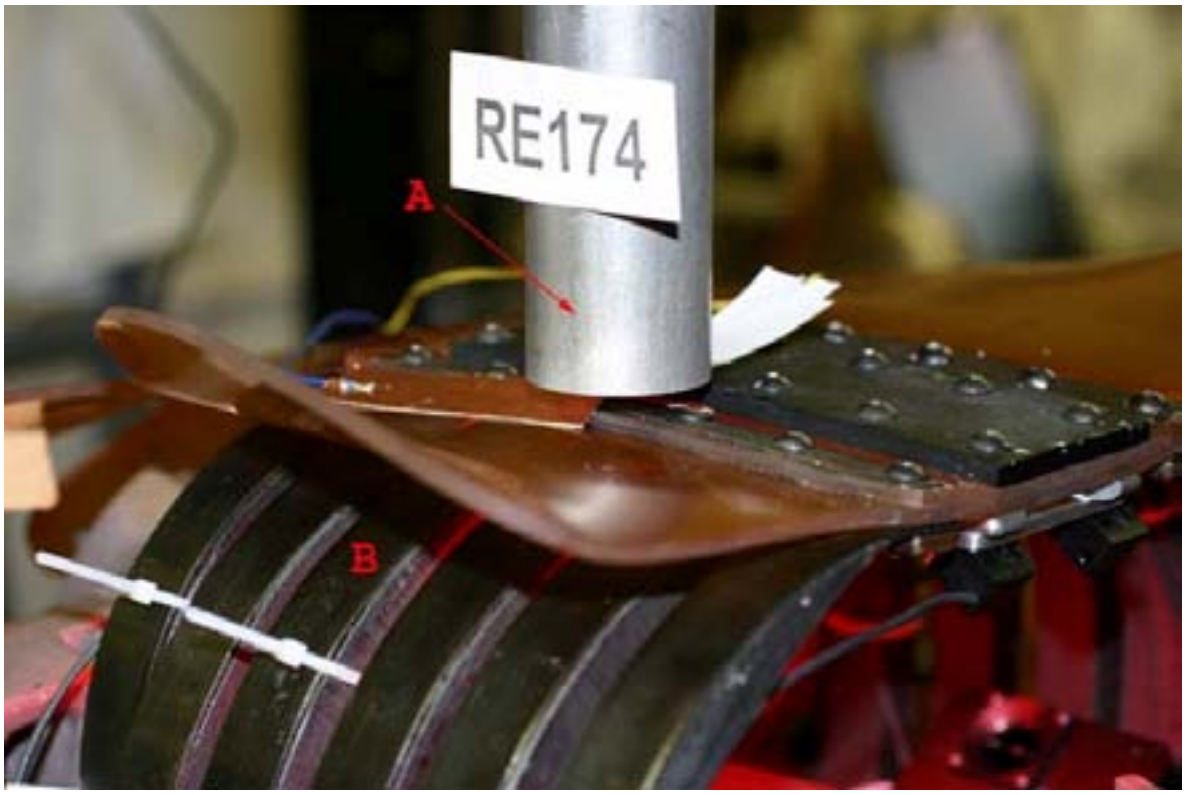

Figure 49: Test configuration for rib-mounted loading. A: indenter, B: right third rib.

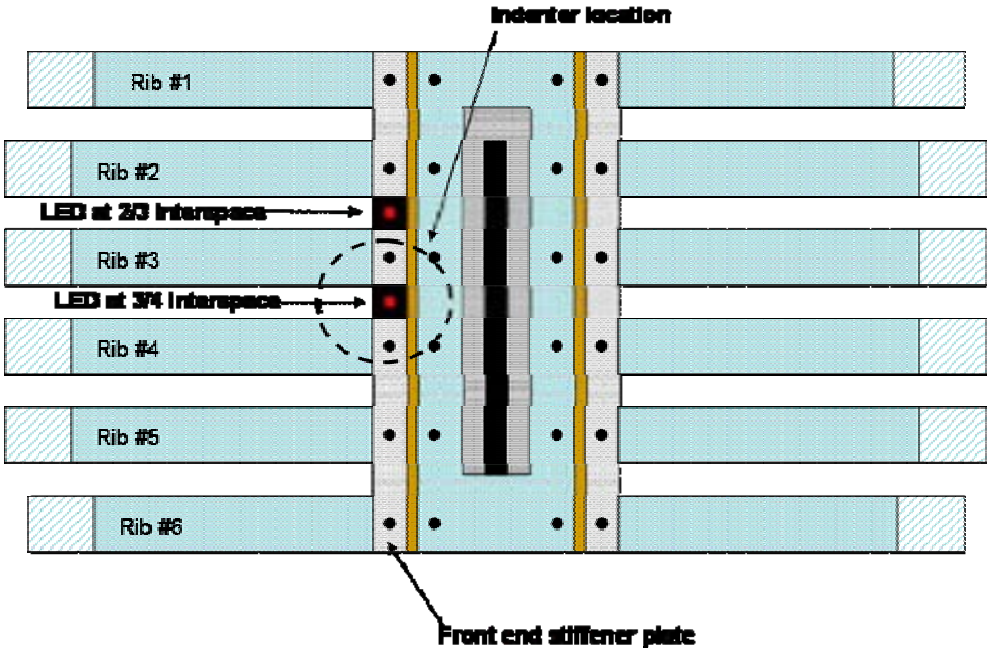

Figure 50: LED configurations used in rib-mounted LED tests. Dashed circle shows the outline of the indenter centered at the interspace between ribs three and four.

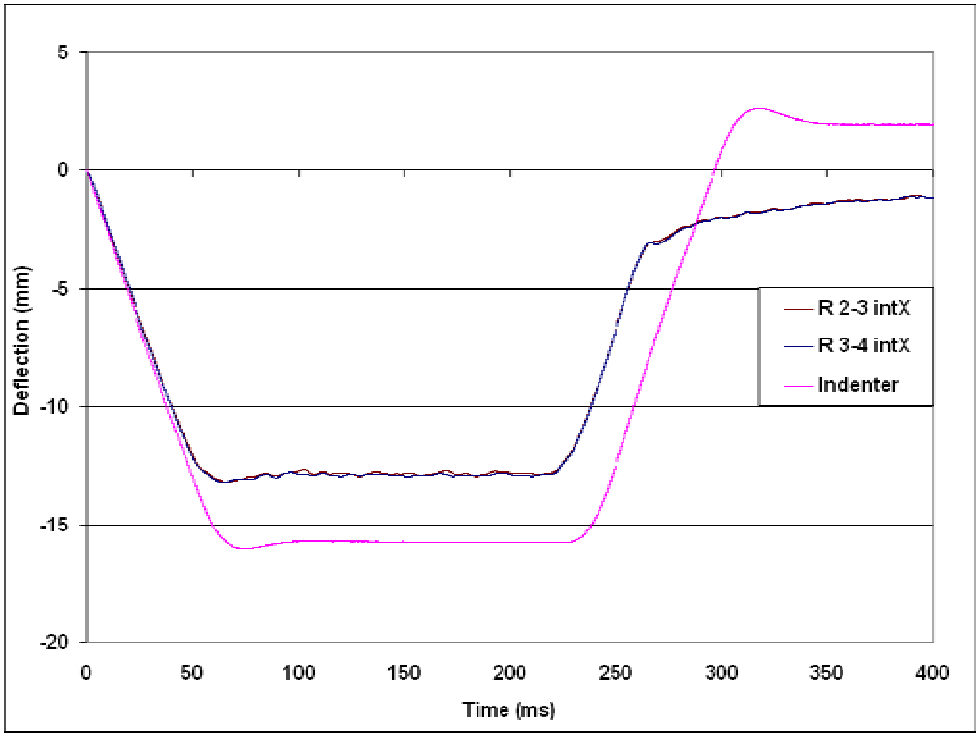

Figure 51: Comparison of deflection data along the x-direction from LEDs positioned at the right 2-3 and 3-4 interspaces. Indenter displacements are also shown.

3.2.3 Rib-mounted LED tests with rotated chest:

In the subsequent subseries of accuracy tests, the dummy chest was rotated 13 degrees about its z-axis, as shown in Figure 53, and securely fixed to the "x-y" cross table. The small circular indenter was placed directly over an LED attached to the right fourth rib at 8 cm from the sternum midline (Figures 52-53) and chest compression tests were performed. Table 12 compares peak LED deflections with indenter displacements corrected for the initial rotation. A representative plot comparing LED deflections and indenter displacements is shown (Figures 54-55). Deflections measured by LEDs were lower than indenter displacements (difference: -0.7 mm to -1.5 mm; -1.9 to -9.4%, Table 12).

Table 12: Right rib 4 LED deflections compared to indenter displacement in rotated thorax tests

Test ID	Peak Indenter Displacement (mm)	Resultant peak R Rib 4 Displacement (mm)	Difference (mm)	% R Rib 4 Difference
179	-15.8	-14.3	-1.5	-9.4
180	-21.9	-21.2	-0.7	-3.4
181	-28.5	-27.6	-0.9	-3.1
182	-40.8	-40.0	-0.8	-1.9

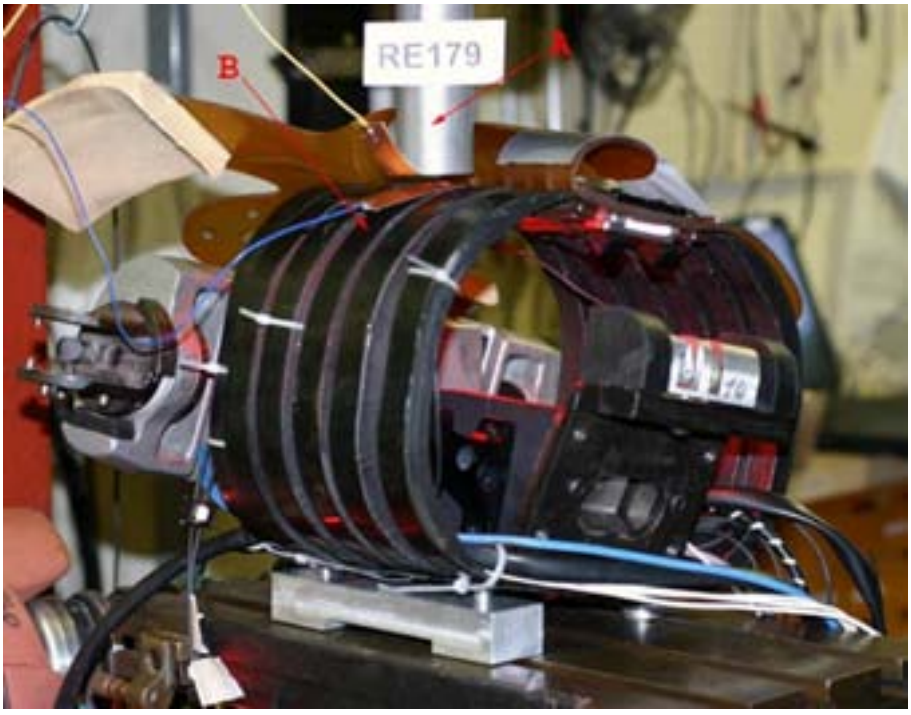

Figure 52: Photograph showing the setup for thorax rotated loading tests. A: indenter and B; right fourth rib.

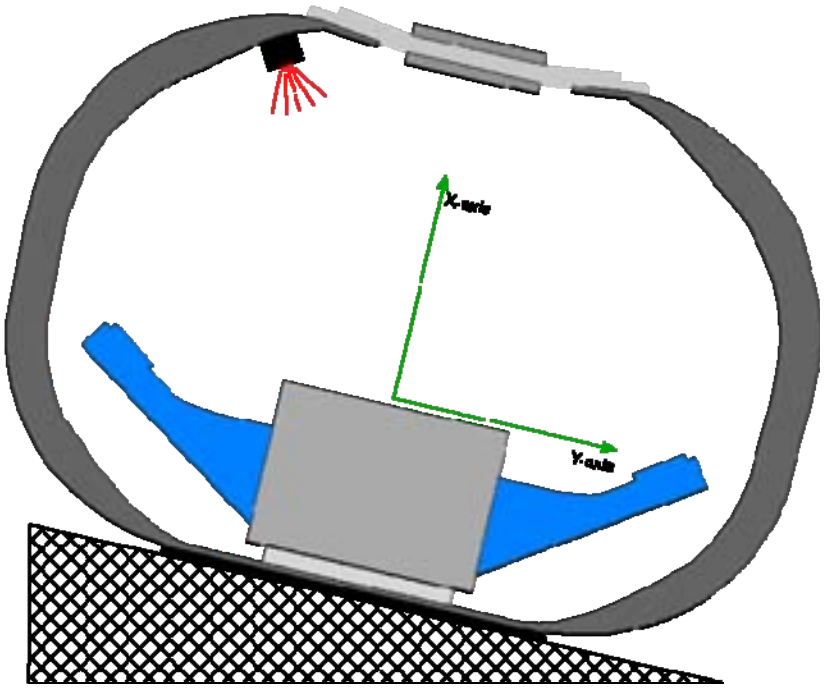

Figure 53: Schematic showing the setup for thorax rotated loading tests. Only one LED is shown in the illustration.

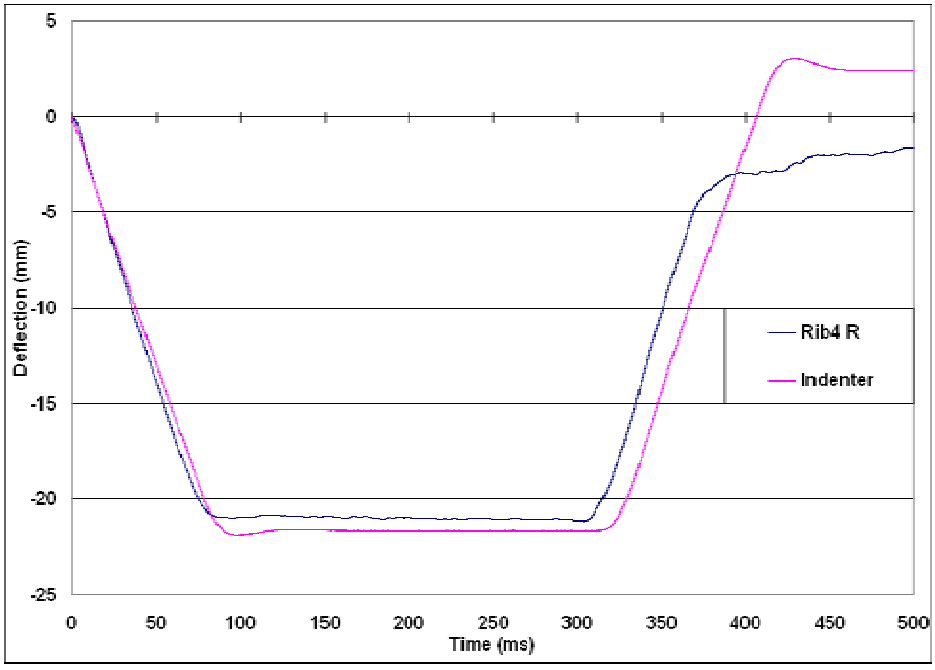

Figure 54: Comparison of deflection data along the vertical direction from the right fourth rib and indenter in rotated thorax tests.

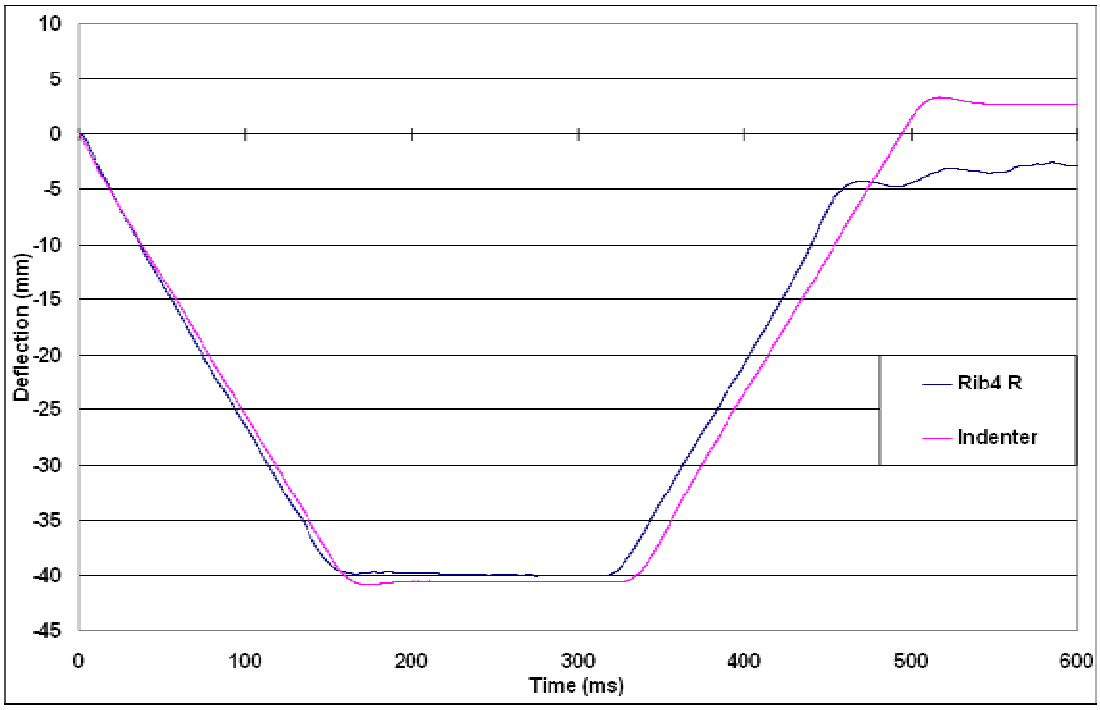

Figure 55: Comparison of deflection data along the vertical direction from the right fourth rib and indenter in rotated thorax tests.

3.2.4 Indenter-mounted LED tests:

In the subsequent subseries of accuracy tests, an LED was mounted to an extension of the indenter that allowed for positioning of the LED directly under the rib of interest. The Hybrid III sternum was modified to allow the indenter extension to pass between the ribs, but maintain the original thorax geometry (Figures 56-58). This configuration essentially produced an accuracy bench test that maintained ATD and RibEye integrity. Compression tests were performed at the left third and right sixth ribs (Figures 59-60). Indenter velocities ranged from 0.08 m/s to 0.25 m/s with nominal deflections of 12 to 60 mm. Representative plots comparing LED and indenter displacements are shown in figures 61-62. The difference between RibEye and indenter displacements ranged from -1.92 mm to 0.49 mm (-3.75% to 2.24%, Table 13). These findings indicate that, under pure x-deformations, the RibEye LED can effectively follow the vertical indenter path and hence produce reasonable output.

Table 13: Summary of data

Test #	Indenter Velocity (m/s)	Test Location	Peak Y RibEye Disp (mm) CFC60	Peak X Indenter Disp (mm) CFC1000	Peak X RibEye Disp (mm) CFC60	Difference in X (mm)	Percent Difference in X (%)
208	0.08	Rib 3L	0.30	-12.8	-13.0	0.15	1.20
209	0.08	Rib 3L	0.30	-12.8	-13.1	0.26	2.01
210	0.08	Rib 3L	0.39	-19.3	-19.5	0.20	1.01
211	0.08	Rib 3L	0.59	-25.6	-25.7	0.11	0.43
212	0.08	Rib 3L	0.96	-32.0	-31.9	-0.09	-0.27
213	0.08	Rib 3L	1.34	-38.3	-37.8	-0.51	-1.32
214	0.12	Rib 3L	1.44	-38.4	-37.7	-0.63	-1.65
215	0.15	Rib 3L	2.24	-44.8	-43.7	-1.12	-2.49
216	0.20	Rib 3L	3.69	-51.2	-49.3	-1.92	-3.75
217	0.20	Rib 3L	6.48	-56.4	-54.7	-1.74	-3.08
218	0.08	Rib 6R	-0.37	-12.8	-13.1	0.29	2.24
219	0.08	Rib 6R	-0.60	-19.3	-19.7	0.42	2.17
220	0.08	Rib 6R	-0.76	-25.6	-26.1	0.48	1.89
221	0.08	Rib 6R	-1.00	-32.0	-32.5	0.49	1.53
222	0.15	Rib 6R	-1.41	-38.4	-38.7	0.28	0.74
223	0.15	Rib 6R	-1.66	-44.8	-45.1	0.24	0.54
224	0.20	Rib 6R	-2.23	-51.2	-51.2	0.09	0.18
225	0.25	Rib 6R	-2.71	-57.7	-57.7	0.02	0.03

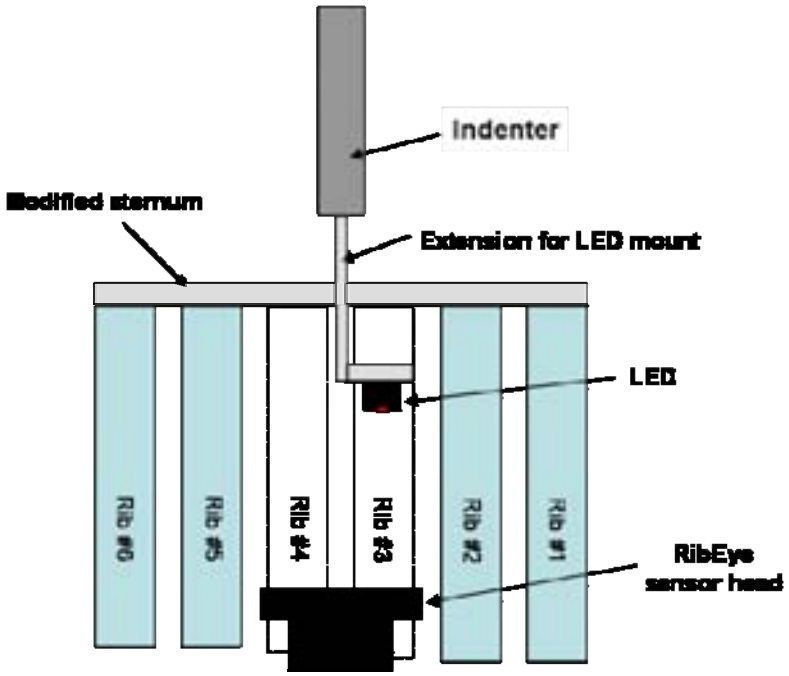

Figure 56: Schematic of the test with sternum modification with the indenter attached to the testing device.

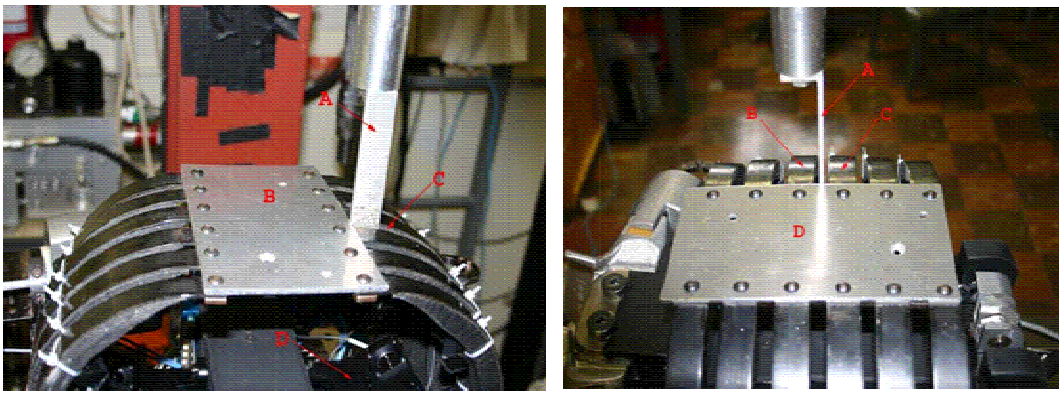

Figure 57: Photograph of the setup used in indenter-mounted LED tests. Left: A: indenter extension, B: sternum modification, C: left 3-4 interspace, and D: RIbEye sensor head. Right: A: indenter extension, B and C: left third and fourth ribs, and D: sternum

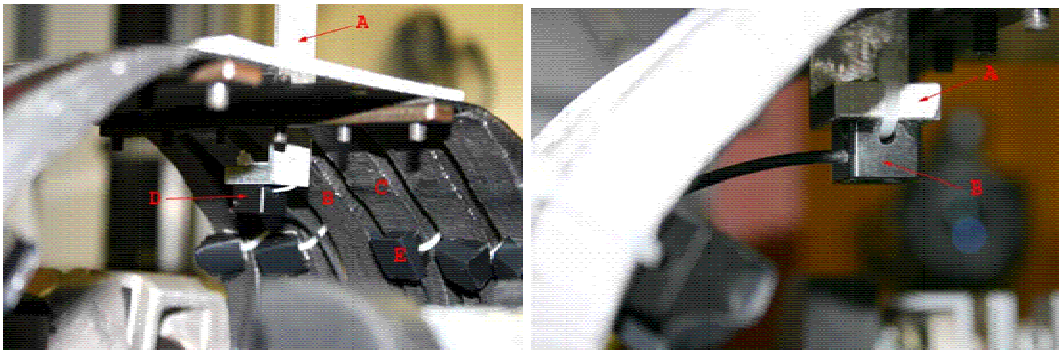

Figure 58: Photograph of the setup used in indenter-mounted LED tests. Left: A: indenter extension, B: left third rib, C: left fourth rib, D: LED being evaluated, and E: LED on the fourth rib. Right: A: indenter extension, B: LED being evaluated.

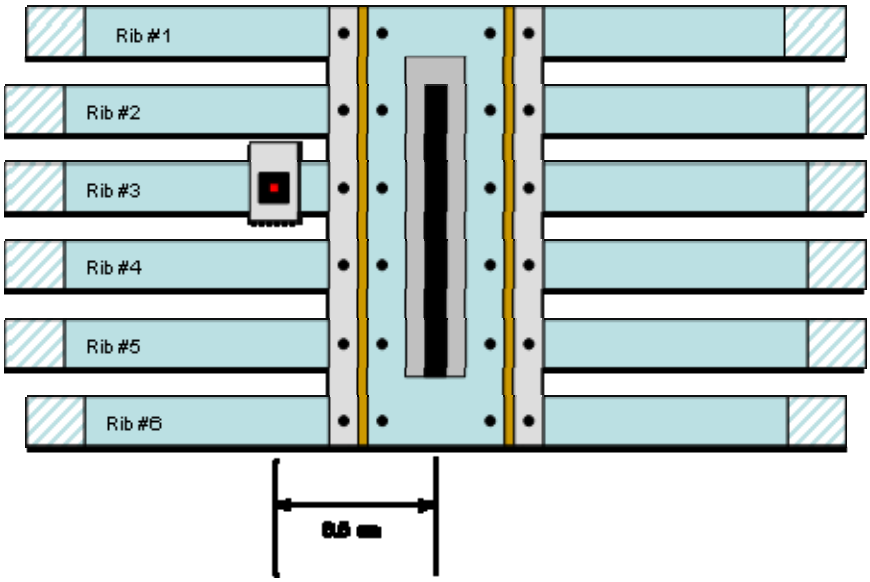

Figure 59: Configuration for left third rib accuracy evaluation.

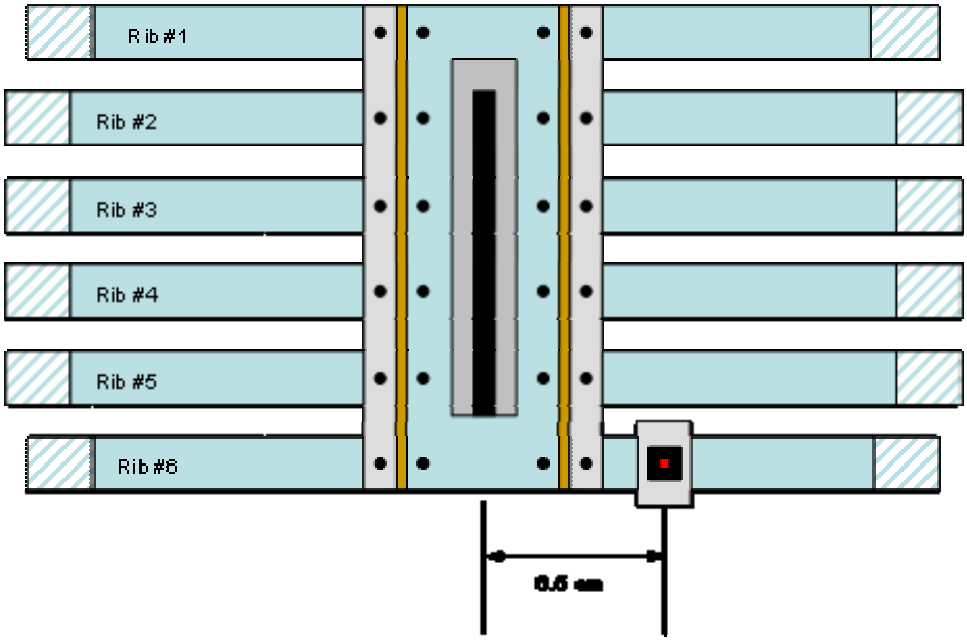

Figure 60: Configuration for right sixth rib accuracy evaluation.

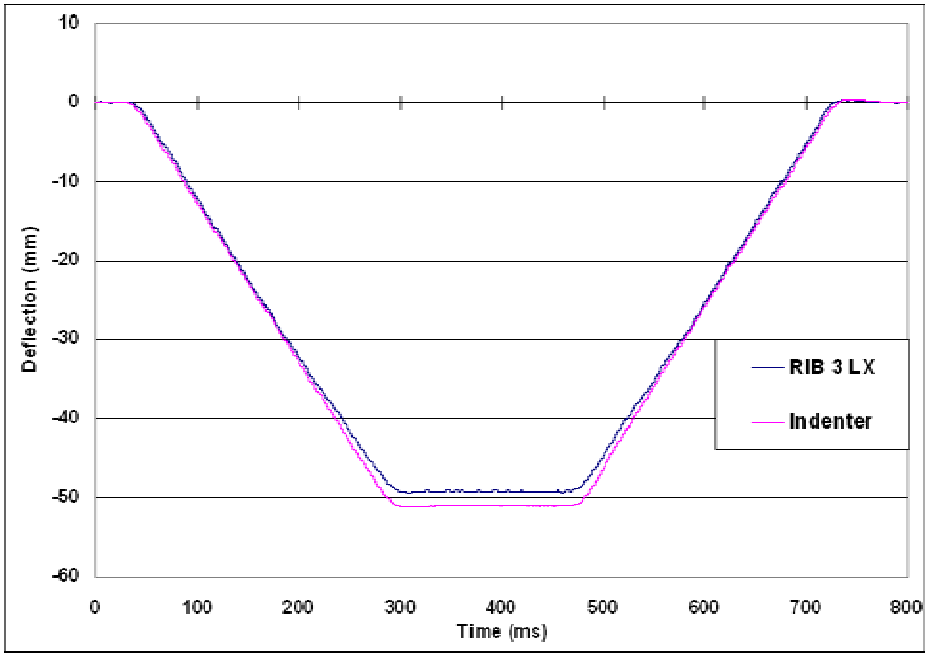

Figure 61: Comparison of displacements from the indenter and LED mounted to the extension arm of the indenter for assessing the accuracy of an LED attached to the arm. The LED was positioned under the left third rib.

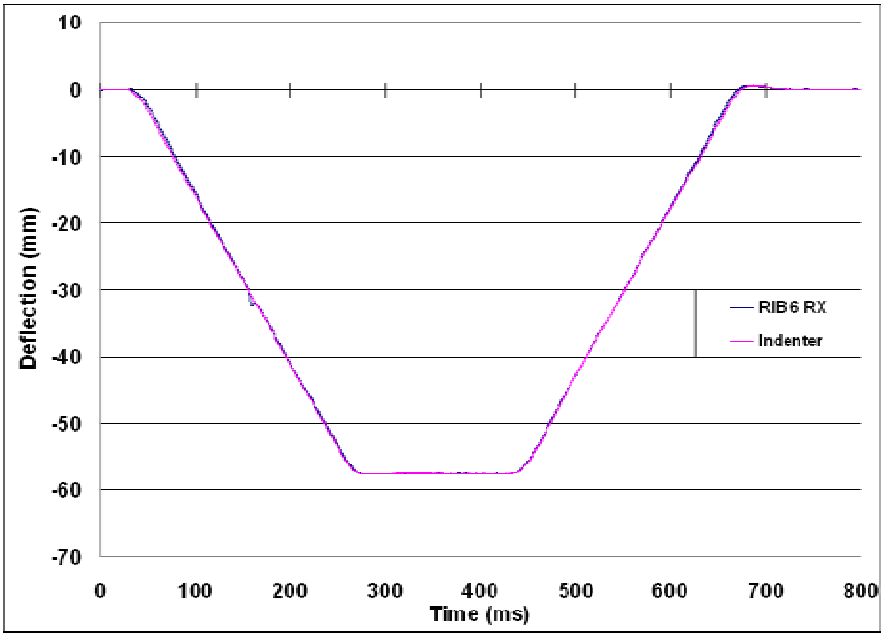

Figure 62: Comparison of displacements from the indenter and LED mounted to the extension arm of the indenter for assessing the accuracy of an LED attached to the arm. The LED was positioned under the right sixth rib.

4.0 EVALUATIONS BASED ON DYNAMIC LOADING

The purpose of this series of tests was to further evaluate the performance of RibEye-based deflection measurements using pendulum impactor and full-scale vehicle crash tests. LEDs were affixed to ribs using double-sided tape and nylon cable ties. Based on results from quasi-static tests, LEDs were positioned at the optimal location, 9 cm from mid sternum (Figure 63).

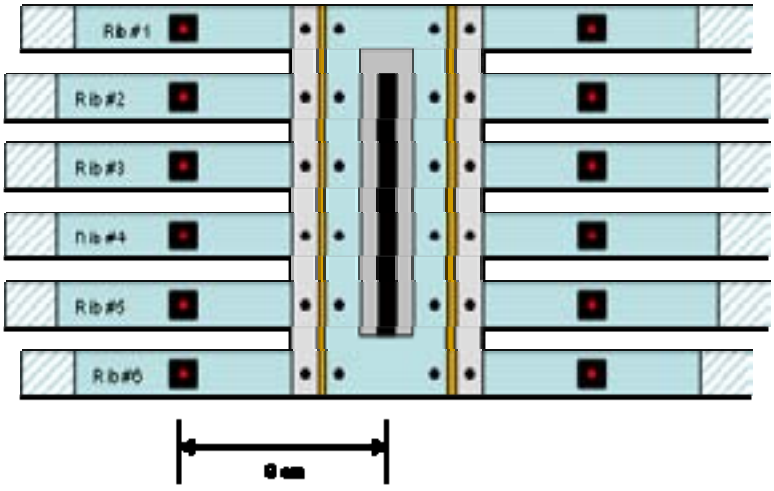

Figure 63: LED configuration for dynamic test procedures.

4.1 Pendulum Tests

The RibEye system was subjected to nine tests. Seven tests were conducted with the dummy in the neutral and two tests were conducted with the dummy in the 25-degree rotated position about the vertical (z) axis so that the pendulum impacted the right side of the thorax. The neutral positioning followed specifications according to 49 CFR 572.34 (Figure 64)[3]. Impact velocity, measured with an optical system for Hybrid III thorax qualification tests, ranged from 3.0 m/s to 6.6 m/s. The internal chest potentiometer was used in four of the neutral tests. It was not used in any oblique test. The initial test in this series (Test 1, probe velocity = 6.60 m/s) served as a thoracic impact calibration test. The maximum sternum deflection measured by the internal chest potentiometer, 66.8 mm, was within the qualification corridor in 49 CFR 572.34. Drop-out did not occur in tests conducted at velocities ranging from 3.0 to 4.8 m/s, regardless of the presence of the chest potentiometer (Table 14). However, drop-out occurred in three of twelve (25%) LEDs in the 6.6 m/s test in the neutral position with inclusion of the internal chest potentiometer. The analogous test without the potentiometer produced no drop-out and implicated the chest pot slider arm as the source of sensor interference. Figures 65-67 include deflections along the x-direction from the upper, middle, and lower ribs with LED drop-out demonstrated in the lower rib output. The internal chest potentiometer data are included in all plots. Rib deflection curves closely followed the sternum deflection measured by the chest potentiometer in both timing and shape. As expected, rib deflections were lower than the sternum deflection secondary to positioning of LEDs on the ribs and rib motion during compression. Because of the three-dimensional nature of the ribcage and off-central locations of the LEDs, sternum-measured displacements were greater than the displacements recorded by the LEDs positioned on the ribs. Figure 68 shows deflections along the y-direction. The ribs on the right side deflect along the positive y-direction while the opposite is true for the left side (hoop deformation). This is reflective of central loading of the chest during impact. Figures 69-71 include deflections along the x-direction from the upper, middle, and lower ribs for the test without the internal chest potentiometer. No signal drop-out occurred in these evaluations. Figure 72 shows deflections along the y-direction for all LEDs, again demonstrating no drop-out.

Figure 64: Hybrid III dummy set-up for neutral position pendulum testing according to CFR § 572.34

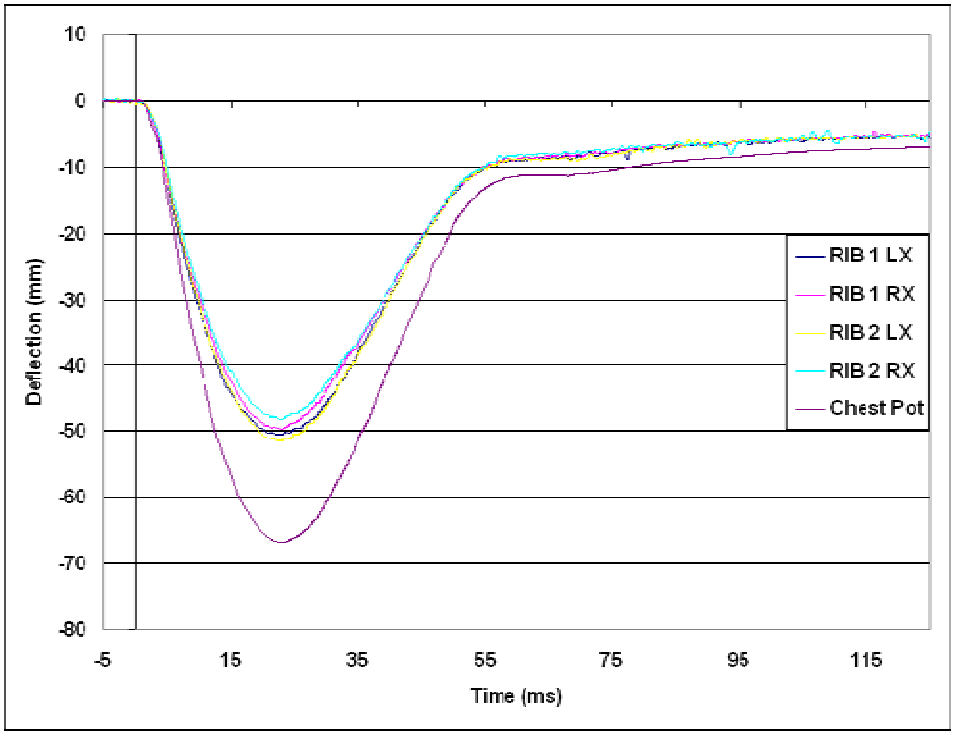

Figure 65: Comparison of deflections in the x-direction from the internal chest potentiometer and LED positioned at 9 cm on ribs one and two during 6.6 m/s pendulum test.

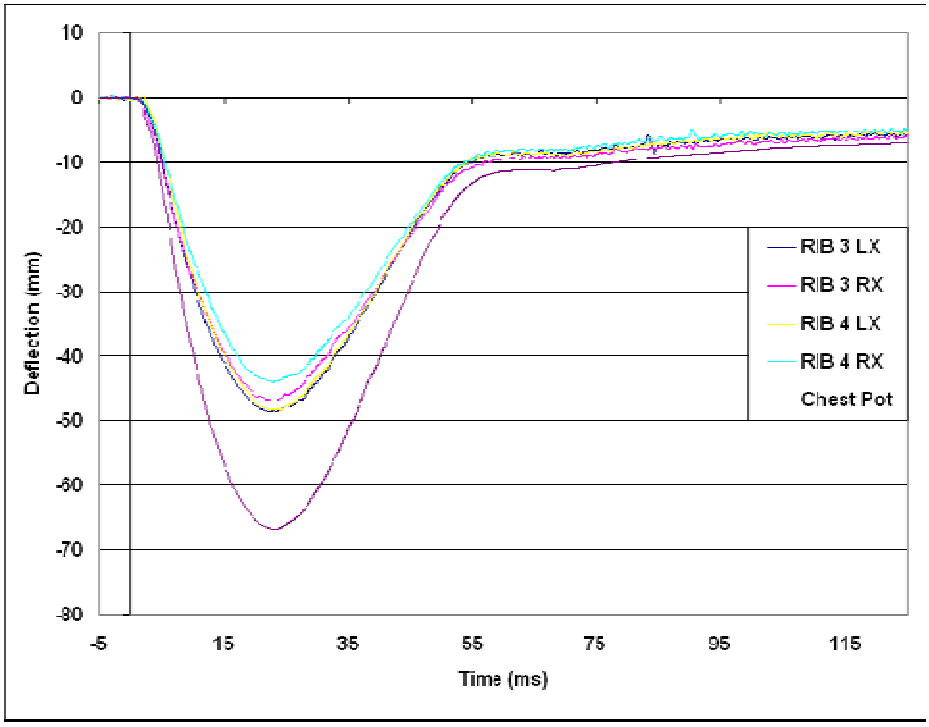

Figure 66: Comparison of deflections in the x-direction from the internal chest potentiometer and LED positioned at 9 cm on ribs three and four during 6.6 m/s pendulum test.

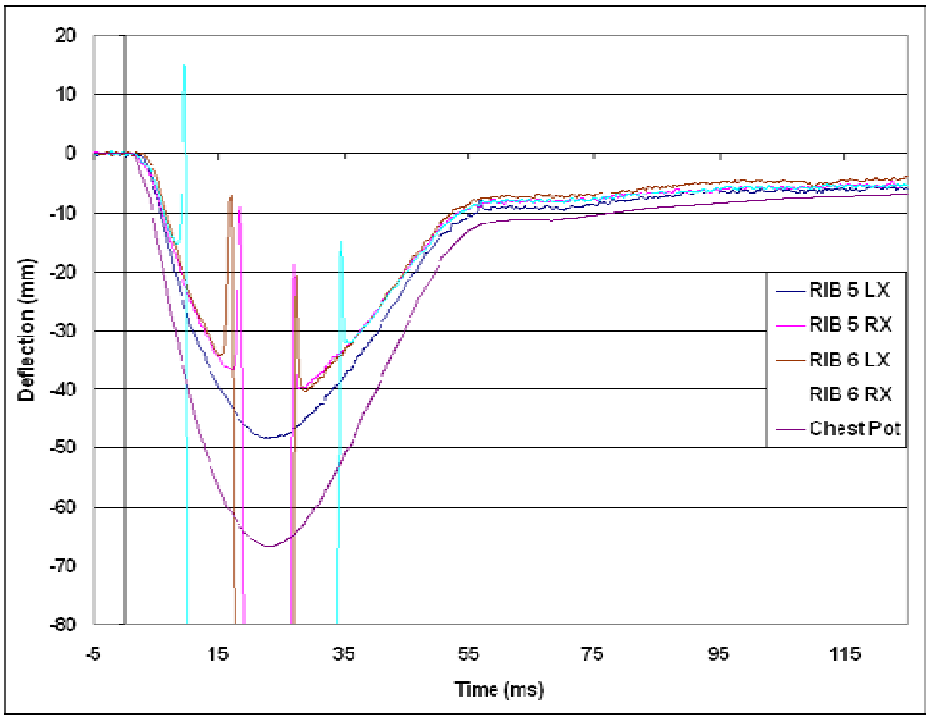

Figure 67: Comparison of deflections in the x-direction from the internal chest potentiometer and LEDs positioned at 9 cm on ribs five and six during 6.6 m/s pendulum test. Drop-out occurred in three LEDs.

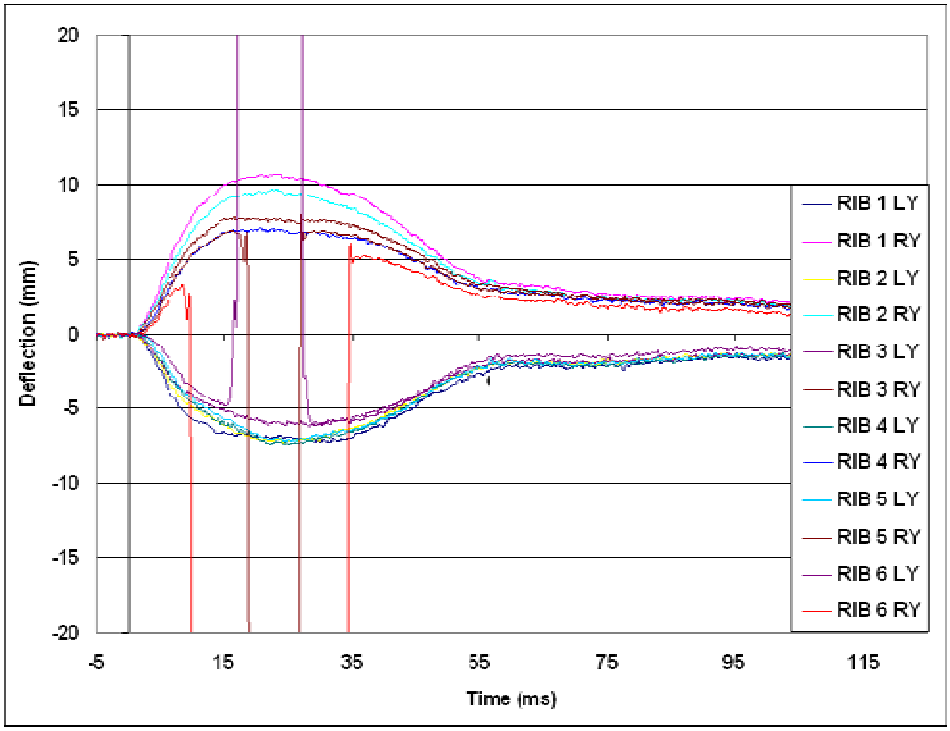

Figure 68: Deflections in the y-direction from LEDs positioned at 9 cm on all ribs during 6.6 m/s pendulum test. Drop-out occurred in three LEDs.

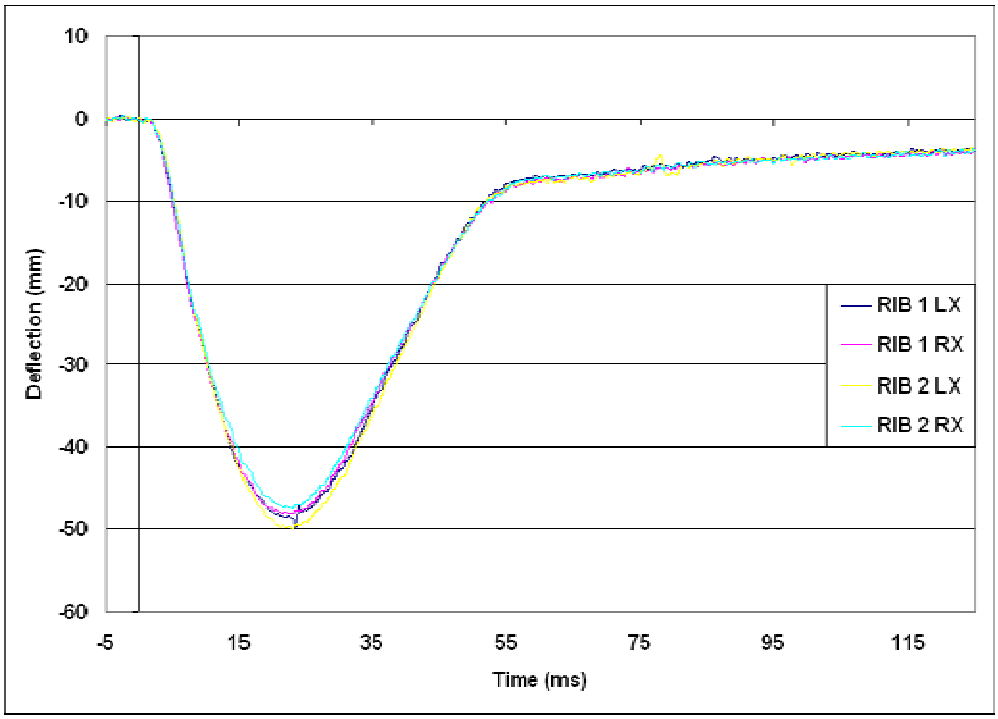

Figure 69: Deflections in the x-direction from LEDs positioned at 9 cm on ribs one and two during 6.6 m/s pendulum test.

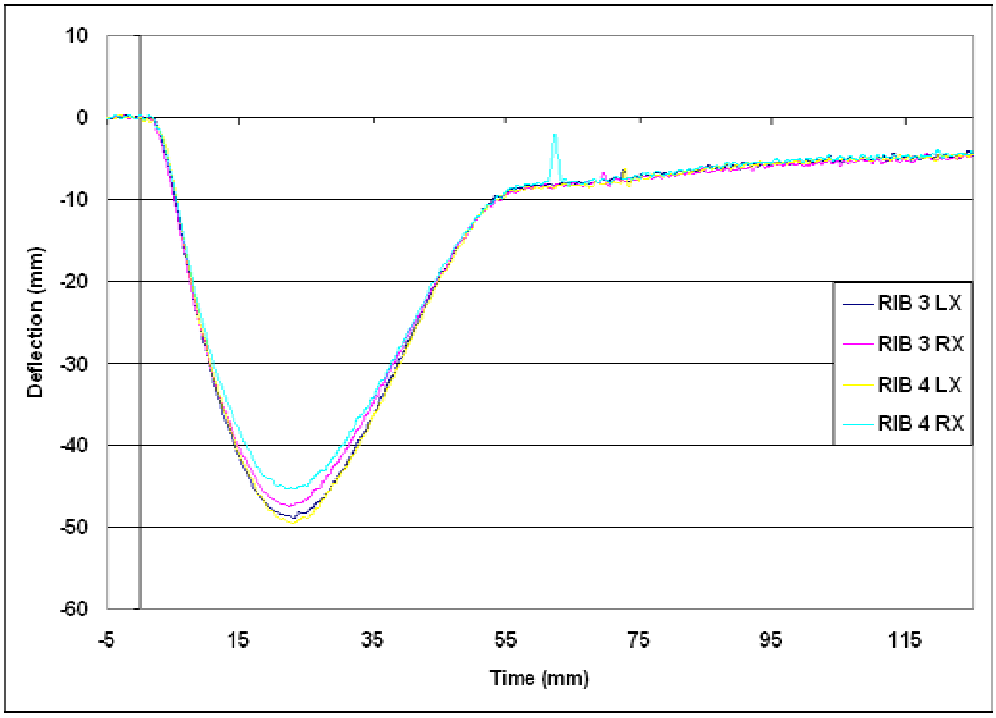

Figure 70: Deflections in the x-direction from LEDs positioned at 9 cm on ribs three and four during 6.6 m/s pendulum test.

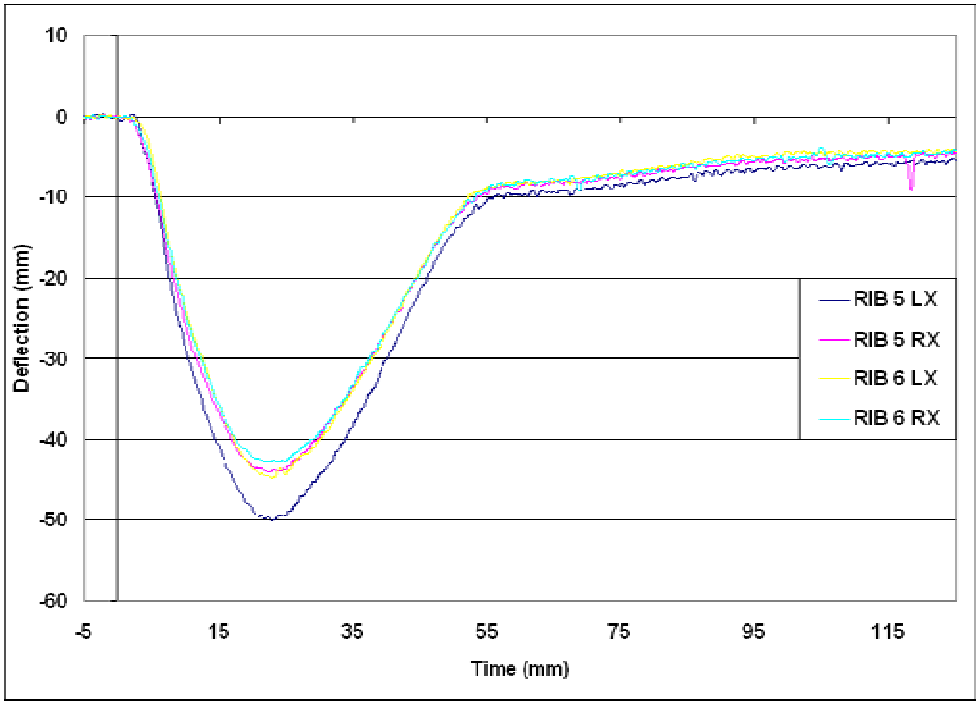

Figure 71: Deflections in the x-direction from LEDs positioned at 9 cm on ribs five and six during 6.6 m/s pendulum test.

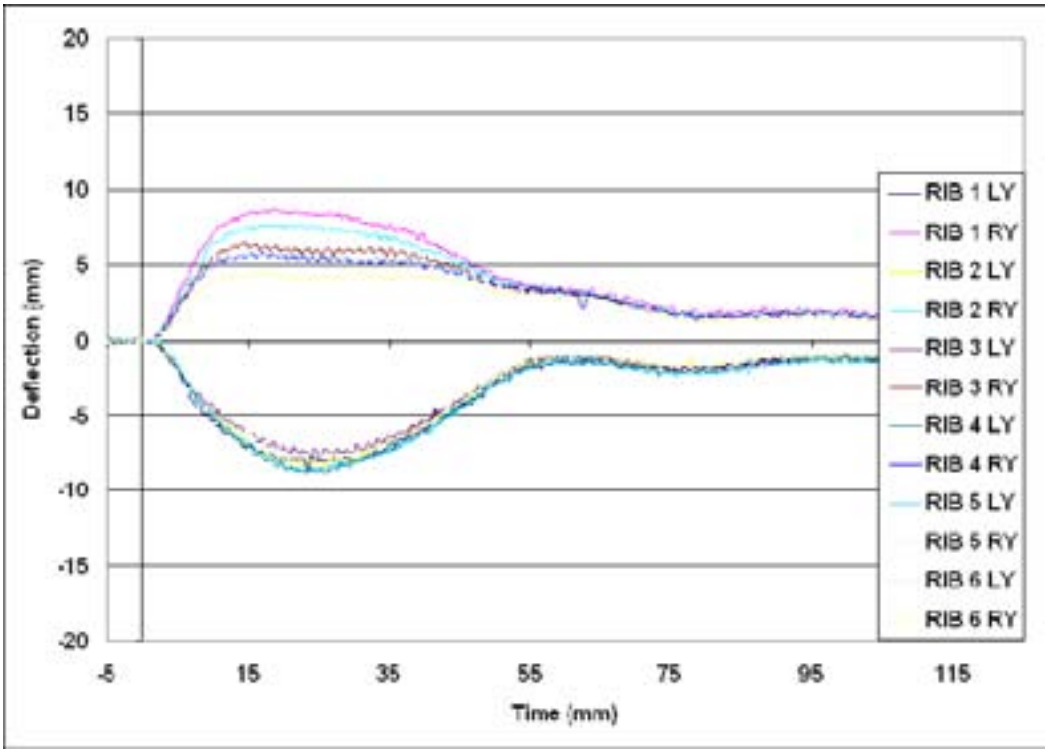

Figure 72: Deflections in the y-direction from LEDs positioned at 9 cm on all ribs during 6.6 m/s pendulum test.

Figures 73-75 include deflections along the x-direction from the upper, middle, and lower ribs for the oblique test. Right-sided ribs demonstrated greater deflection magnitudes in the x direction compared to left-sided ribs. This is reflective of the right oblique chest loading imparted by the pendulum. No signal drop-out occurred in these evaluations. Figure 76 shows deflections along the y-direction for all LEDs, again demonstrating no drop-out. Deflections in the y direction were approximately the same magnitude, which would be expected because the loading is from the right to the left side causing a deflection of all ribs toward the left side.

These findings suggest that, in the absence of light interference during impact, at velocities used in the current subseries of tests, the RibEye system can capture rib deformations along both x- and y-directions and at multiple locations. Table 14 summarizes the data.

Table 14: Summary of pendulum test data

Test ID	Dummy Position	Velocity (m/s)	Chest Pot Used	Max Chest Potentiometer Deflection (mm)	LED Drop-out	% LED Drop out
1	Neutral	6.6	Y	66.8	3	25.0
2	Neutral	4.1	Y	39.5	0	0.0
3	Neutral	3.0	Y	27.0	0	0.0
4	Neutral	4.1	Y	41.1	0	0.0
5	Neutral	4.1	N	-	0	0.0
6	Neutral	3.0	N	-	0	0.0
7	Neutral	6.6	N	-	0	0.0
8	Oblique	4.1	N	-	0	0.0
9	Oblique	4.8	N	-	0	0.0

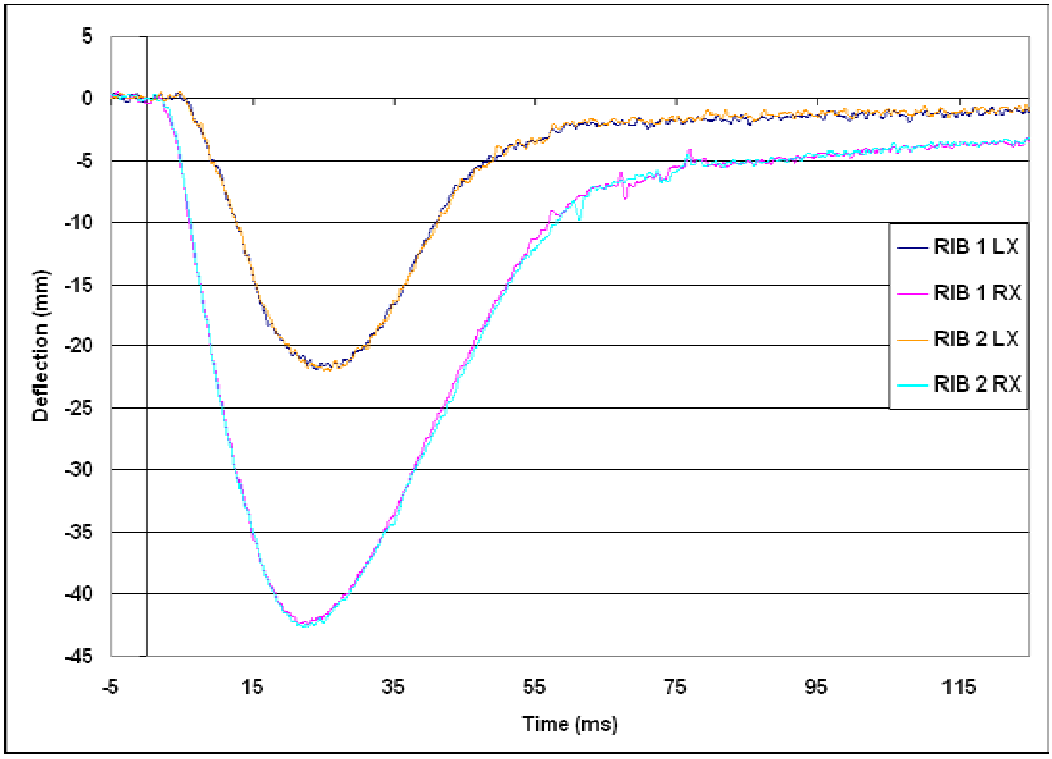

Figure 73: Deflections in the x-direction from LEDs positioned at 9 cm on ribs one and two during 4.8 m/s oblique pendulum test.

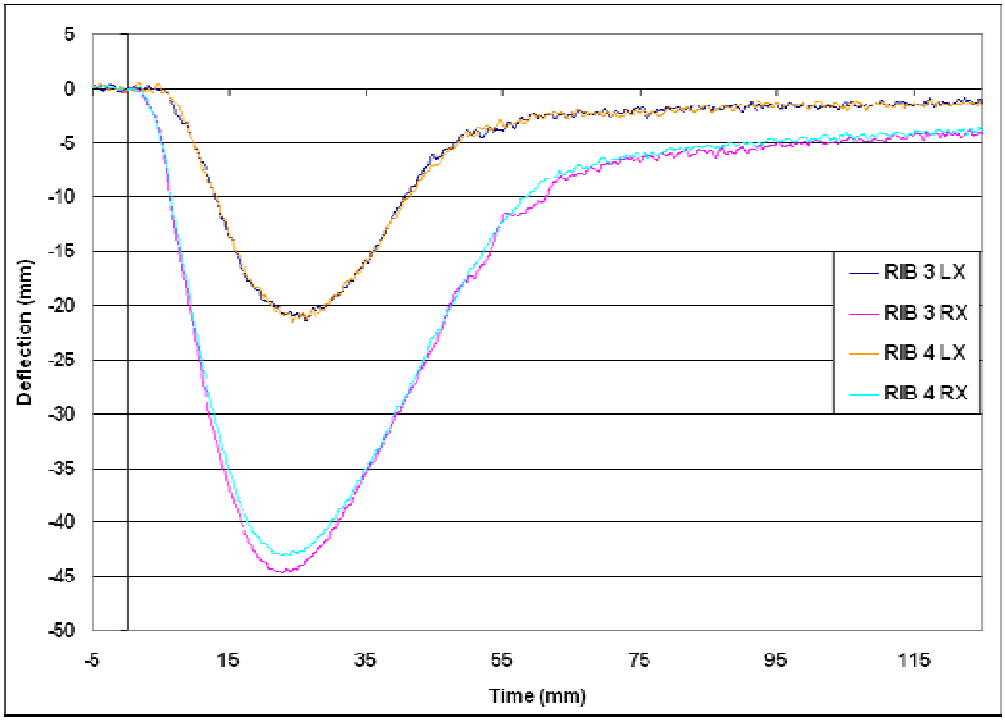

Figure 74: Deflections in the x-direction from LEDs positioned at 9 cm on ribs three and four during 4.8 m/s oblique pendulum test.

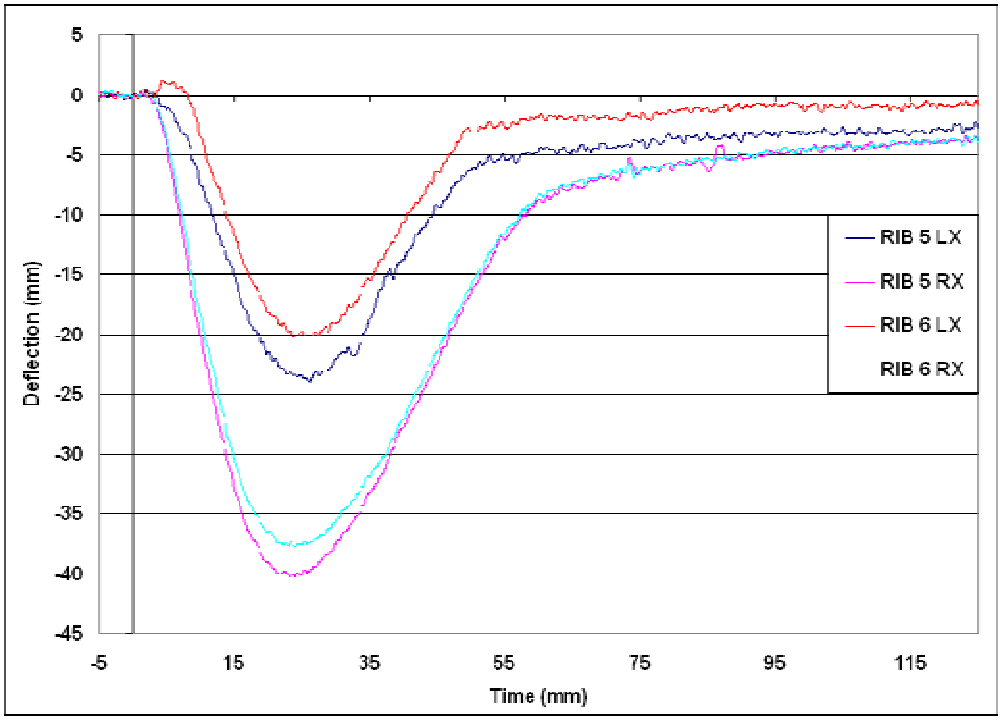

Figure 75: Deflections in the x-direction from LEDs positioned at 9 cm on ribs five and six during 4.8 m/s oblique pendulum test.

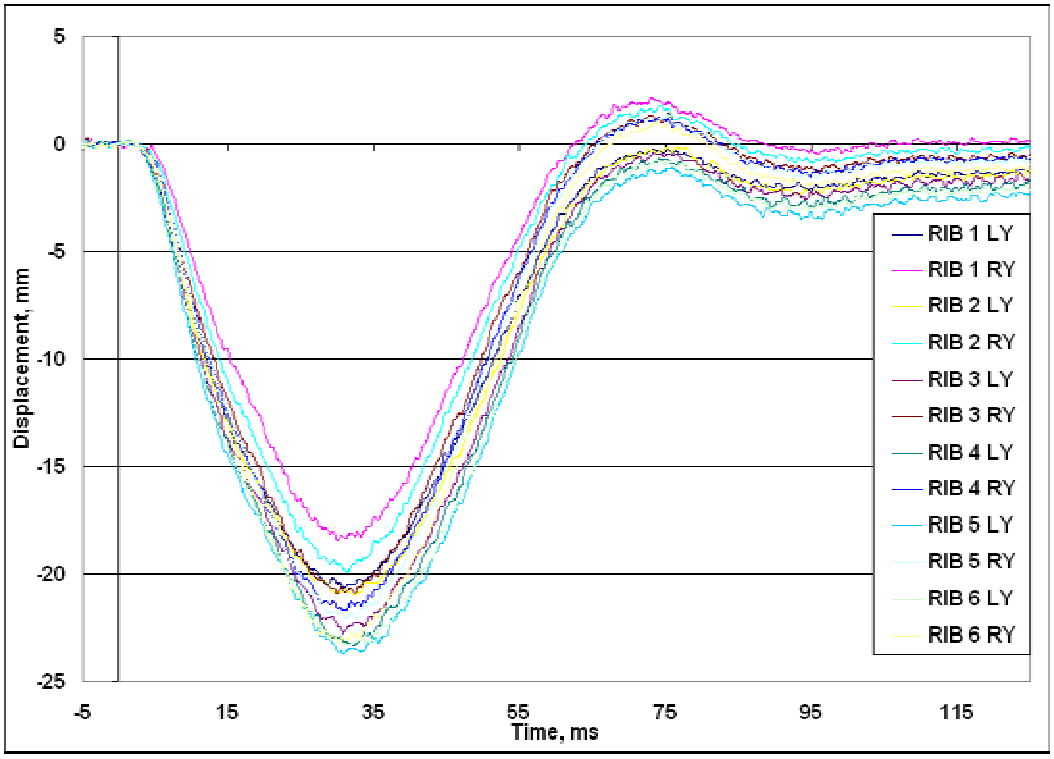

Figure 76: Deflections in the y-direction from LEDs positioned at 9 cm in all ribs during 4.8 m/s oblique pendulum test.

4.2 Full-scale vehicle frontal offset pole test

The 50th percentile Hybrid III dummy with the RibEye system was used as a belted right front occupant in a left frontal offset pole crash test (Figure 77). The vehicle was a 1994 Chevrolet Cavalier without frontal air bags and the impact speed was 45 kilometers/hour. LEDs were arranged at the 9 cm position on ribs one through six bilaterally and the chest potentiometer was excluded (Figure 32). Table 15 summarizes peak rib deflections of all LEDs. Peak deflections (Table 15) in the x-direction were greater on the left than right ribs, ranging from -19.7 mm at rib one to -14.9 mm at rib six. Right side x-direction deflections ranged from -7.0 mm at rib one to -3.8 mm at rib six. In contrast, peak deflections in the y-direction were greater on the right than the left, ranging from 8.5 mm at rib one to 8.0 mm at rib six. Left side y-direction deflections ranged from -6.1 at rib five to -4.9 mm at rib one. Figures 78-80 demonstrate the rib deflection profiles along the x-direction. LED drop-out occurred in the first left rib for two short durations (Figure 78). Figures 81 and 82 illustrate the rib deflection

profiles along the y-direction. For the sake of comparison, while the x-direction profiles are plotted based on upper, middle, and lower ribs pairs in Figures 78-80, y-direction deflection profiles are plotted as left and right pairs for all the six ribs in Figures 81 and 82. As can be seen, drop-outs are distinguishable in Figure 78 for the x- (as indicated in Figure 78) and for the y-direction in Figure 81 on the left side.

Table 15: Summary of peak deflections from frontal offset test

Rib Level	Left		Right	
	x (mm)	y (mm)	x (mm)	y (mm)
Rib 1	-19.7	-4.9	-7.0	8.5
Rib 2	-19.1	-5.0	-5.2	8.2
Rib 3	-18.3	-5.1	-5.7	8.4
Rib 4	-17.6	-5.4	-4.5	8.1
Rib 5	-17.5	-6.1	-3.8	8.0
Rib 6	-14.9	-5.8	-3.8	8.0

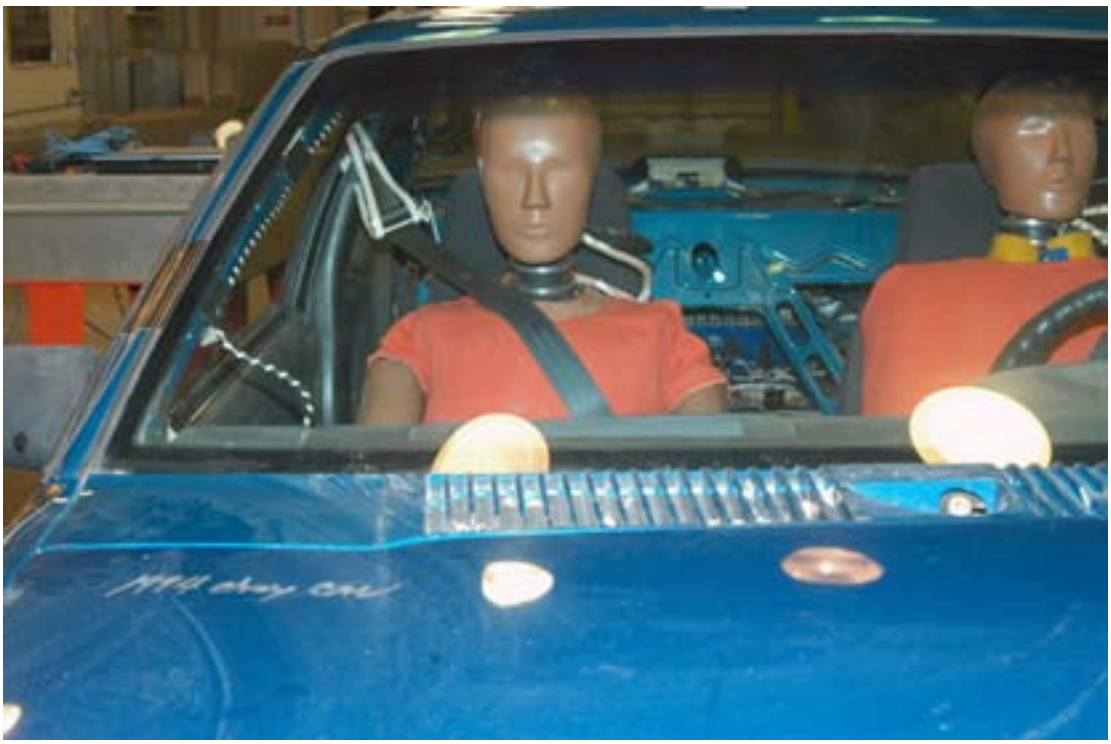

Figure 77: Photograph of pre-test position of Hybrid III/RibEye dummy in offset frontal crash test.

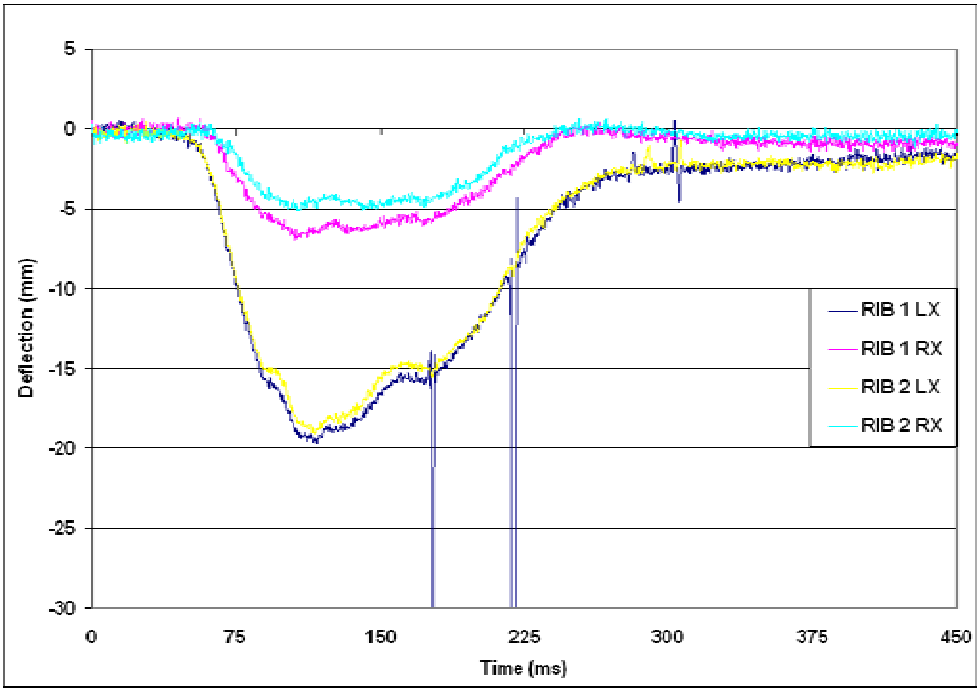

Figure 78: Deflections in the x-direction from LEDs mounted to ribs one and two as recorded by the LEDs positioned at 9 cm, during offset frontal pole test. Note that drop-outs occurred in left rib one at 175 and 220 ms.

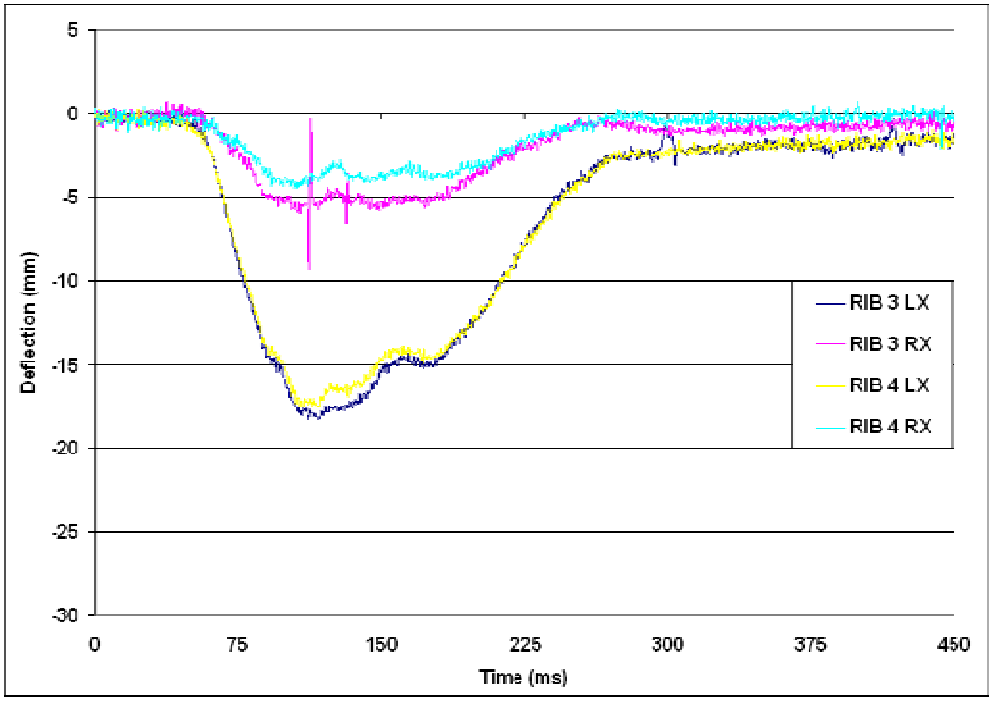

Figure 79: Deflections in the x-direction from LEDs mounted to ribs three and four as recorded by the LEDs positioned at 9 cm, during offset frontal pole test.

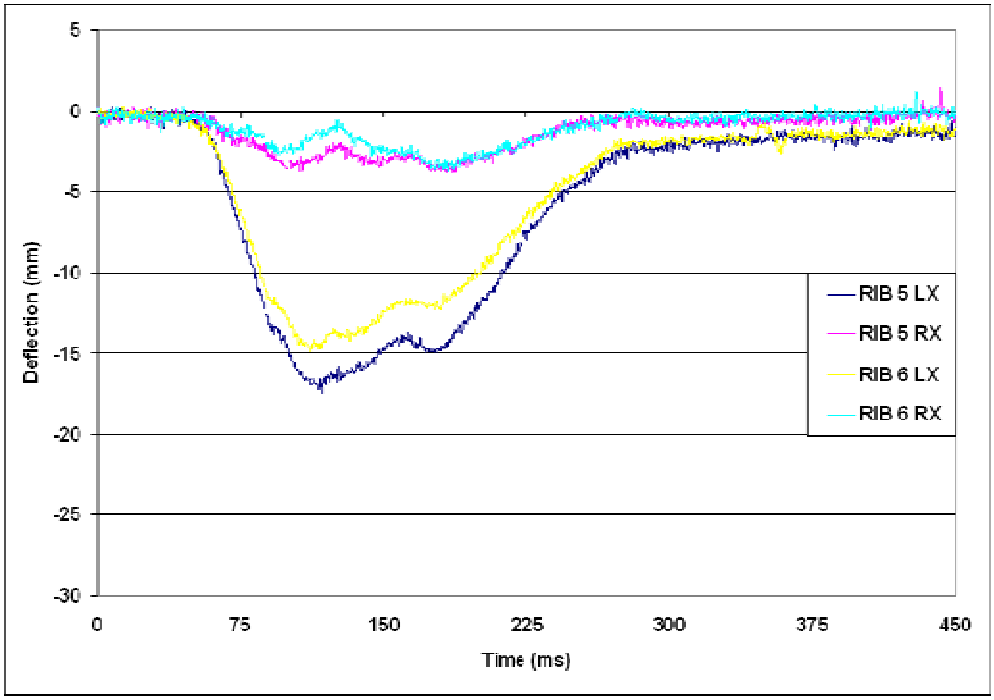

Figure 80: Deflections in the x-direction from LEDs mounted to ribs five and six as recorded by the LEDs positioned at 9 cm, during offset frontal pole test.

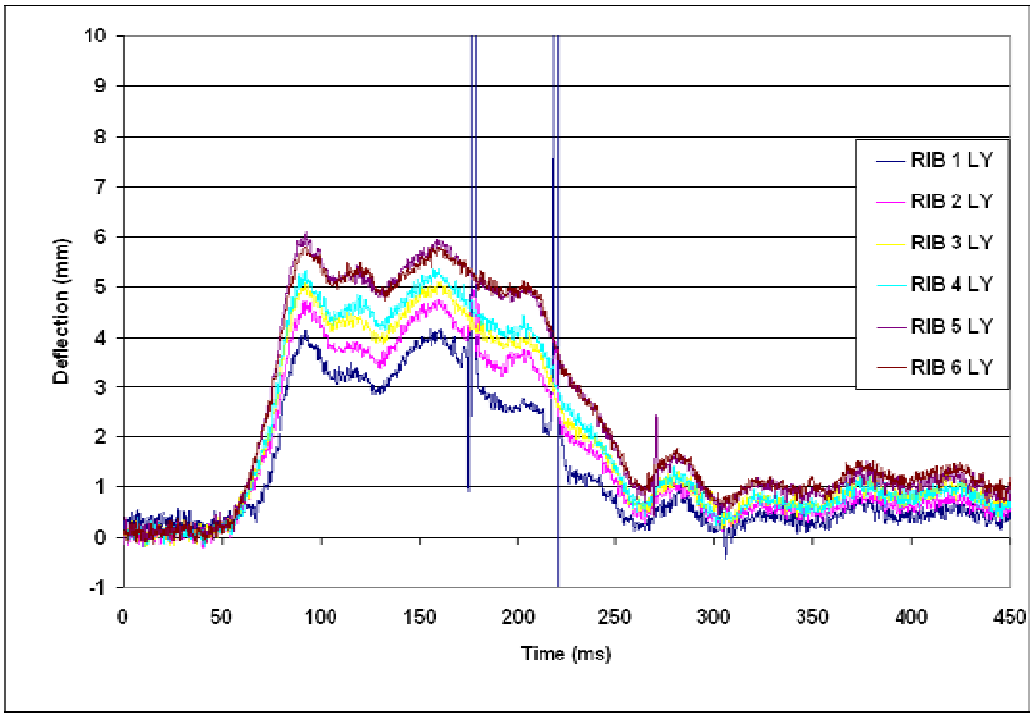

Figure 81: Deflections in the y-direction from LEDs positioned at 9 cm on left ribs during frontal offset pole test. Note that drop-outs occurred in left rib one at 175ms and 220 ms.

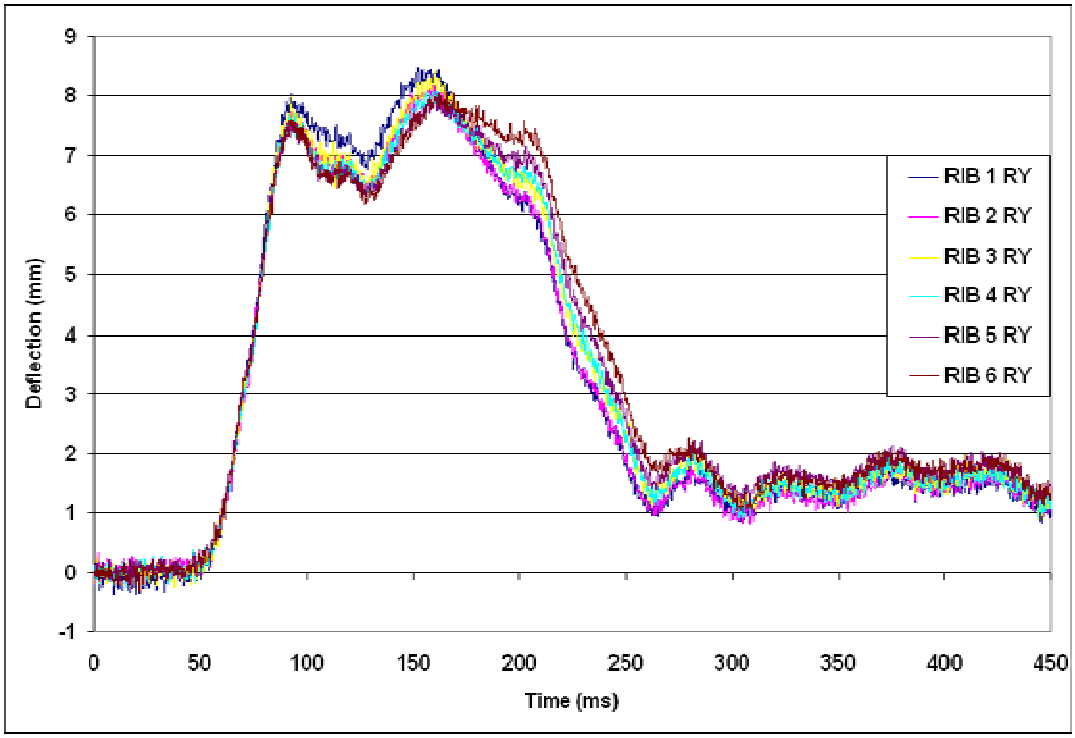

Figure 82: Deflections in the y-direction from LEDs positioned at 9 cm on right ribs during frontal offset pole test.

A comparison between the left and right rib deflections for both x- and y-components is included in Figures 83-84. The decreased x-direction deflections in the right ribs of the dummy compared to the left ribs reflected the asymmetric loading of the chest induced by frontal offset impact and routing of the shoulder belt such that upper left-sided thorax interaction was enhanced. The y-direction deflections of all ribs to the right provided additional evidence of asymmetric loading and are expected in a frontal left offset impact. Observation of these consequences of asymmetric thorax loading would not be possible using the standard HIII chest potentiometer. Although the purpose of the test was not to evaluate the accuracy of the system, acknowledging the limitations in the sample size, the optics-based deflection measurement device appears to capture asymmetric loading and motions of the chest in real-world simulations. Additionally, RibEye system performance was not affected by the high intensity lighting system used during this vehicle crash test. There was no indication of LED drop-out secondary to extraneous light interference which typically manifests as signal drop-out in all LEDs. However, additional studies are needed to confirm these observations.

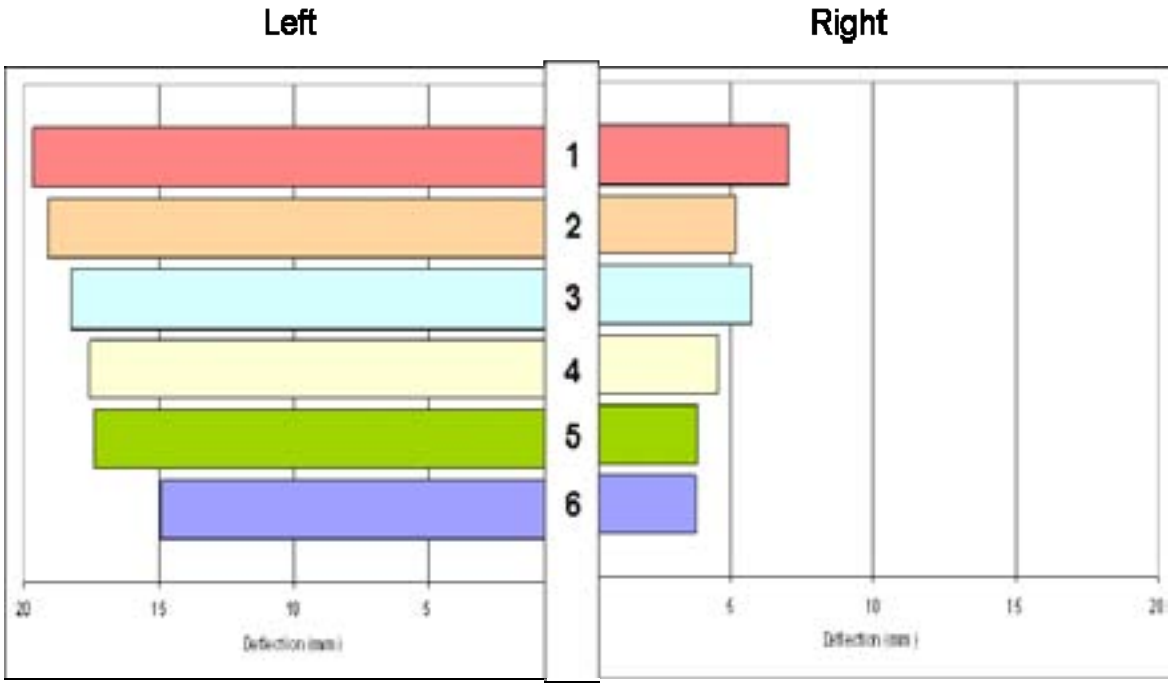

Figure 83: Peak rib deflections (x direction) in left frontal offset crash test. Rib numbers are shown in the center.

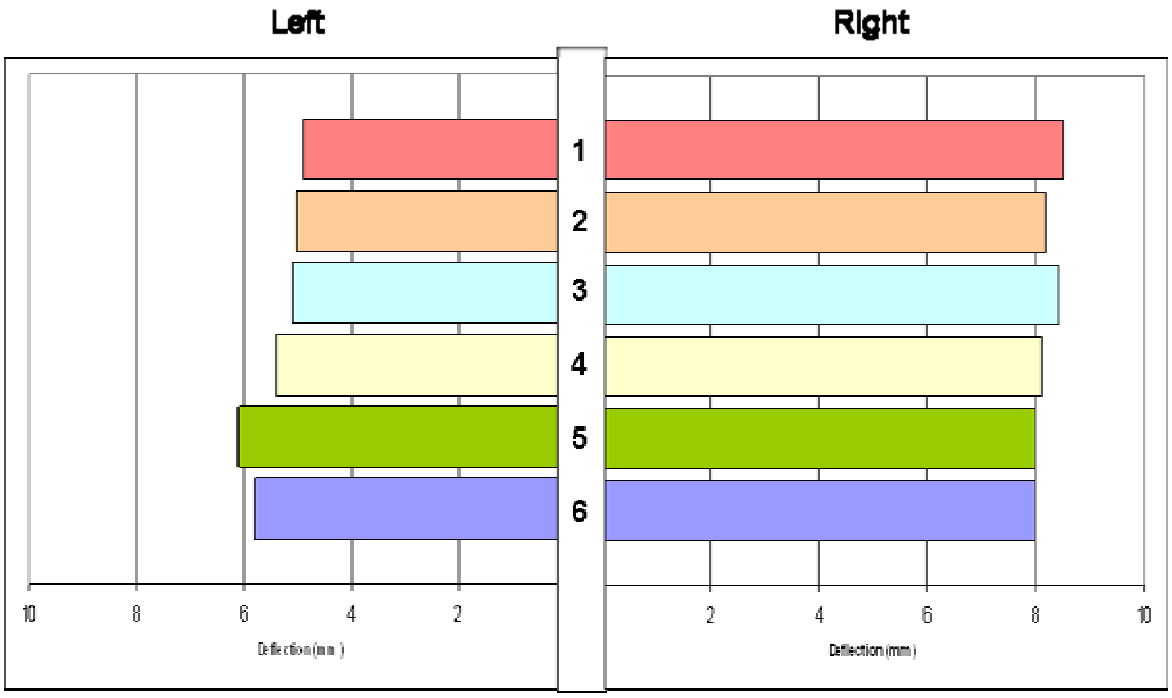

Figure 84: Peak rib deflections (y direction) in left frontal offset crash test. Rib numbers are shown in the center. All deflections are positive, i.e., toward the right.

5.0 OTHER CONSIDERATIONS

The system evaluated is with specific reference to the Hybrid III 50th percentile male dummy. Because the construction of the dummies is different for different sizes in the Hybrid III family, the same system cannot be incorporated into the other dummies. In the same vein, while a modified system has the potential to be incorporated into other types of dummies, the present evaluations should be considered only as a first step in the performance of such systems. It should be noted that the system is stand-alone and requires integration into standard data acquisition systems that are used in routine crashworthiness tests, and the sample frequency and recording time are fixed for the current version. In the 141 tests conducted in the present evaluation study, none resulted in data loss, occasional data download issues included browser re-boot in 20 tests and system reboot in two tests. Data delimiters were missing in six tests. These issues may need further consideration.

6.0 SUMMARY

For the evaluation of RibEye system, quasi-static and dynamic tests were conducted in this study. Quasi-static signal drop-out evaluations included mid-sternum compression tests replicating symmetrical, and offset and diagonal compression tests replicating asymmetric loading to the chest. Quasi-static accuracy assessment evaluations included tests using sternum-mounted LEDs, rib-mounted LEDs with and without initial chest rotation, and indenter-mounted LEDs. The Hybrid III dummy internal chest potentiometer was included in some tests. For dynamic evaluations, pendulum tests with LEDs positioned at the optimal location of 9 cm were conducted with the dummy in the neutral (with and without the chest potentiometer) and oblique positions. This was followed by a full-scale vehicle frontal offset test was conducted with the RibEye system in the dummy positioned in the right front passenger seat.

Quasi-static test results indicated that the RibEye system captures ribcage deformations effectively. LEDs on the sternum responded similar to the chest potentiometer. The accuracy

of the system depends on the location where the LEDs are positioned on the rib, magnitude of rib deformation, and potential interference from devices such as the presence of the internal chest potentiometer. Optimum locations appear to be at a distance of 9 cm measured along the outer curvilinear path of the rib from mid-sternum on either side. At this positioning, the system showed no signal drop-out at deflections representative of current frontal impact IARV. At suboptimal positions, drop-out may occur. Positioning LEDs away from the rib center, i.e., eccentric z-axis placement may result in accuracy loss. Signal drop-out depended on the type of loading, asymmetric loading produced more signal loss. The deflection responses along the x-and y-directions were deemed reasonable in oblique loading tests.

Dynamic testing results indicated that light interference from internal components restricts the ability of the system to obtain deflections including signal drop-out. In oblique tests, the system captured the asymmetric motions of the chest by demonstrating greater x-deflections on all left side ribs than right side ribs, demonstrating its potential under this loading condition. Results from the full-scale vehicle frontal offset test indicated that the RibEye performed well with minor signal drop-outs. The deflections from the RibEye system were in-line with the frontal offset principal direction of force with x-direction component magnitudes more on left chest than the right chest, and the y-direction components of all ribs were from the left-to-right and consistent with the expected y-direction response. These quasi-static and dynamic evaluations have provided a fundamental understanding of the performance of the RibEye system and its ability to measure chest deflections at multiple locations including the sternum and along the two principal axes in frontal impact simulations.

7.0 NOMENCLATURE

A-P	Antero-posterior
ATD	Anthropomorphic Testing Device
NHTSA	National Highway Traffic Safety Administration
Hybrid III	Hybrid III dummy developed for frontal impact crashworthiness
FMVSS	Federal Motor Vehicle Safety Standards
SAE	Society of Automotive Engineers
IARV	Injury Assessment Reference Value
LED	Light Emitting Diodes
RAM	Random Access Memory
Hz	Hertz, sampling frequency
W	Watts, units of power
mm	millimeter
DC	Direct Current

8.0 BIBLIOGRAPHY

1. Society of Automotive Engineers, in Human tolerance to impact conditions as related to motor vehicle design-J885. Warrendale, PA: SAE, 1980
2. 49-CFR: Code of Federal Regulations, Part 571, in. Washington, DC: US Department of Transportation, 2000
3. 49-CFR: Code of Federal Regulations, Part 572, in. Washington, DC: US Department of Transportation, 2000
4. Backaitis SH, Mertz HJ (eds): Hybrid III: The First Human-Like Crash Test Dummy. Warrendale, PA: Society of Automotive Engineers, 1994
5. Eppinger RH: On the development of deformation measurement system and its application toward developing mechanically based indices, in Stapp Car Crash Conf. Washington, DC, 1989, pp 209-268
6. Handman DF: Multipoint position measuring and recording system for anthropomorphic test devices, in. USA: Boxboro systems, LLC, Newton, NA, 2007
7. Kroell CK, Schneider DC, Nahum AM: Impact tolerance and response to the human thorax, in Stapp Car Crash Conf. Coronado, CA, 1971, pp 84-134
8. Kroell CK, Schneider DC, Nahum AM: Impact tolerance and response to the human thorax II, in Stapp Car Crash Conf. Ann Arbor, MI: SAE, Warrendale, PA, 1974, pp 123-142
9. Kuppa S, Eppinger RH, McKoy F, et al: Development of Side Impact Thoracic Injury Criteria and Their Application to the Modified ES-2 Dummy with Rib Extensions (ES-2re). Stapp Car Crash J 47:189-210, 2003
10. Mertz HJ, Irwin AL, Prasad P: Biomechanical and scaling bases for frontal and side impact injury assessment reference values. Stapp Car Crash J 47:155-188, 2003
11. Morgan RM, Eppinger RH, Haffner MP, et al: Thoracic trauma assessment formulations for restrained drivers in frontal impact, in Stapp Car Crash Conf. Ft. Lauderdale, FL, 1994, pp s12-34
12. Neathery RF: Analysis of chest impact response data and scaled performance recommendations, in Stapp Car Crash Conf, 1974
13. Yoganandan N, Morgan RM, Eppinger RH, et al: Mechanisms of thoracic injury in frontal impact. J Biomech Eng 118:595-597, 1996
14. Yoganandan N, Pintar FA, Skrade D, et al: Thoracic biomechanics with air bag restraint, in Stapp Car Crash Conf. San Antonio, TX, 1993, pp 133-144
15. Yoganandan N, Skrade D, Pintar F, et al: Thoracic deformation contours in a frontal impact, in Stapp Car Crash Conf. San Diego, CA, 1991, pp 47-63

DOT HS 811 102
March 2009

U.S. Department
of Transportation
**National Highway
Traffic Safety
Administration**

www.nhtsa.gov